

DIMETHYL ETHER (DME) SYNTHESIS USING MESOPOROUS SAPO-34 LIKE
CATALYTIC MATERIALS

A THESIS SUBMITTED TO
THE GRADUATE SCHOOL OF NATURAL AND APPLIED SCIENCES
OF
MIDDLE EAST TECHNICAL UNIVERSITY

BY

HAKAN DEMİR

IN PARTIAL FULFILLMENT OF THE REQUIREMENTS
FOR
THE DEGREE OF MASTER OF SCIENCE
IN
CHEMICAL ENGINEERING

AUGUST 2011

Approval of the thesis:

**DIMETHYL ETHER (DME) SYNTHESIS USING MESOPOROUS SAPO-34
LIKE CATALYTIC MATERIALS**

submitted by **HAKAN DEMİR** in partial fulfillment of the requirements for the degree of Master of Science in **Chemical Engineering Department, Middle East Technical University** by,

Prof. Dr. Canan ÖZGEN
Dean, Graduate School of **Natural and Applied Sciences**

Prof. Dr. Deniz ÜNER
Head of Department, **Chemical Engineering**

Assoc. Prof. Dr. Naime Aslı SEZGİ
Supervisor, **Chemical Engineering Dept., METU**

Prof. Dr. Timur DOĞU
Co-supervisor, **Chemical Engineering Dept., METU**

Examining Committee Members:

Prof. Dr. Suna BALCI
Chemical Engineering Dept., Gazi University

Assoc. Prof. Dr. Naime Aslı SEZGİ
Chemical Engineering Dept., METU

Prof. Dr. Timur DOĞU
Chemical Engineering Dept., METU

Prof. Dr. Göknur BAYRAM
Chemical Engineering Dept., METU

Assoc.Prof.Dr. Nuray OKTAR
Chemical Engineering Dept., Gazi University

Date: 08.08.2011

I hereby declare that all information in this document has been obtained and presented in accordance with academic rules and ethical conduct. I also declare that, as required by these rules and conduct, I have fully cited and referenced all material and results that are not original to this work.

Name, Last name: Hakan DEMİR

Signature :

ABSTRACT

DIMETHYL ETHER (DME) SYNTHESIS USING MESOPOROUS SAPO-34 LIKE CATALYTIC MATERIALS

Demir, Hakan

M.Sc., Department of Chemical Engineering

Supervisor: Assoc.Prof.Dr. Naime Aslı Sezgi

Co-supervisor: Prof.Dr. Timur Doğu

August 2011, 123 pages

In 21st century, researchers make great effort of finding a clean transportation fuel to diminish the severe effects of conventional transportation fuel combustion such as global warming and air pollution. Dimethyl ether is considered as a strong fuel alternative due to its good burning characteristics and environmentally friendly properties. In order to produce dimethyl ether, different synthesis routes and solid acid catalysts are being utilized. SAPO-34 is an aluminophosphate based catalyst having moderate acidity. This property makes it a good candidate for the synthesis of dimethyl ether. However, SAPO-34 has microporous structure causing diffusion limitations.

The objective of this study is to synthesize, characterize mesoporous SAPO-34 like catalytic materials and test the activity of them in methanol dehydration reaction.

The benefit of obtaining mesoporous structure is that the diffusion limitations can be eliminated.

Mesoporous SAPO-34 like catalysts were synthesized through hydrothermal synthesis route. BET surface areas of these catalysts were 117-133 m²/g. All methanol dehydration reactions were carried out at a space time of 0.14 s.g/cm³. By using mesoporous SAPO-34 like catalysts, the highest methanol conversion was 48% obtained at 550°C with DME selectivity and yield values of 1 and 0.49, respectively. Since utilizing microporous SAPO-34 catalyst gave higher methanol conversion, 67%, at lower temperature, 250°C, with dimethyl ether selectivity of around 1, mesoporous SAPO-34 like catalysts are not suitable for this reaction.

Keywords: Dimethyl ether, methanol dehydration, SAPO-34, mesoporous catalyst

ÖZ

MEZOGÖZENEKLİ SAPO-34 BENZERİ KATALİTİK MALZEMELER KULLANARAK DİMETİL ETER (DME) SENTEZİ

Demir, Hakan

Yüksek Lisans, Kimya Mühendisliği

Tez Yöneticisi: Doç. Dr. Naime Aslı Sezgi

Ortak Tez Yöneticisi: Prof.Dr. Timur Doğu

Ağustos 2011, 123 sayfa

21.yüzyılda, arařtırmacılar, geleneksel ulaşım yakıtının yanmasıyla oluşan ciddi etkilerin, örneğın küresel ısınma ve hava kirliliğı, azaltılması amacıyla temiz bir ulaşım yakıtı bulmak için büyük bir çaba göstermektedirler. Dimetil eter sahip olduğı iyi yanma karakteristiğı ve çevre dostu özellikleri sebebiyle güçlü bir yakıt alternatifi olarak değerlendirilmektedir. Dimetil eter üretmek için farklı sentez yolları ve katı asit katalizörleri kullanılmaktadır. SAPO-34 orta derecede asidikliğıe sahip alümino fosfat bazlı bir katalizördür. Bu özellik, SAPO-34'ü dimetil eter üretimi için iyi bir aday yapmaktadır. Fakat, SAPO-34 difüzyon kısıtlamasına sebep olan mikrogözenekli yapıya sahiptir.

Bu çalışmanın amacı mezogözenekli SAPO-34 benzeri katalitik malzemeler sentezlemek, karakterize etmek ve onların etkinliğini metanol dehidrasyon tepkimesinde

test etmektir. Mezogözenekli yapı elde etmenin faydası difüzyon kısıtlamalarını ortadan kaldırmaktır.

Mezogözenekli SAPO-34 benzeri katalizörler hidrotermal sentez yoluyla sentezlenmiştir. Bu katalizörlerin BET yüzey alanları 117-133 m²/g'dır. Bütün metanol dehidrasyon tepkimeleri 0.14 s.g./ cm³ alıkonma süresinde gerçekleştirilmiştir. Mezogözenekli SAPO-34 benzeri katalizörler kullanarak 550°C'de en yüksek metanol dönüşümü %48 olarak elde edilip dimetil eter seçiciliği ve dimetil eter verimi sırasıyla 1 ve 0.49 olmuştur. Mikrogözenekli SAPO-34 katalizörü kullanıldığında daha düşük sıcaklıkta, 250°C, daha yüksek metanol dönüşümü, 67%, elde edilmesi ve dimetil eter seçiciliğinin 1 civarında olması, mezogözenekli SAPO-34 benzeri katalizörlerin bu tepkime için uygun olmadığını göstermiştir.

Anahtar sözcükler: Dimetil eter, metanol dehidrasyonu, SAPO-34, mezogözenekli katalizör

To my family

ACKNOWLEDGEMENTS

Firstly, I would like to thank to my thesis supervisor Assoc.Prof.Dr. Naime Aslı Sezgi. She has always intimately helped me to deepen my knowledge about every theoretical and experimental issue that I have dealt with during my master's thesis studies. Her encouragement and support have enabled me to sustain my motivation throughout my thesis studies.

Besides, I would like to express my gratitude to my thesis co-supervisor Prof.Dr. Timur Dođu for his guidance, inspiration and sharing his vision and immense knowledge not only about catalysis and chemical reaction engineering but also about universities and academic career in the USA. I sincerely thank to both of my thesis supervisors for giving me the opportunity to become a group member of kinetic laboratory research group and develop this thesis work. I am greatly honored to have such wonderful supervisors.

I deeply thank to faculty members of METU Chemical Engineering Department for their invaluable comments on this study. I would like to show my appreciation to staff of METU Central Laboratory for the analyses of XRD, N₂ physisorption, ²⁷Al and ²⁹Si NMR, SEM-EDS. I would like to offer my sincere thanks to Prof.Dr. Suna Balcı and Assoc.Prof.Dr. Meltem Dođan at Gazi University for their valuable contributions about characterization analyses. Thanks are due to Mihrican Açıkgöz from METU Chemical Engineering Department for thermal analysis. I thank to Necmi Avcı from METU Metallurgical and Materials Engineering Department for XRD analyses. Thanks are due to Aylin Önder for her assistance about XRD analysis and staff of workshop in METU Chemical Engineering Department for technical and equipment assistance.

I thank to Seval Gündüz, Gökhan Çelik, Caner Hoccođlu, Canan Şener, Dr. Zeynep Obalı, Kenan Cem Tokay, Sultan Orman, Ayça Arınan, Buğçe Aydemir, Birce

Pekmezci, Özge Aktaş Panta, Arzu Solmaz, İlhan Ayas and Filiz Aktı for their invaluable friendship and support. I will always remember the moments we have shared. Thanks are due to Assist.Prof.Dr. Dilek Varışlı for her help about the experimental setup used for activity test.

TÜBİTAK support through BİDEB scholarship programme is gratefully acknowledged.

TABLE OF CONTENTS

ABSTRACT	iv
ÖZ	vi
ACKNOWLEDGEMENTS	ix
TABLE OF CONTENTS.....	xi
LIST OF TABLES	xiv
LIST OF FIGURES	xvii
NOMENCLATURE	xxii
CHAPTERS	
1. INTRODUCTION	1
2. DIMETHYL ETHER (DME) : A DIESEL FUEL ALTERNATIVE.....	3
3. DME SYNTHESIS VIA METHANOL DEHYDRATION REACTION	11
4. SILICOALUMINOPHOSPHATES (SAPO).....	15
5. EXPERIMENTAL STUDIES	22
5.1.SYNTHESIS OF MICROPOROUS SAPO-34 CATALYST USING TETRAETHYLAMMONIUM HYDROXIDE(TEAOH) AS SURFACTANT	22
5.2. SYNTHESIS OF MESOPOROUS SAPO-34 LIKE CATALYSTS USING CETYLTRIMETHYLAMMONIUM BROMIDE (CTMABr) AS SURFACTANT	26
5.3. CATALYST CHARACTERIZATION	29
5.3.1. X-Ray Diffraction (XRD)	30
5.3.2. N ₂ Physisorption.....	31

5.3.3. Scanning Electron Microscopy (SEM) and Energy Dispersive X-Ray Spectroscopy (EDS)	31
5.3.4. Thermal Analyses (TGA + DTA)	32
5.3.5. Nuclear Magnetic Resonance (NMR)	32
5.4. EXPERIMENTAL SETUP	33
6. RESULTS AND DISCUSSION	36
6.1. CHARACTERIZATION OF MICROPOROUS SAPO-34 CATALYST	36
6.1.1. X-Ray Diffraction (XRD)	36
6.1.2. Scanning Electron Microscopy (SEM)	42
6.1.3. Energy Dispersive X-Ray Spectroscopy (EDS).....	45
6.1.4. N ₂ Physisorption	46
6.1.5. TGA and DTA	49
6.1.6. Nuclear Magnetic Resonance (NMR).....	50
6.2.CHARACTERIZATION OF MESOPOROUS SAPO-34 LIKE CATALYSTS	52
6.2.1. X-Ray Diffraction (XRD)	52
6.2.2. N ₂ Physisorption	56
6.2.3. Scanning Electron Microscopy (SEM)	64
6.2.4. Energy Dispersive X-Ray Spectroscopy (EDS).....	65
6.2.5. Nuclear Magnetic Resonance (NMR).....	65
6.3.ACTIVITY RESULTS OF SYNTHESIZED CATALYSTS	66
7. CONCLUSIONS AND RECOMMENDATIONS	77
REFERENCES	79
APPENDICES	
A. XRD DATA AND PATTERNS	86

A1. XRD DATA OF SAPO-34	86
A2. XRD PATTERNS OF THE SYNTHESIZED CATALYSTS	88
B. CONVERSION, YIELD AND SELECTIVITY CALCULATIONS ABOUT METHANOL DEHYDRATION REACTION SYSTEM	98
B1. RELATIONS FOR THE CALCULATIONS OF CONVERSION, SELECTIVITY AND YIELD.....	98
B2. CALCULATION OF METHANOL FLOW RATE	99
B3. CALCULATION OF HELIUM FLOW RATE	99
B4. CALCULATION OF TOTAL FLOW RATE	100
B5. GC CALIBRATION FACTORS AND RETENTION TIMES OF COMPONENTS	100
C. EDS RESULTS OF THE SYNTHESIZED CATALYSTS	101
D. SEM IMAGES OF SYNTHESIZED CATALYSTS	104
E. CONVERSION, SELECTIVITY AND YIELD VALUES	109
F. REACTION RAW DATA.....	116
G. EQUILIBRIUM CONVERSION FOR METHANOL DEHYDRATION REACTION	123

LIST OF TABLES

TABLES

Table 1. DME Properties [7]	5
Table 2. Physical properties comparison for several fuels [1, 5, 9]	6
Table 3. Reactions leading to synthesis of dimethyl ether [5, 12]	10
Table 4. Structural properties of aluminophosphate based structures[23]	16
Table 5. AlPO ₄ based molecular sieves [24].....	17
Table 6. Parameters used for the synthesis of microporous SAPO-34 samples.....	25
Table 7. Synthesis parameters for the mesoporous SAPO-34 like catalysts.....	29
Table 8. Temperature ranges investigated for the catalysts synthesized.....	35
Table 9. Optimum synthesis parameters for microporous SAPO-34.....	41
Table 10. EDS results for SAPO-34 #14.....	45
Table 11. EDS results for SAPO-34 #19.....	46
Table 12. Physical properties of SAPO-34 #19	47
Table 13. Nitrogen adsorption desorption analysis results for SAPO-34 #21, SAPO-34 #26 and SAPO-34 #28.....	57

Table 14. EDS results for SAPO-34 #21 and SAPO-34 #26	65
Table 15. Generalized X-ray powder diffraction data of SAPO-34 [33]	86
Table 16. XRD data of SiO ₂ [55]	93
Table 17. XRD data of AlPO ₄ [55]	94
Table 18. XRD data of α-Al ₂ O ₃ [55].....	95
Table 19. XRD data of Al(PO ₃) ₃ [55]	96
Table 20. XRD data of C [55]	97
Table 21. Calibration factors and retention times for the species obtained	100
Table 22. EDS analysis results of several catalysts	101
Table 23. Atomic percentages of Al, Si and P in several catalysts obtained by EDS	102
Table 24. Atomic percentages of Al, Si and P in several catalysts obtained by EDS	102
Table 25. Conversion, selectivity and yield obtained by SAPO-34 #19	109
Table 26. Conversion, selectivity and yield obtained by SAPO-34 #19 (repeated)	110
Table 27. Conversion, selectivity and yield obtained by SAPO-34 #19 (regenerated)	111
Table 28. Conversion, selectivity and yield obtained by SAPO-34 #20	112
Table 29. Conversion, selectivity and yield obtained by SAPO-34 #21	112

Table 30. Conversion, selectivity and yield obtained by using SAPO-34 #22	113
Table 31. Conversion, selectivity and yield obtained by using SAPO-34 #24	113
Table 32. Conversion, selectivity and yield obtained by using SAPO-34 #25	114
Table 33. Conversion, selectivity and yield obtained by using SAPO-34 #26	114
Table 34. Conversion, selectivity and yield obtained by using SAPO-34 #27	115
Table 35. Conversion, selectivity and yield obtained by using SAPO-34 #28	115
Table 36. Experimental data for SAPO-34 #19	116
Table 37. Experimental data for SAPO-34 #19 (repeated)	117
Table 38. Experimental data for SAPO-34 #19 (regenerated)	118
Table 39. Experimental data for SAPO-34 #20	119
Table 40. Experimental data for SAPO-34 #21	119
Table 41. Experimental data for SAPO-34 #22	120
Table 42. Experimental data for SAPO-34 #24	120
Table 43. Experimental data for SAPO-34 #25	121
Table 44. Experimental data for SAPO-34 #26	121
Table 45. Experimental data for SAPO-34 #27	122
Table 46. Experimental data for SAPO-34 #28	122

LIST OF FIGURES

FIGURES

Figure 1. Dimethyl ether structure [8].....	4
Figure 2. Representation of indirect route (on the left) and direct route (on the right)	9
Figure 3. Chabazite structure [26].....	18
Figure 4. XRD pattern of SAPO-34 [32]	21
Figure 5. Microporous SAPO-34 synthesis steps	26
Figure 6. Representation of synthesis steps of mesoporous SAPO-34 like catalyst	28
Figure 7. Bragg diffraction [37].....	30
Figure 8. Schematic of the reaction system utilized to produce dimethyl ether	34
Figure 9. Comparison of XRD patterns of microporous SAPO-34 catalysts for the determination of mixing temperature effect (Hydrothermal synthesis time: 2 days, hydrothermal synthesis temperature: 200°C, addition rate of	

phosphoric acid: slow)	37
Figure 10. Comparison of XRD patterns of SAPO-34 catalysts for the determination of hydrothermal synthesis time effect (Mixing temperature: 40°C, hydrothermal synthesis temperature: 200°C, addition rate of phosphoric acid: slow).....	38
Figure 11. XRD pattern of SAPO-34 #14.....	39
Figure 12. XRD pattern of SAPO-34 #19.....	40
Figure 13. Comparison of XRD patterns of SAPO-34 #19 and SAPO-34 #195	41
Figure 14. SEM images of SAPO-34 #14.....	43
Figure 15. SEM images of SAPO-34 #19.....	44
Figure 16. Nitrogen adsorption desorption isotherms of SAPO-34 #19.....	47
Figure 17. BJH adsorption pore size distribution of SAPO-34 #19.....	48
Figure 18. BJH desorption pore size distribution of SAPO-34 #19.....	49
Figure 19. Thermal analysis of uncalcined SAPO – 34 # 19.....	50
Figure 20. ²⁷ Al NMR of SAPO-34 #19.....	51
Figure 21. ²⁹ Si NMR of SAPO-34 #19	52
Figure 22. XRD pattern of SAPO-34 #26 (Mixing temperature: 40°C, initial pH: 6.70, hydrothermal synthesis temperature: 70°C).....	54
Figure 23. XRD pattern of SAPO-34 #21(Mixing temperature: 30°C, initial pH: 2.33, hydrothermal synthesis temperature: 70°C).....	54

Figure 24. XRD pattern of SAPO-34 #20 (Mixing temperature: 30°C, initial pH: 2.28, hydrothermal synthesis temperature: 200°C).....	55
Figure 25. XRD pattern comparison of SAPO-34 #19 and SAPO-34 #24.....	56
Figure 26. Nitrogen adsorption-desorption isotherms for SAPO-34 #21	58
Figure 27. Nitrogen adsorption-desorption isotherms for SAPO-34 #26	58
Figure 28. Nitrogen adsorption-desorption isotherms for SAPO-34 #28	59
Figure 29. Pore size distribution of SAPO-34 #21 based on BJH adsorption	60
Figure 30. Pore size distribution of SAPO-34 #21 based on BJH desorption	60
Figure 31. Pore size distribution of SAPO-34 #26 based on BJH adsorption	61
Figure 32. Pore size distribution of SAPO-34 #26 based on BJH desorption	62
Figure 33. Pore size distribution of SAPO-34 #28 based on BJH adsorption	63
Figure 34. Pore size distribution of SAPO-34 #28 based on BJH desorption	63
Figure 35. SEM images of (a) SAPO-34 #21, (b) SAPO-34 #26, (c) SAPO-34 #20 catalysts.....	64
Figure 36. ²⁷ Al NMR analysis result for SAPO-34 #28	66
Figure 37. Methanol conversion on SAPO-34 #19 at 0.14 s.g/cm ³	67
Figure 38. Selectivity values obtained by using SAPO-34 #19 at 0.14 s.g/cm ³	68
Figure 39. Yield values attained using SAPO-34 #19 catalyst at 0.14 s.g/cm ³	69
Figure 40. TGA analysis of spent SAPO-34 #19 catalyst.....	70
Figure 41. XRD pattern of spent SAPO-34 #19 catalyst	70

Figure 42. Activity test results of fresh and regenerated SAPO-34 #19 catalysts at 0.14 s.g/cm ³	71
Figure 43. Activity results of SAPO-34 #21, SAPO-34 #26, SAPO-34 #27 and SAPO-34 #28 catalysts at 0.14 s.g/cm ³	72
Figure 44. Activity results of SAPO-34 #20, SAPO-34 #22, SAPO-34 #24 and SAPO-34 #25 catalysts at 0.14 s.g/cm ³	73
Figure 45. Selectivities obtained by using SAPO-34 #28 at 0.14 s.g/cm ³	74
Figure 46. Yields obtained by using SAPO-34 #28 at 0.14 s.g/cm ³	74
Figure 47. Selectivities obtained by using SAPO-34 #21 at 0.14 s.g/cm ³	75
Figure 48. Yields obtained by using SAPO-34 #21 at 0.14 s.g/cm ³	75
Figure 49. XRD pattern of SAPO-34 #22 (Mixing temperature: 40°C, initial pH: 2.14, hydrothermal synthesis temperature: 200°C).....	88
Figure 50. XRD pattern of SAPO-34 #24 (Mixing temperature: 40°C, initial pH: 6.70, hydrothermal synthesis temperature: 200°C).....	88
Figure 51. XRD pattern of SAPO-34 #25 (Mixing temperature: 30°C, initial pH: 6.71, hydrothermal synthesis temperature: 200°C).....	89
Figure 52. XRD pattern of SAPO-34 #27 (Mixing temperature: 30°C, initial pH: 6.71, hydrothermal synthesis temperature: 70°C).....	89
Figure 53. XRD pattern of SAPO-34 #28 (Mixing temperature: 40°C, initial pH: 2.13, hydrothermal synthesis temperature: 70°C).....	90

Figure 54. Low angle XRD pattern of SAPO-34 #20 (Mixing temperature: 30°C, initial pH: 2.28, hydrothermal synthesis temperature: 200°C)	90
Figure 55. Low angle XRD pattern of SAPO-34 #26 (Mixing temperature: 40°C, initial pH: 6.70, hydrothermal synthesis temperature: 70°C)	91
Figure 56. Low angle XRD pattern of SAPO-34 #27 (Mixing temperature: 30°C, initial pH: 6.71, hydrothermal synthesis temperature: 70°C)	91
Figure 57. Low angle XRD pattern of SAPO-34 #28 (Mixing temperature: 40°C, initial pH: 2.13, hydrothermal synthesis temperature: 70°C)	92
Figure 58. EDS spectrum and data of SAPO-34 #28	103
Figure 59. SEM images of SAPO-34 #20	104
Figure 60. SEM images of SAPO-34 #21	105
Figure 61. SEM images of SAPO-34 #22	105
Figure 62. SEM images of SAPO-34 #24	106
Figure 63. SEM images of SAPO-34 #25	106
Figure 64. SEM images of SAPO-34 #26	107
Figure 65. SEM images of SAPO-34 #27	107
Figure 66. SEM images of SAPO-34 #28	108
Figure 67. Effect of temperature on equilibrium conversion for methanol dehydration reaction [5]	123

NOMENCLATURE

A_i : Area obtained from gas chromatography analysis for species i

AlPO, AlPO₄: Aluminophosphate

CTMABr: Cetyltrimethylammonium bromide

d : Spacing between the planes in the atomic lattice

DME: Dimethyl Ether

DTA: Differential Thermal Analysis

EDS: Energy Dispersive X-Ray Spectroscopy

F : Volumetric flow rate (mL/min)

FA: Formaldehyde

GC: Gas chromatograph

H : Enthalpy (kJ/mol)

I : Intensity

IUPAC: International Union of Pure and Applied Chemistry

LHV: Lower heating value

LPG: Liquefied petroleum gas

M : Molecular weight (g/mol)

MeOH: Methanol

n : Order of reflection

n_{Total} : Total moles of carbon

NMR: Nuclear Magnetic Resonance

P: Pressure (bar)

P123: Pluronic 123

R: Gas constant ($83.14 \text{ cm}^3 \cdot \text{bar/mol/K}$)

S: Selectivity

SAPO: Silicoaluminophosphate

SBA: Santa Barbara Amorphous type material

SEM: Scanning Electron Microscopy

T: Temperature ($^{\circ}\text{C}$)

TCD: Thermal conductivity detector

TEAOH: Tetraethylammonium hydroxide

TGA: Thermogravimetric Analysis

WHSV: Weight hourly space velocity

X: Conversion

XRD: X- Ray Diffraction

Y: Yield

ρ : Density (g/cm^3)

ΔH_r° : Standard enthalpy of reaction

β : Calibration factor

θ : Angle between the incident ray and the scattering planes

λ : Wavelength of incident wave

CHAPTER 1

INTRODUCTION

In this century, excessive usage of oil reserves leads to several serious problems threatening human lifestyle such as global warming, air pollution and shortage of fuel and petrochemical feedstock. Since the major usage area of petroleum is transportation, finding a clean transportation fuel as a substitute for petroleum derived fuels is very essential in today's world to lessen the effects of fossil fuel combustion [1]. Dimethyl ether (DME) is considered as a strong candidate for the substitution of petroleum derived fuel due to its environmentally benign characteristics. It is possible to produce this "green" fuel via methanol dehydration reaction by using catalysts with acidic property.

Silicoaluminophosphate-34 (SAPO-34) is an acidic catalyst having microporous structure utilized for many reactions such as chloromethane transformation to light olefins, oxidative dehydrogenation of ethane etc. [2, 3]. It can also be utilized for methanol dehydration reaction producing dimethyl ether since it has moderate acidity. However, due to its small pore sizes, diffusion limitation comes into play. This limitation can be eliminated by having a catalyst with larger pore sizes. At this point, it should be noted that expanding the pores is not sufficient since acidity also plays an important role in methanol dehydration reaction. Therefore, having a mesoporous catalyst with medium acidity should be the aim for high rates of dimethyl ether production.

In this study, both microporous and mesoporous SAPO-34 like catalysts were synthesized, characterized and their catalytic performances were tested in methanol dehydration reaction in order to produce dimethyl ether.

In Chapters 2, 3 and 4 give detailed information about dimethyl ether, methanol dehydration reaction and SAPO structure are given. In Chapter 2, properties that make dimethyl ether a strong fuel alternative are described together with the production routes of it. Some comparisons are made between dimethyl ether and conventional transportation fuels. In Chapter 3, the studies about the methanol dehydration reaction are explained. The catalysts and the experimental systems utilized for dimethyl ether synthesis are indicated along with the operation conditions. In Chapter 4, silicoaluminophosphate structure is described and types of SAPO are explained. Specifically, chabazite, the structural analog of SAPO-34, is illustrated.

Chapter 5 provides detailed information about the synthesis procedures of both microporous and mesoporous SAPO-34 like catalysts. Several characterization techniques applied to reveal the properties of the synthesized catalysts are briefly mentioned. In this chapter, lastly, the experimental setup established for methanol dehydration reaction is described.

Chapter 6 presents the characterization results of the synthesized catalysts together with the activity test results. Comparisons between catalysts are made based on their structural characteristics and reaction performances. The effect of temperature on methanol conversion, dimethyl ether selectivity and yield values are discussed.

Last but not the least, conclusions and recommendations are presented in Chapter 7.

CHAPTER 2

DIMETHYL ETHER (DME): A DIESEL FUEL ALTERNATIVE

Basically, diesel fuel and gasoline are two traditional transportation fuels that are utilized widespread in the today's world. Similar to gasoline, diesel fuel consists of many hydrocarbons with a wide boiling point range. However, both the physical and chemical properties of diesel fuel are quite different than those of gasoline. Principally, diesel fuel is comprised of straight-chain alkanes having ten to twenty carbon atoms. On the other hand, gasoline possesses both aromatic compounds and branched alkanes with 3-10 carbon atoms [4]. Diesel fuel is heavier and it has lower vapor pressure, higher energy density compared to gasoline [5]. Similar to gasoline engine, a diesel engine is an internal combustion engine utilized for the transformation of fuel's chemical energy into mechanical energy enabling the up and down movement of pistons in cylinders. The pistons have connection with the crankshaft of engine which converts linear motion to rotary motion for the propulsion of vehicle's wheels. In gasoline and diesel engines, energy is obtained by a series of explosions caused by the reaction of fuel with oxygen in the air. The principal difference between these engines is in the way of explosions taking place. In diesel engines, fuel ignites on its own contrary to the case of gasoline engine where the explosions are initiated by sparks from spark plugs [6]. Typically, compression ratio in gasoline engines is 8-9 to 1, whereas in diesel engines this ratio is higher than 17 to 1 [4]. High compression of air makes fuel-burning oxygen concentrated and diesel fuel, having high energy content per volume, is able to react with that concentrated oxygen [6]. Starting from 1970's, diesel engines are preferred to gasoline engines due to better fuel economy. However, both diesel fuel and gasoline

cause detrimental effects on human and ecosystem health. Usage of diesel fuel results in emissions of particulate matter and nitrogen compounds leading to acid rains and deterioration in human health. The emissions owing to the combustion of fossil fuels such as oxides of carbon, sulfur and nitrogen contribute to global warming effect. Thus, an environmentally friendly transportation fuel is needed and dimethyl ether is regarded as a promising fuel alternate due to its superior properties [5].

Dimethyl ether (DME) is the simplest form of diesel ethers, which can be obtained by alcohol dehydration, having the chemical formula CH_3OCH_3 [7]. The figure below shows the chemical structure of dimethyl ether.

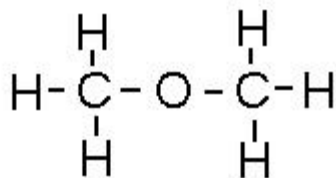


Figure 1. Dimethyl ether structure [8]

DME, whose several properties are listed in Table 1, is gaseous ether under ambient pressure.

Table 1. DME Properties [7]

Formula	C ₂ H ₆ O, CH ₃ OCH ₃
Molar Mass (g/mol)	46.07
Normal Boiling Point (K)	248.25
Specific Density (gas vs. air)	1.59
Cetane Number	55-60
Vapor Pressure at 298 K (kPa)	510
Autoignition Temperature (K)	508

As a diesel fuel alternative, dimethyl ether presents superior properties which were found out in the beginning of 1990's. First of all, DME possesses higher cetane number (55-60) compared to that of conventional diesel fuel (40-55) indicating higher auto-ignition property which is the key parameter for a diesel fuel. Besides, dimethyl ether is a non-toxic, non-carcinogenic, non-corrosive and environmentally benign chemical. Gaseous DME is almost odorless in low concentrations and it does not have detrimental effects on human health. Its usage in compression ignition engines causes low NO_x and CO₂ emissions along with no particulate matter, SO_x or smoke emissions [1, 7]. As shown in Table 2, dimethyl ether possesses higher cetane number compared to other several fuels.

Table 2. Physical properties comparison for several fuels [1, 5, 9]

	DME	Diesel	Gasoline	Methane	Methanol	Ethanol
Formula	CH ₃ OCH ₃	C ₁₄ H ₃₀	C ₇ H ₁₆	CH ₄	CH ₃ OH	C ₂ H ₅ OH
Molecular weight (g mol ⁻¹)	46.07	198.4	100.2	16.04	32.04	46.07
Density (g cm ⁻³)	0.661 ^b	0.856	0.737	0.00072 ^a	0.792	0.785
Normal boiling point (°C)	-24.9	125-400	38-204	-162	64	78
Cetane number ^d	55-60	40-55		3	5	8
LHV (kJ cm ⁻³)	18.92	35.66	32.05	0.0346 ^a	15.82	21.09
LHV (kJ g ⁻¹)	28.62	41.66	43.47	47.79	19.99	26.87
Autoignition temperature (°C)	235	250		650	450	420
Carbon content (wt%)	52.2	87	85.5	74	37.5	52.2
Sulfur content (ppm ^c)	0	~250	~200	~7-25	0	0

^a Values per cm³ of vapor at STP; ^b Density at P = 1 atm and T = -25 °C; ^c Mass basis; ^d Data taken from [1]

The reason why DME is considered as the fuel of 21st century is that it can be obtained from various sources such as natural gas, coal and biomass other than the conventional crude oil source [7]. However, DME has still few shortcomings as a diesel fuel alternate. Since its energy density is approximately half of the energy density of diesel oil, a storage tank for DME fuel should have twice the size of a conventional diesel fuel storage tank to attain an equivalent driving range [9]. Another disadvantage

of DME is that it has low normal boiling point, but it can readily be liquefied under modest pressure (6 bar) so that it is easy to transport and store dimethyl ether [7, 10]. For dimethyl ether engine operation, new storage and fuel delivery systems are needed but no alteration is required for the engine itself. Since viscosity of DME is less than the viscosity of diesel by a factor of 20, higher amount of leakage may be observed in pumps and fuel injectors [9]. Besides that, dimethyl ether has low lubricity leading to quick wear and failure of pumps and fuel injectors. In order to enhance the lubricity of DME several additives namely Lubrizol and Hitec 560 are utilized. Exposing dimethyl ether to several kinds of rubbers and plastics deteriorates the seals. Therefore, material compatibility is another issue that should be under consideration. Vessels containing dimethyl ether can be sealed by polytetrafluoroethylene (PTFE) and butyl-*n* (Buna-N) rubber. Non-sparking metal-to-metal seal, which has resistance against high temperature, is another option [4].

Traditionally, DME has been utilized as an aerosol propellant and for ultra-pure glass production. Now, other than being used as a fuel, its usage areas are much wider. It can be used for power generation and cooking & heating purposes. General Electric proved that dimethyl ether is an attractive fuel to be used for power generation in gas turbines due to the similar emissions and performances compared to those obtained with natural gas usage. By some modifications especially in the fuel delivery system, existing turbines, where natural gas, liquid naphtha or distillate oil is currently fired, can be made compatible to DME usage. On the other hand, cooking stoves built for natural gas do not require any modifications for DME usage. For cooking and heating purposes, dimethyl ether can be mixed with LPG, in a maximum ratio of 20%, and utilized without any alterations in the equipment or distribution network. As DME usage and blending becomes more popular in the wide LPG market, use of DME will enhance in domestic applications [4, 11].

For the handling and storage of DME, similar methods used for LPG fuels should be followed. Dimethyl ether can utilize the already constructed land and ocean-based LPG infrastructures. In order to transport dimethyl ether through oceans,

conventional LPG tankers can be used. DME can be gathered and stored at receiving stations utilizing the same equipment and methods used for LPG except few alterations in pumps, seals and gaskets. Several changes should also be done for the land-based infrastructure. There are many established refilling stations for LPG and these stations can be used for refilling purposes of dimethyl ether. As dimethyl ether demand rises up, extra refilling stations can be set up but the cost of building up these additional units would be quite lower compared to setting up a completely new infrastructure for storage and distribution. Other than cost of it, establishing a new infrastructure requires time which postpones the transition to the widespread usage of a fuel alternate. It was estimated that the required capital investment including production plants and infrastructure was US \$4 billion for dimethyl ether whereas that investment was US\$ 18 billion for hydrogen, US\$ 4 billion for methanol and US\$ 5 billion for ethanol [9].

Up to 2004, the global dimethyl ether demand was around 150,000 tonnes per year but since then DME synthesis increased substantially. For instance, in 2008, DME production was more than 2 million tonnes per year in China. DME synthesis is still increasing since usage of it becomes more widespread around the world. There are many companies and institutions developing vehicles running on DME. Companies such as Volvo, Isuzu tested DME-powered trucks, buses and concluded that DME was one of the strongest candidates as diesel oil alternate. In China, a DME-powered transit bus was developed with the cooperation of researchers in Jiao Tong University and several companies. The production of 30 transit buses was endorsed by Chinese Ministry of Science [4].

There are two routes for the production of dimethyl ether. One of them is the indirect route in which methanol is firstly synthesized from syngas originated from feedstocks such as natural gas, coal or biomass and then dehydrated to produce DME. Thus, it is a two-step process. The other route for DME production is the direct route in which syngas is converted to dimethyl ether in one step. The schematic of these processes is shown in Figure 2.

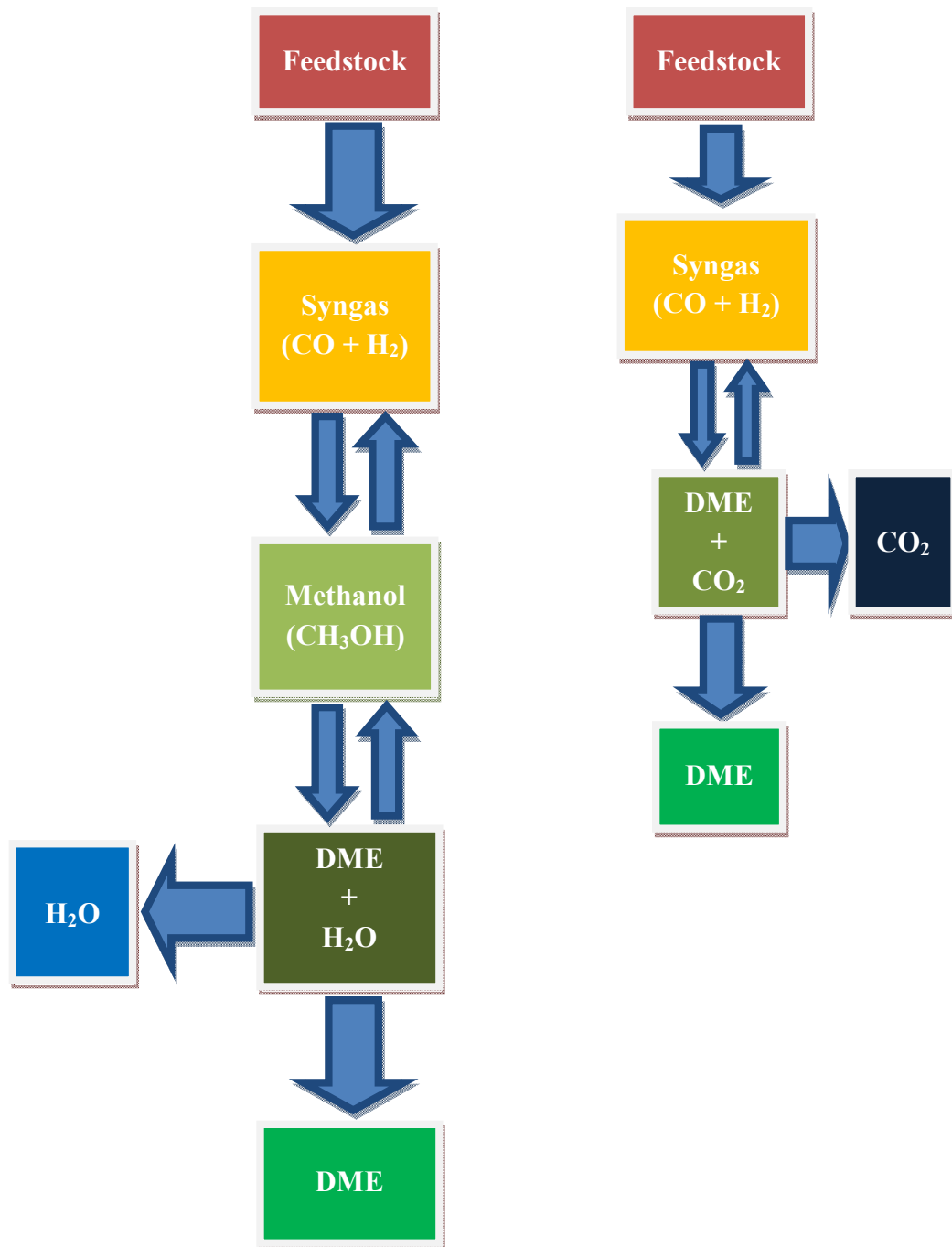


Figure 2. Representation of indirect route (on the left) and direct route (on the right)

Table 3 shows the reactions that are included in dimethyl ether production. As can be seen, there are many options to produce syngas, thus, dimethyl ether.

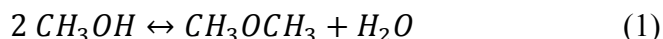
Table 3. Reactions leading to synthesis of dimethyl ether [5, 12]

Reaction Names	Reaction Chemistry	ΔH°_{298K} (kJ/mol)
Partial oxidation reforming	$\text{CH}_4 + \frac{1}{2} \text{O}_2 \longrightarrow \text{CO} + 2\text{H}_2$	-36.0
Steam reforming	$\text{CH}_4 + \text{H}_2\text{O} \longleftrightarrow \text{CO} + 3 \text{H}_2$	206.0
Water gas shift reaction	$\text{CO} + \text{H}_2\text{O} \longleftrightarrow \text{CO}_2 + \text{H}_2$	-40.9
Methanol synthesis	$\text{CO} + 2 \text{H}_2 \longleftrightarrow \text{CH}_3\text{OH}$	-90.7
	$\text{CO}_2 + 3 \text{H}_2 \longleftrightarrow \text{CH}_3\text{OH} + \text{H}_2\text{O}$	-50.1
Methanol dehydration	$2 \text{CH}_3\text{OH} \longleftrightarrow \text{CH}_3\text{OCH}_3 + \text{H}_2\text{O}$	-23.3
DME direct synthesis	$2 \text{CO} + 4 \text{H}_2 \longleftrightarrow \text{CH}_3\text{OCH}_3 + \text{H}_2\text{O}$	-205.0
	$3 \text{CO} + 3 \text{H}_2 \longleftrightarrow \text{CH}_3\text{OCH}_3 + \text{CO}_2$	-246.2
Overall DME synthesis	$2 \text{CH}_4 + \text{O}_2 \longrightarrow \text{CH}_3\text{OCH}_3 + \text{H}_2\text{O}$	

CHAPTER 3

DME SYNTHESIS VIA METHANOL DEHYDRATION REACTION

Dimethyl ether can be obtained from the dehydration of two methanol molecules giving out one molecule of water



The methanol dehydration reaction is exothermic having ΔH_r° (gas phase) = -24 kJ / mol. It is thermodynamically limited at high temperatures. At 200°C, the equilibrium methanol conversion is 92 % when pure methanol is fed to the system [7].

Xu et al. [13] synthesized Pd/Cab-O-Sil catalyst by impregnation method. They tested the activity of that catalyst for methanol dehydration reaction in a plug flow reactor made of fused quartz. At 225°C, they achieved to synthesize dimethyl ether with DME selectivity and methanol conversion of 78% and 38%, respectively. When the temperature was raised to 280°C, conversion of methanol was enhanced to 77% whereas dimethyl ether selectivity diminished to 47%. As partial pressure of methanol was decreased, DME selectivity diminished. It was found that methanol consumption rate and DME formation rate were half-order with respect to partial pressure of methanol.

Seo et al. [14] synthesized zeolite W catalysts via hydrothermal and microwave methods with a synthesis gel having SiO₂ to Al₂O₃ ratio of 6.4. Two of zeolite W catalysts were synthesized by adding ethylene glycol to the solution gel in order to have a much more uniform morphology. The catalysts synthesized by these two methods were tested in methanol dehydration reaction to produce dimethyl ether. The reaction was

carried out in a fixed bed reactor. Maximum methanol conversion value was obtained as 43% at 325°C with the catalyst synthesized through conventional hydrothermal method. However, at 250°C using that catalyst gave only 3% methanol conversion. The performance of zeolite W catalyst synthesized by microwave method was worse in methanol dehydration reaction. At 250°C no methanol conversion was obtained and after increasing the temperature to 325°C, the methanol conversion could reach to 28%. All the catalysts yielded 100% dimethyl ether selectivity due to their mild acidity.

Dai et al. [15] worked on the synthesis of AlPO-5, AlPO-11, AlPO-41, SAPO-5, SAPO-11, and SAPO-41 and tested their performances on methanol dehydration reaction in the temperature range of 250-400°C. The methanol dehydration reaction was carried out in a fixed-bed flow microreactor under atmospheric pressure. SAPO-11, having weak acid sites together with moderate acid sites in low concentration, showed high activity for DME synthesis through methanol dehydration at 250 °C. As temperature was increased to 300-400°C, moderate acid sites in silico-aluminophosphates caused side reaction to proceed and yield of dimethyl ether decreased. By using SAPO-11 at 250°C, methanol conversion over 85% with dimethyl ether selectivity higher than 99.9 could be attained for 200 hours. It was observed that by using AlPO-5, AlPO-11 and AlPO-41 catalysts, DME became the primary product in the temperature range of 250-400°C. The maximum dimethyl ether yield values, which were slightly higher than 80%, were obtained at 350°C for AlPO-5, AlPO-11 and AlPO-41. It was found that those three catalysts possess good durability for methanol dehydration at 350 °C.

In the work of Liu et al. [16], several samples of γ -Al₂O₃ were synthesized by precipitation and impregnation methods. By impregnating Nb₂O₅ and Nb₂O₅-(NH₄)₂SO₄ on alumina catalysts, modifications were done. Methanol dehydration reaction was performed at 0.1 MPa in a quartz tubular reactor having 700 mm length and 12 mm internal diameter. The temperature range investigated was 240-340°C. By the help of Nb₂O₅ modification, number of acid sites and methanol conversion were increased whereas strength of acid sites was lowered. Alumina catalysts which underwent Nb₂O₅

and $\text{Nb}_2\text{O}_5-(\text{NH}_4)_2\text{SO}_4$ modifications exhibited higher performance compared to the unmodified alumina catalyst at lower temperature. Alumina catalyst with 10 wt. % of Nb_2O_5 showed highest activity at low temperatures.

Raouf et al. [17] studied the methanol dehydration reaction on an adiabatic fixed bed reactor. They used γ -alumina, having 1-2 mm particle size, in the reactor in the operating temperature range of 233-303°C. They found out that below 230°C methanol conversion was insignificant but as the temperature was raised to 250°C, methanol conversion reached to 85%. For 30 hours of experimentation, the activity of the catalyst was almost unchanged. They fed water and methanol mixture to the reactor in order to see its effect on deactivation of catalyst. Combining water with methanol in the feed stream caused faster deactivation of γ -alumina compared to the deactivation observed while using pure methanol as feed. In order to have a relation between the pure methanol conversion to the reactor operating temperature, a mathematical model was developed which was consistent with the experimental data.

Keshavarz et al. [18] synthesized nanocrystalline γ -alumina catalysts by thermal decomposition, precipitation and sol-gel method in which sucrose and hexadecyltrimethyl ammonium bromide were utilized as surfactant. These catalysts were tested on methanol dehydration reaction. The reaction was carried out at 300°C at atmospheric pressure. It was found that the catalyst synthesized via thermal decomposition method exhibited the lowest methanol conversion at WHSV of 1.75 h^{-1} and 11.66 h^{-1} . Samples synthesized by precipitation and sol-gel methods showed similar activity at WHSV of 1.75 h^{-1} but when WHSV was set as 11.66 h^{-1} , the catalyst synthesized by sol-gel method using hexadecyltrimethyl ammonium bromide gave the highest activity. They discovered that surfactant addition lowered the crystallite size and increased surface area. It was concluded that smaller crystallite size had more preferable acid sites for methanol dehydration reaction since their accessibility was enhanced.

In the study of Ciftci et al. [19], Nafion-silica nanocomposites with mesoporous structure were hydrothermally synthesized. In order to remove the surfactant, as-

synthesized catalysts were either washed with sulfuric acid and ethanol (SAE) solution or calcined. Nafion/silica ratio was varied for the syntheses and the optimum ratio was found as 0.15. Increasing this ratio further causes decrease in Bronsted acidity. It was found out that the catalysts possess well-dispersed structures together with high surface areas (595-792 m²/g). The synthesized acidic catalysts were tested between 120-300°C in methanol dehydration reaction to synthesize dimethyl ether. As the Bronsted acidity of the catalysts increased, dimethyl ether selectivity was enhanced. Methanol conversion increased as the temperature was increased in 120-300°C. The catalyst having the highest Bronsted acidity with a surface area of 595 m²/g exhibited 40% methanol conversion at 300°C when space time was 0.27 s.g/cm³. This catalyst was found to be stable for 6 hours.

Varisli et al. [20] studied the activities of pure silicotungstic acid (STA), mesoporous aluminosilicate catalysts and STA impregnated aluminosilicate catalysts in methanol dehydration reaction to synthesize dimethyl ether. Mesoporous aluminosilicate catalysts, involving Al/Si atomic ratios of 0.09 and 0.18, were synthesized via hydrothermal synthesis route. A commercial mesoporous aluminosilicate catalyst with Al/Si ratio of 0.03 was also tested in the methanol dehydration reaction. Besides, this aluminosilicate material was utilized as a supporting material and STA was impregnated to it. Because of the surface area and acid strength effects, it was found that there existed an optimum Al/Si ratio of 0.09 to have highest methanol conversion and dimethyl ether yield. STA impregnated aluminosilicate catalyst gave higher methanol conversion compared to pure STA and aluminosilicates even at low temperatures such as 250°C. STA loaded aluminosilicates together with pure aluminosilicate catalysts exhibited high dimethyl ether selectivity.

CHAPTER 4

SILICOALUMINOPHOSPHATES (SAPO)

SAPO's are aluminophosphate (AlPO_4) based materials which were discovered in the 1980's. SAPO can be generated by incorporating silicon into AlPO_4 framework. SAPO molecular sieves consist of tetrahedral oxide frameworks involving silicon, phosphorus and aluminium. The incorporation of silicon into the structure can be possible theoretically in three ways. In the first route, silicon substitutes for aluminium whereas in the second route phosphorus is substituted by silicon. The third route is the substitution of two silicon atoms for one aluminum atom and one phosphorus atom. It has been shown that silicon does not incorporate into the structure through the first route. Thus, Si-O-P linkage does not exist in SAPO structure. In silicoaluminophosphate structure, coordination environment of silicon is quite important in terms of acidity. The acidic property of SAPO is due to the surface hydroxyl group formed by protons balancing the net negative framework charge. This negative framework charge is caused by silicon incorporation into the neutral AlPO_4 framework. Acidity of SAPO structure increases in the order of $\text{Si (0Al)} < \text{Si (4Al)} < \text{Si (3Al)} < \text{Si (2Al)} < \text{Si (1Al)}$. Brønsted acid sites can be shown as Si-O(H)-Al . Besides acidic property, silicoaluminophosphate has high thermal stability like aluminophosphates [21, 22].

AlPO_4 based materials have many structure types. These structure types are indicated by a number such as AlPO_4 -34 where 34 designates the structure of chabazite. Same number is given to the materials having the same structure types even their compositions differ. For instance, AlPO_4 -34 and SAPO-34 possess the same structure, chabazite. Table 4 shows the pore sizes of aluminophosphate based structures [23].

Table 4. Structural properties of aluminophosphate based structures[23]

Pore size	Number of tetrahedral atoms in largest ring	Structure type
Very large	18	VPI-5
Large	12	5, 36, 37, 40, 46, 50
Medium	10	11, 31, 41
Small	8	14, 17, 18, 22, 26, 33, 34, 35, 39, 42, 43, 44, 47, 52
Very small	6	16, 20

Anhydrous composition of SAPO can be represented as $0-0.3 R(\text{Si}_x\text{Al}_y\text{P}_z) \text{O}_2$, in which R, x, y and z designate template, the mole fraction of silicon, aluminium and phosphorus elements, respectively. Many aluminophosphate based molecular sieves have analogous structures to zeolites. Table 5 lists several structure types with their physical properties [24]. As can be seen, some species have structure analogous to zeolites whereas some have new structure types. This table reveals that, for instance, SAPO-20 has different structure than SAPO-34 with different pore size and pore volume.

Table 5. AlPO₄ based molecular sieves [24]

Structure number	Structure type	Pore size, nm	Saturation H ₂ O pore volume, cm ³ /g
8	Novel	0.9	0.24
5	Novel	0.8	0.31
41	Novel	0.6	0.22
34	Chabazite	0.43	0.3
20	Sodalite	0.3	0.24

In this study, SAPO-34 is the material focused on to synthesize dimethyl ether. It can be synthesized by using various templates namely tetraethylammonium hydroxide, morpholine, dipropylamine, piperidine and triethylamine [25]. As Table 5 implies SAPO-34 has a structure analogous to natural zeolite chabazite with a pore size of 0.43 nm. Then, it is useful to understand the chabazite structure. The idealized form of chabazite structure is $\text{Ca}_2(\text{Al}_4\text{Si}_8)\text{O}_{24}\cdot 12\text{H}_2\text{O}$. The chabazite structure is composed of double 6-rings (4^66^2) and one cavity per unit cell of the form $[4^{12}6^28^6]$. This cavity shares 8-ring windows by which it is connected to 6 other cavities [26]. Figure 3 depicts the chabazite structure. Dots correspond to Si, Al or P which are connected to each other by oxygen atoms.

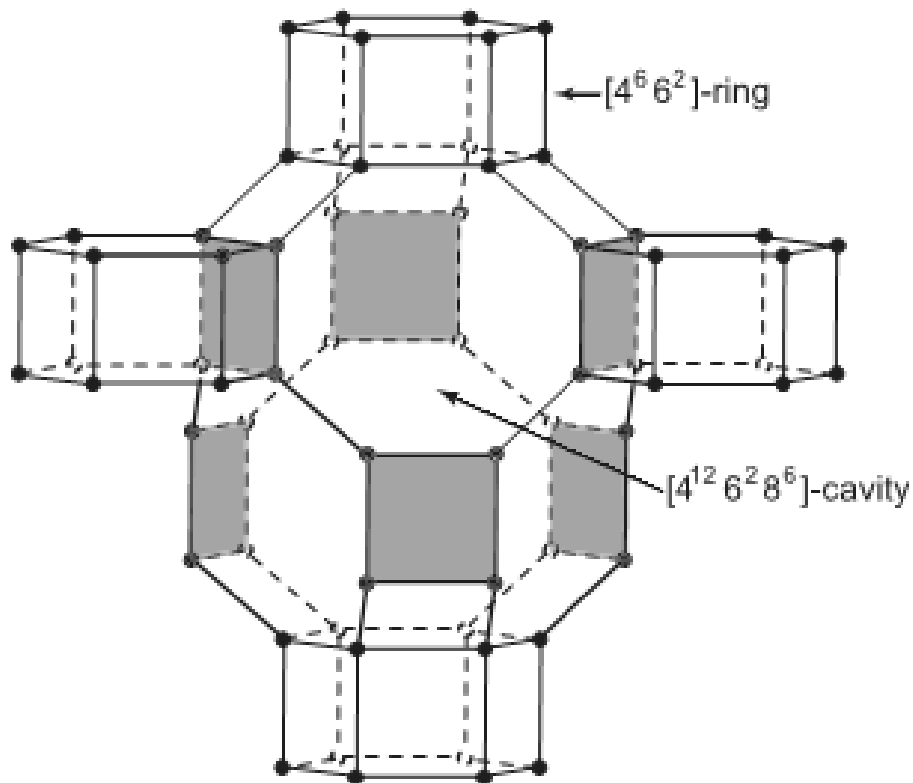


Figure 3. Chabazite structure [26]

There are many studies in the literature about SAPO synthesis and their applications. For instance, Liu et al. [27] hydrothermally synthesized mesoporous SAPO-34 catalysts by using NaF as modifier. In order to synthesize them, firstly aluminium source was mixed with deionized water. Then, silica source and phosphorus source were added successively. Lastly, NaF and template were put into the synthesis solution after which hydrothermal synthesis was done. Afterwards, washing, drying and calcinations steps were performed to produce mesoporous SAPO-34 catalyst. For the syntheses where NaF was utilized, F/Si ratio was changed in the range of 0.02-0.2. In order to see the effect of salts in the synthesis of mesoporous SAPO-34 syntheses,

different salts, NH_4F , NaCl and NH_4Cl , were utilized with the ratio of salts/ $\text{SiO}_2 = 0.1$. XRD patterns of the synthesized materials indicated that increasing F/Si up to 0.1 enhanced the crystallinity. The highest crystallinity was attained when F/Si was 0.1 but increasing this ratio further caused crystallinity loss and phase transformation to SAPO-5. Syntheses performed using NH_4F , NaCl and NH_4Cl led to SAPO-34 catalysts having cubic shaped particles whereas adding NaF to the synthesis solution caused floral SAPO-34 catalyst synthesis. Ammonia temperature programmed desorption and nitrogen sorption analyses revealed that floral SAPO-34 structure possessed the lowest strong acidity and highest pore volume among all the catalysts synthesized in this work. The floral SAPO-34 had both micropores and mesopores which were mostly in the diameter of 0.9 nm and 10 nm, respectively.

In the study of Izadbakhsh et al. [28], SAPO-34 samples were prepared by using tetraethylammonium hydroxide as surfactant and these catalysts were tested in methanol dehydration reaction in a U-shaped continuous plug flow reactor. Those catalytic materials were synthesized at hydrothermal synthesis temperature of 190-215°C by changing Si/Al ratio in the range of 0.05-0.5. EDX analysis presented that elemental compositions of Al, Si, and P in the products were different than the compositions used in the synthesis gels. However, EDX analysis verified that Si/Al ratio increased for the samples where higher Si/Al was utilized. Based on SEM and XRD results, it was concluded that the crystallinity was enhanced up to Si/Al ratio of 0.13. On the other hand, increasing this ratio further resulted in crystallinity loss. It was observed that SAPO-34 samples with higher crystallinity had longer life time in the methanol to olefins reaction.

Zhang et al. [29] synthesized SAPO-34 and MgAPSO-34 with varying Mg compositions in the synthesis gel. These catalysts were utilized in chloromethane transformation in order to generate light olefins. The reaction was carried out under atmospheric pressure in a fixed bed reactor. It was seen that samples containing Mg had higher unit cell parameter and bigger particle size. Addition of Mg into the synthesis gel caused a reduction in silicon incorporation. Moreover, it affected the chemical

environment of silicon. The results of ammonia temperature programmed desorption technique and FT-IR indicated that samples in which Mg incorporated had less acid sites together with weaker acidity compared to SAPO-34. SAPO-34 and MgAPSO-34 catalysts were tested for chloromethane transformation and it was observed that MgAPSO-34 caused higher conversion and light olefin selectivity. Besides, it had longer life time.

In the study of Nishiyama et al. [30], several SAPO-34 crystals were hydrothermally synthesized. For their syntheses, morpholine (Mor), tetraethylammonium hydroxide (TEAOH), N,N,N',N'-tetraethylethane-1,2-diamine (TEEDA) and a combination of TEAOH with Mor were utilized as templates. By using a fixed-bed reactor made up of quartz glass, the methanol to olefins reaction was carried out with these catalysts at atmospheric pressure. Sizes of SAPO-34 crystals were adjusted in the range of 1.5-7 μm by utilizing combined surfactant (TEAOH + Mor) in the synthesis. It was understood that for the methanol to olefins reaction particle size was an important parameter and as the particle size got smaller SAPO-34 catalysts had longer lifetime. By using tetraethylammonium hydroxide as surfactant, SAPO-34 structure having the smallest crystals (800 nm) was obtained. This catalyst exhibited the longest lifetime in the methanol to olefins reaction.

Liu et al. [31] utilized uncalcined SBA-15 as silica source to synthesize layered mesoporous SAPO-34 having 20 μm particle. Besides that, three other syntheses were performed using calcined SBA-15, mixture of colloidal silica and Pluronic P123, and mixture of calcined SBA-15 and Pluronic P123. It was concluded from XRD results that SAPO-34 structure was obtained by all synthesis routes, but only SAPO-34 catalyst prepared by using uncalcined SBA-15 exhibited mesoporous structure.

XRD pattern of SAPO-34 synthesized according to the procedure described in the SAPO-34 patent is shown in Figure 4 [32]. The tabulated form of 2θ versus intensity ratio (I/I_0) values is given in Table 15 in Appendix A [33].

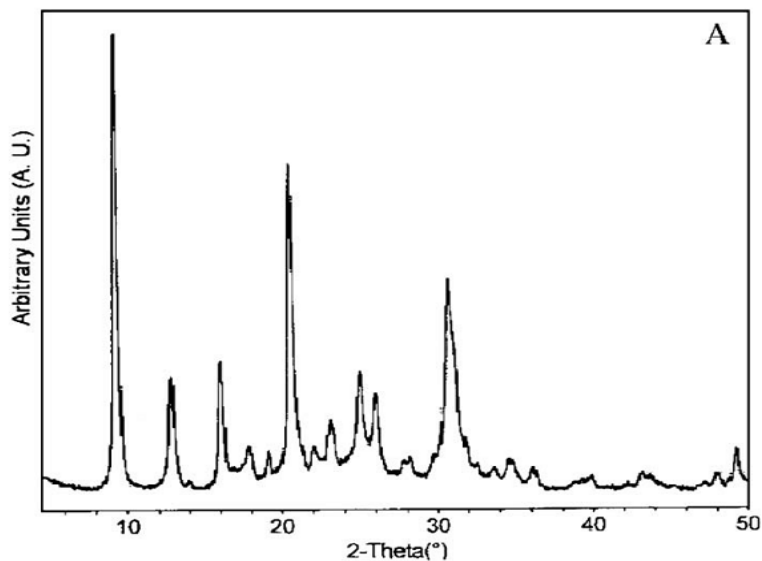


Figure 4. XRD pattern of SAPO-34 [32]

SAPO-34 has various application areas in both catalysis and adsorption processes. It can be used for methanol conversion to dimethyl ether, methanol to olefin process, CO₂/CH₄ separation, hydrogen purification, kinetic separation of propylene from propane etc [34, 35].

Although there are numerous studies in the literature on the synthesis and testing of microporous SAPO-34, there are quite few researches on SAPO-34 catalysts having mesoporous structure. Obtaining a SAPO-34 like catalyst with mesoporous structure can be very beneficial since diffusion limitations are much lower in greater pore sizes. Previously, microporous SAPO-34 catalysts have already been utilized to produce dimethyl ether. In order to attain higher conversion in the dimethyl ether synthesis, it might be better to utilize a similar catalytic material with larger pore sizes to eliminate diffusion limitation which is the idea behind this study. Thus, in this study, it is aimed to synthesize microporous SAPO-34 and mesoporous SAPO-34 like catalytic materials and test the activity of them in methanol dehydration reaction to synthesize dimethyl ether.

CHAPTER 5

EXPERIMENTAL STUDIES

In this study, both microporous SAPO-34 and mesoporous SAPO-34 like catalyst were synthesized by following hydrothermal synthesis route. The synthesized catalysts were characterized by several techniques namely XRD, N₂ physisorption, SEM-EDS, NMR and TGA-DTA. The activities of the catalysts were tested in the methanol dehydration reaction to synthesize dimethyl ether. These experimental studies are explained successively.

5.1. SYNTHESIS OF MICROPOROUS SAPO-34 CATALYST USING TETRAETHYLAMMONIUM HYDROXIDE (TEAOH) AS SURFACTANT

Microporous SAPO-34 catalysts were synthesized via hydrothermal route. The synthesis procedure followed was similar to the one described by Dubois et al. [32]. The chemicals listed below were utilized in the synthesis without any purification treatment. The molar composition of the synthesis mixture was Al₂O₃ / P₂O₅ / 0.30 SiO₂ / 2.0 TEAOH / 50 H₂O.

- Surfactant source: Tetraethylammonium hydroxide (TEAOH), [(H₅C₂)₄N]⁺OH⁻ (20 weight % aqueous solution) (Merck)
- Silica source: Fumed silica (S5380), SiO₂ (particle size: 0.011 μm, surface area: 255 m²/g ± 15 m²/g, 99% pure, Sigma-Aldrich)

- Aluminium source: Aluminium isopropoxide, $\text{Al}[\text{OCH}(\text{CH}_3)_2]_3$ (Merck)
- Phosphorus source: Ortho-phosphoric acid, H_3PO_4 (85%) (Merck)
- Base source: 1N Sodium hydroxide, NaOH (Merck)
- Solvent source: Deionized water

For the synthesis of microporous SAPO-34 catalyst, the following steps were taken.

- **Preparing synthesis solution:** 15.1 grams of aluminium isopropoxide was mixed with 54 mL of tetraethylammonium hydroxide at 350 rpm. Having stirred the solution for 1.5 hour, 0.66 grams of fumed silica was combined with the mixture. 10 minutes after adding the fumed silica, 5 mL of phosphoric acid diluted with 12.2 grams of water was added dropwise to the solution. After adding all the reagents, pH of the mixture was measured around 6.70. The mixture was kept stirring for 1 hour and pH of the mixture was measured again after one hour. This time, pH of the solution was around 6.80. Having measured the pH of the mixture for the second time, pH of the solution was made 7.40 by adding 1 N NaOH drop by drop. The mixture was stirred for another one hour and pH of the mixture was measured around 7.60 after all. Throughout the synthesis, mixing temperature was kept constant.
- **Hydrothermal synthesis:** The synthesis mixture was taken into a Teflon bottle and the bottle was put into a stainless steel autoclave. Hydrothermal synthesis was performed at 200°C under autogenous pressure without agitation. The hydrothermal synthesis duration was varied for some samples in order to observe how it would affect the structure.
- **Cooling & Aging:** After the hydrothermal synthesis, the autoclave was taken out of the oven and left for cooling for 24 hours. After cooling period, the material was picked out of the autoclave and deionized water was added to obtain 300 mL of mixture. The mixture was aged for 24 hours at room temperature.
- **Centrifuging:** 300 mL of mixture was divided into 6 centrifuge tubes of 50 mL and centrifugation was carried out for 30 minutes at 15°C with 7000 rpm. After

30 minutes, the solid product was separated from the liquid portion. The centrifuge tubes were filled with deionized water and the centrifugation was carried out again. The centrifugation has been done for 4 times in total.

- **Drying:** The solid material recovered by centrifugation was placed into the oven and it was dried at 100°C for 24 hours. After drying, the product was crushed in order to have it in powder form.
- **Calcination:** Quartz tubular reactors placed in the temperature controlled tubular furnace were used for calcinations of all samples. For all samples, the furnace was heated from room temperature to 550°C by 1°C/min and kept at that temperature for 8 hours while dry air passed through the reactor at 1 dm³/min to burn the surfactant and open up the pores.

By following the steps mentioned above, 6 samples were synthesized as listed in Table 6. Parameters other than the ones listed in Table 6 that could affect the synthesis, such as hydrothermal synthesis temperature, pH of synthesis gel, were kept same. In order to see the effect of phosphoric acid addition rate, one of the samples was synthesized by adding phosphoric acid rapidly contrary to the all other samples.

Table 6. Parameters used for the synthesis of microporous SAPO-34 samples

Catalyst number	Mixing temperature of the solution(°C)	Hydrothermal synthesis time (days)	Addition rate of phosphoric acid*
SAPO-34 #14	40	2	fast
SAPO-34 #15	40	3	slow
SAPO-34 #16	40	6	slow
SAPO-34 #17	50	2	slow
SAPO-34 #18	30	2	slow
SAPO-34 #19	40	2	slow
SAPO-34 #195	40	2	slow

* fast: few seconds, slow: 10 minutes

As can be seen from the table above, synthesis of SAPO-34 #19 was repeated to check the reproducibility of it and the synthesized material was called as SAPO-34 #195. Figure 5 below summarizes the steps involved in the synthesis of microporous SAPO-34 catalyst.

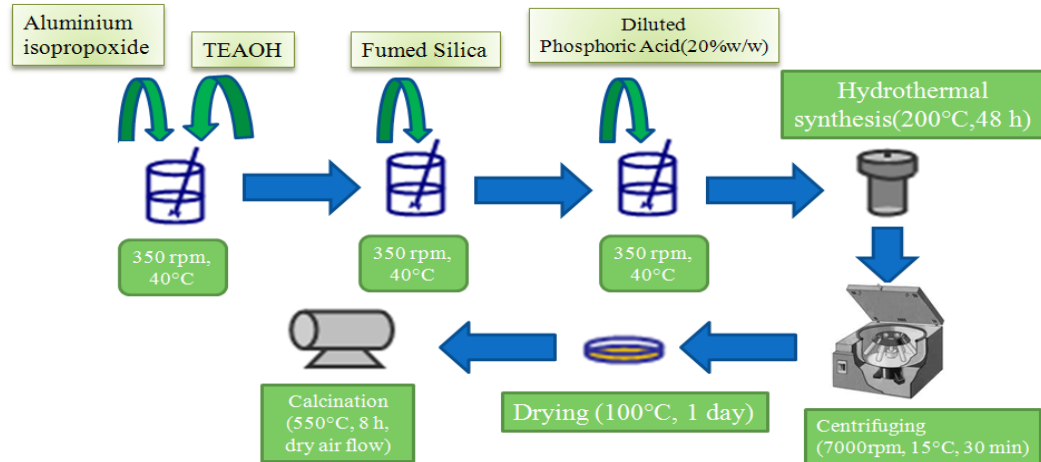


Figure 5. Microporous SAPO-34 synthesis steps

5.2. SYNTHESIS OF MESOPOROUS SAPO-34 LIKE CATALYSTS USING CETYLTRIMETHYLAMMONIUM BROMIDE (CTMABr) AS SURFACTANT

Mesoporous SAPO-34 like catalytic materials were also synthesized hydrothermally. The synthesis procedure followed was a modified form of the synthesis procedure described by Dubois et al. [32]. The reagents shown below were used in the synthesis without any purification. The molar composition of the synthesis mixture was $\text{Al}_2\text{O}_3 / \text{P}_2\text{O}_5 / 0.30 \text{ SiO}_2 / 2.0 \text{ CTMABr} / 50 \text{ H}_2\text{O}$.

- Surfactant source: Cetyltrimethylammonium bromide (CTMABr), $\text{C}_{19}\text{H}_{42}\text{BrN}$ (purity $\geq 98\%$, Merck)
- Silica source: Fumed silica (S5505), SiO_2 (particle size: $0.014 \mu\text{m}$, surface area: $200 \text{ m}^2/\text{g} \pm 25 \text{ m}^2/\text{g}$, 99% pure, Sigma-Aldrich)
- Aluminium source: Aluminium isopropoxide, $\text{Al}[\text{OCH}(\text{CH}_3)_2]_3$ (Merck)
- Phosphorus source: Ortho-phosphoric acid, H_3PO_4 (85%) (Merck)
- Base source: 1N Sodium hydroxide, NaOH (Merck)

- Solvent source: Deionized water

For the synthesis of mesoporous SAPO-34 like catalyst, the following steps were taken.

- **Preparing synthesis solution:** 13.6 grams of cetyltrimethylammonium bromide was mixed with 87 mL of deionized water at 350 rpm. Having stirred the solution for 45 minutes, 7.55 grams of aluminium isopropoxide was combined. After stirring for 1.5 hours, 0.33 grams of fumed silica was added to the solution. 10 minutes after adding the fumed silica, 2.5 mL of phosphoric acid diluted with 6.1 grams of water was added dropwise to the solution. After adding all the reagents, pH of the mixture was measured around 2.10. The mixture was kept stirring for 1 hour and pH of the mixture was measured again after one hour. This time, pH of the solution was around 2.20. Having measured the pH of the mixture, pH of the solution was made 7.40 by adding 1 N NaOH drop by drop. The mixture was stirred for another one hour and pH of the mixture was measured around 7.30.

In order to observe the effect of initial pH of the synthesis solution, several samples were synthesized by changing the initial pH. For those samples, after measuring pH of the mixture for the first time around 2.10, pH was increased to 6.70 by adding 1 N NaOH dropwise. Then the solution was mixed for 1 hour. Afterwards, pH of the mixture was altered to 7.40 with the dropwise addition of NaOH. Finally, the solution was stirred for another hour. Throughout the syntheses, mixing temperature was kept constant.

- **Hydrothermal synthesis:** The synthesis mixture was taken into a Teflon bottle and the bottle was put into a stainless steel autoclave. Hydrothermal synthesis was performed at 70°C and 200°C under autogenous pressure without agitation.
- **Cooling & Aging:** After hydrothermal synthesis, the autoclave was removed from the oven and left for cooling for 24 hours. After cooling, the material was taken out of the autoclave and deionized water was added to get 300 mL mixture. The mixture was aged for 24 hours at room temperature.

- **Centrifuging:** 300 mL of mixture was divided into 6 centrifuge tubes of 50 mL and centrifugation was carried out for 30 minutes at 15°C with 7000 rpm. After 30 minutes, the solid product was separated from the liquid portion. The centrifuge tubes were filled with deionized water and the centrifugation was carried out again. The centrifugation was done for 4 times totally.
- **Drying:** The solid material recovered by centrifugation was put into the oven and it was dried at 100°C for 24 hours. After drying, the product was crushed in order to have it in powder form.
- **Calcination:** Calcination was done under dry air flow at 1 dm³/min by heating the samples from room temperature to 550°C by 1°C/min and keeping at 550°C for 8 hours.

Figure 6 depicts the synthesis steps for mesoporous SAPO-34 like catalysts.

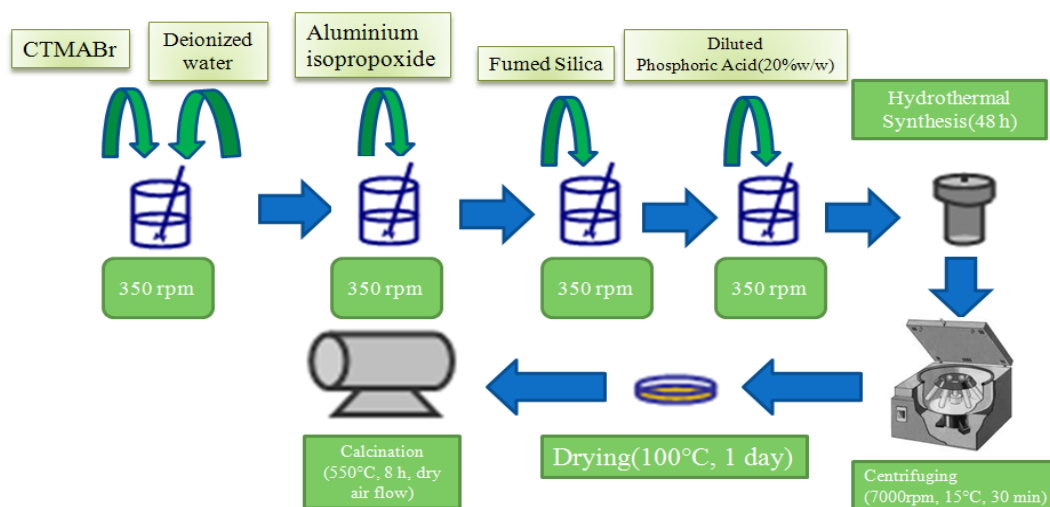


Figure 6. Representation of synthesis steps of mesoporous SAPO-34 like catalyst

By applying the abovementioned procedure, 8 samples with the parameters given in Table 7 were synthesized.

Table 7. Synthesis parameters for the mesoporous SAPO-34 like catalysts

Catalyst name	Mixing T(°C)	Initial pH	Final pH	Hydrothermal T(°C)
SAPO-34 #20	30	2.28	7.40	200
SAPO-34 #21	30	2.33	7.40	70
SAPO-34 #22	40	2.14	7.40	200
SAPO-34 #24	40	6.70	7.40	200
SAPO-34 #25	30	6.71	7.40	200
SAPO-34 #26	40	6.70	7.40	70
SAPO-34 #27	30	6.71	7.40	70
SAPO-34 #28	40	2.13	7.40	70

5.3. CATALYST CHARACTERIZATION

In order to reveal properties of catalysts such as surface area, morphology, acidity, chemical composition etc. several characterization techniques were applied. These techniques are briefly explained below.

5.3.1 X-Ray Diffraction (XRD)

X-ray diffraction is a non-destructive technique used to have information about chemical composition, crystallographic structure and particle size of the material investigated. XRD is the elastic scattering of X-rays by the atoms in a periodic lattice. X-ray diffraction caused by crystal planes enables finding out lattice spacing by using Bragg's Law, $n\lambda=2d\sin\theta$, where d is the distance between two lattice planes, θ is the angle between the incident X-ray and the normal to the reflecting plane, λ is the wavelength of X-ray, n is the order of reflection. Figure 7 depicts Bragg diffraction. In this technique, the sample must have sufficiently long ordered structure to have clear diffraction peaks [36, 37].

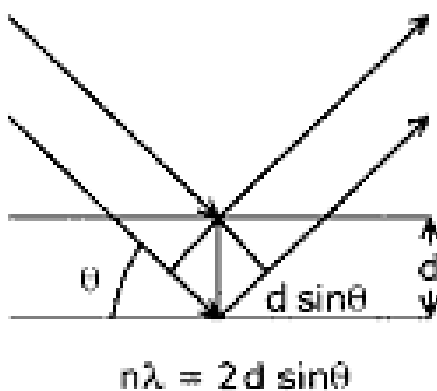


Figure 7. Bragg diffraction [37]

The synthesized catalysts were characterized by XRD technique using a Rigaku D/MAX2200 diffractometer having CuK radiation source in 2θ range of $1-60^\circ$ with a scanning rate of $2^\circ/\text{min}$. The low angle XRD analyses were performed using a

Rigaku Ultima IV diffractometer with CuK radiation source in 2θ range of $0.1-8^\circ$ with a scanning rate of $1^\circ/\text{min}$.

5.3.2 N₂ Physisorption

Gas adsorption is a common method utilized for the measurement of surface area, pore size and pore volume of materials. Usually, nitrogen is used for this purpose due to its appropriate molecular size and inertness. Prior to the surface area characterization analysis, solid surface must be cleaned from contaminations such as water, oil. Surface cleaning, in other words degassing, is done by putting a solid sample in a cell and heating it under inert gas flow or vacuum. When the sample is degassed, it is brought to constant temperature by a bath involving cryogen such as nitrogen. Then, the adsorption process begins and gas molecules enter to the pores of material [38, 39].

Nitrogen adsorption-desorption analyses were carried out using a Quantachrome Autosorb-6 instrument. Before starting the analyses, samples were degassed for 16 hours at 110°C . The analyses were performed in the relative pressure range of 10^{-4} to 0.95 at liquid nitrogen temperature (77K). Nitrogen adsorption-desorption isotherms, multipoint BET surface area, pore volume and pore size distribution were obtained.

5.3.3 Scanning Electron Microscopy (SEM) and Energy Dispersive X-Ray Spectroscopy (EDS)

Scanning electron microscope (SEM) utilizes a focused beam with high-energy electrons to produce various signals at the solid sample surfaces. The signals generated from electron-sample interactions give information about morphology, orientation of materials, chemical composition and crystalline structure [40]. SEM-EDS analyses were

performed using the instrument called QUANTA 400F Field Emission SEM. Before the analyses, samples were coated with Au-Pd to prevent charging effect. This technique reveals the morphology of the catalysts synthesized.

EDS is a non-destructive X-ray technique utilized in conjunction with scanning electron microscopy for the determination of elemental composition. In this technique, an electron beam, having an energy value in the range of 10-20 keV, hits the surface of a sample. This strike leads to emission of X-rays, whose energies are characteristic of elements. Since X-rays are produced in a region of 2 microns in depth, EDS is not a surface sensitive technique [41-43].

5.3.4 Thermal Analyses (TGA + DTA)

Thermogravimetric analysis (TGA) measures the weight loss with respect to the temperature changes. It gives information about thermal stability of the sample investigated. In differential thermal analysis (DTA), the material investigated and an inert reference are exposed to the same thermal cycles. Temperature differences between the sample and the reference are recorded. TGA and DTA were performed using Shimadzu DTG-60H. The analysis was done by using air at a flow rate of 60 cc/min and raising temperature of samples from room temperature to 800°C by 5°C/min. This analysis showed at which temperatures weight loss occurred. Thus, based on that result, calcination temperature could be selected. [44]

5.3.5 Nuclear Magnetic Resonance (NMR)

Nuclear magnetic resonance analysis is a technique used for the determination of coordination environment of several elements such as Si and Al. It was carried out using

Bruker Superconducting FT.NMR Spectrometer Avance TM 300 MHz WB instrument with a spinning rate of 8500 Hz. The resonance frequency was set as 78 and 60 MHz for ^{27}Al and ^{29}Si , respectively.

5.4. EXPERIMENTAL SETUP

Methanol dehydration reaction in vapor phase was implemented in a fixed bed reactor system. Helium gas was utilized as both the reference gas for gas chromatograph (GC) and carrier gas. Liquid methanol was sent to an evaporator, which was heated to 150°C, by a syringe pump at a flow rate of 2.1 mL/h. In the evaporator, methanol went into gaseous form and mixed with helium gas. Helium flow rate and the total gaseous flow rate were set as 23 mL/min and 44.14 mL/min, successively. Thus, the ratio of volumetric methanol flow rate to total volumetric flow rate was 0.48. The gaseous mixture passed through a stainless steel tubular reactor, with an outer diameter of 1/4 inch, located in a temperature controlled tubular furnace. In the middle of the reactor, the catalyst to be tested was placed and fixed by quartz wool from both ends. In order to prevent reactant or product condensation along the connection lines, these lines were heated to 150°C. For the analysis of the products and the unreacted methanol, the outlet stream of the reactor was sent to a gas chromatograph (Varian CP 3800 GC) that had a thermal conductivity detector (TCD) and Porapak T column in it. TCD and gas sampling valve were kept at 225°C and 200°C, respectively. In order to separate and distinguish the products, a temperature-ramped program was utilized. The column temperature was set to 75°C and during 2 minutes it was kept constant. By a temperature ramp of 10°C/min, the column temperature was raised to 170°C and the column was kept at this temperature for 3 minutes. In this period, peaks of the products and the unreacted methanol were observed. After each experiment, helium gas passed through the system for 1 hour. The whole reaction system is illustrated in Figure 8. Details about GC calibration factors and retention times are presented in Appendix B.

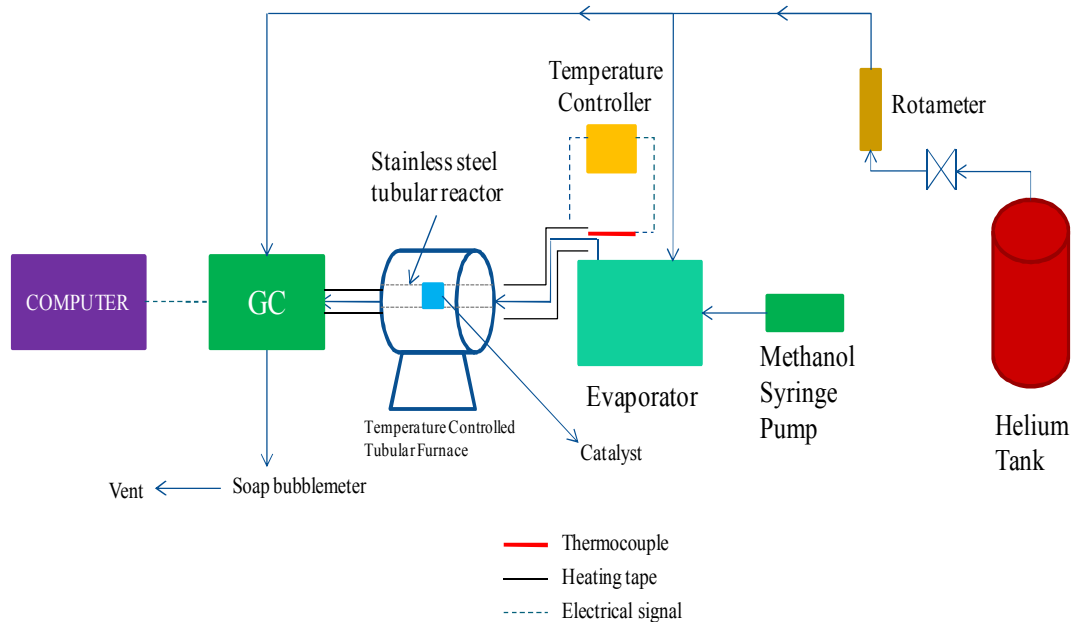


Figure 8. Schematic of the reaction system utilized to produce dimethyl ether

For all the catalysts tested, the used catalyst weight and space time were set as 0.1 g and 0.14 s.g/cm³, respectively. The catalysts were tested in a wide temperature range starting from 150°C up to the temperature at which deactivation was observed. The temperature ranges investigated for each catalyst are shown in Table 8. For the calculations of conversion, selectivity and yield values, average values of 3 successive data points were used.

Table 8. Temperature ranges investigated for the catalysts synthesized

Catalyst name	Reaction temperature range (°C)
SAPO-34 #14	150-300
SAPO-34 #19	150-750
SAPO-34 #20	150-500
SAPO-34 #21	150-700
SAPO-34 #22	150-500
SAPO-34 #24	150-500
SAPO-34 #25	150-550
SAPO-34 #26	150-550
SAPO-34 #27	150-550
SAPO-34 #28	150-550

CHAPTER 6

RESULTS AND DISCUSSION

6.1. CHARACTERIZATION OF MICROPOROUS SAPO-34 CATALYSTS

6.1.1. X-Ray Diffraction (XRD)

In this thesis work, in order to see the effect of mixing temperature of synthesis solution on SAPO-34 catalysts, three samples were synthesized at three different mixing temperatures. SAPO-34 #17, #18 and #19 were the catalysts synthesized for this purpose whose mixing temperatures are 50, 30 and 40°C, respectively. XRD patterns of these three catalysts are shown in Figure 9. As can be seen from the figure, the XRD pattern of the catalyst synthesized at 30°C, that is SAPO-34 #18, was not in compliance with the XRD pattern of SAPO-34 in Figure 4. The main peak around 10° was lost together with several other peaks. For the XRD pattern of SAPO-34 #18, the peaks at 20°, 38° and 55° were attributed to $\text{Al}(\text{PO}_3)_3$ while peaks around 21° and 36° were due to AlPO_4 . Peaks about 35° and 45° were assigned to $\alpha\text{-Al}_2\text{O}_3$ whereas the peak at 22° was observed due to SiO_2 . XRD data of SiO_2 , AlPO_4 , $\alpha\text{-Al}_2\text{O}_3$ and $\text{Al}(\text{PO}_3)_3$ can be found in Appendix A. The peak around 2° might imply a mesoporous structure for SAPO-34 #18 which was not expected in a synthesis where a surfactant, such as TEOH, having short alkyl chain length was utilized. At 30°C the surfactant might not get dissolved totally and the surfactant molecules might stay in a bulky form causing greater pore sizes in the structure than expected.

When the syntheses were made at 40°C and 50°C, XRD pattern of the synthesized materials became consistent with that of presented in Figure 4. It must be noted that increasing mixing temperature from 40°C to 50°C caused a substantial decrease in intensity values. Since this implies a decrease in crystallinity, the optimum mixing temperature was selected as 40°C.

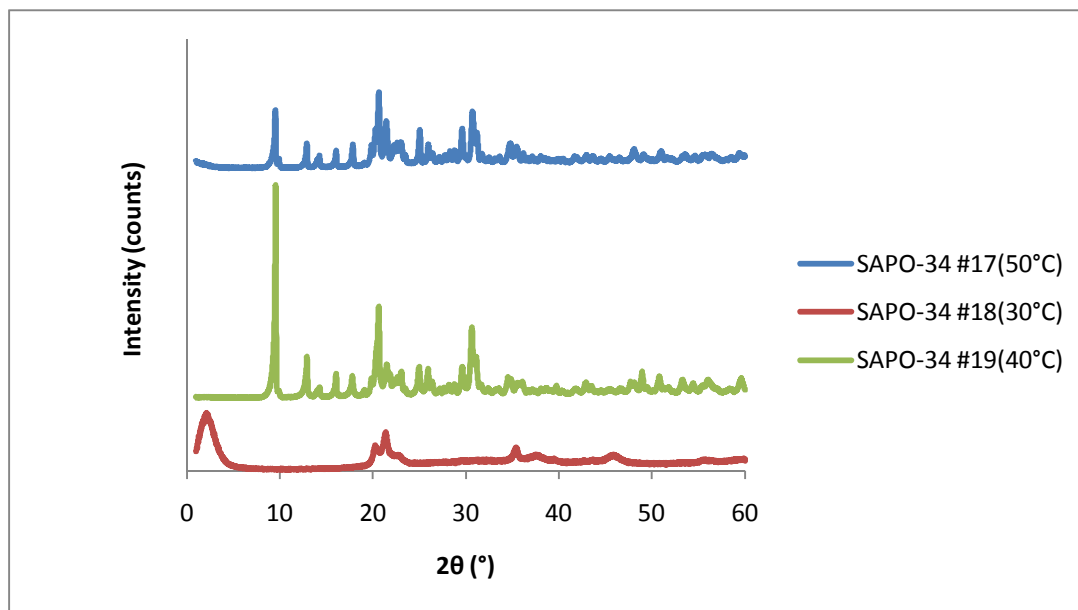


Figure 9. Comparison of XRD patterns of microporous SAPO-34 catalysts for the determination of mixing temperature effect (Hydrothermal synthesis time: 2 days, hydrothermal synthesis temperature: 200°C, addition rate of phosphoric acid: slow)

After choosing the optimum mixing temperature as 40°C, the effect of hydrothermal synthesis time on the structure was investigated. In addition to SAPO-34 #19, whose hydrothermal synthesis time was 2 days, SAPO-34 #15 and SAPO-34 #16 catalysts were synthesized. The hydrothermal synthesis durations were 3 days and 6 days, respectively. As can be seen from Figure 10, raising hydrothermal synthesis time

from 2 days to 3 days caused diminished intensities, thus, crystallinity of the structure was deteriorated. Further increase in the hydrothermal synthesis time led to the distortion of chabazitic structure since main peak of SAPO-34 structure was not observed in the XRD pattern of SAPO-34 #16. For SAPO-34 #16, the peaks around 22° and 36° were attributed to AlPO_4 and SiO_2 peaks. Peaks at 20° , 23° , 26° , 30° , 31° , 38° , 43° and 57° were assigned to $\text{Al}(\text{PO}_3)_3$. Thus, XRD pattern of SAPO-34 #16 consisted of $\text{Al}(\text{PO}_3)_3$, AlPO_4 and SiO_2 peaks. The optimum hydrothermal synthesis duration for microporous SAPO-34 synthesis was found as 2 days.

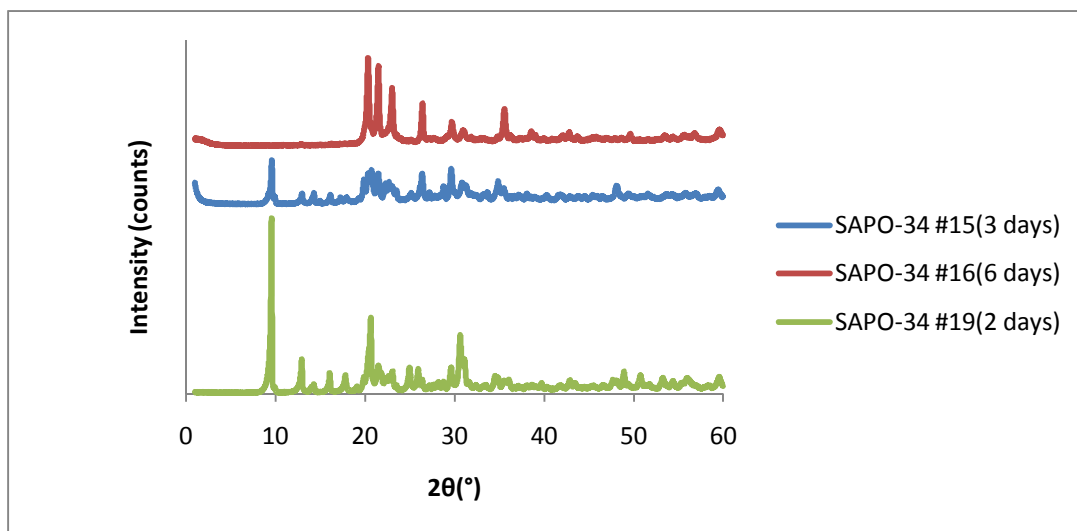


Figure 10. Comparison of XRD patterns of SAPO-34 catalysts for the determination of hydrothermal synthesis time effect (Mixing temperature: 40°C , hydrothermal synthesis temperature: 200°C , addition rate of phosphoric acid: slow)

Having fixed the mixing temperature and the hydrothermal synthesis duration, another parameter, the addition rate of phosphoric acid, was investigated. SAPO-34 #14 was synthesized under the similar conditions at which SAPO-34 #19 was synthesized.

The only difference of these two syntheses was the addition rate of phosphoric acid. SAPO-34 #14 was synthesized by adding phosphoric acid all at once while SAPO-34 #19 was synthesized by combining the phosphoric acid into the solution mixture dropwise. Due to fast addition of phosphoric acid, during the synthesis of SAPO-34 #14, the mixing temperature was not constant unlike SAPO-34 #19. Mixing temperature reached to 50°C, stayed there for several minutes and cooled back to 40°C. As can be seen from the XRD pattern of SAPO-34 #14 in Figure 11, the main peak intensity was around 200. Since TEAOH accepts a limited range of synthesis parameters, increasing hydrothermal synthesis time from 2 days to 6 days or increasing mixing temperature from 40°C to 50°C caused the optimum structure to be lost. TEAOH might template structures other than chabazite under certain conditions [45].

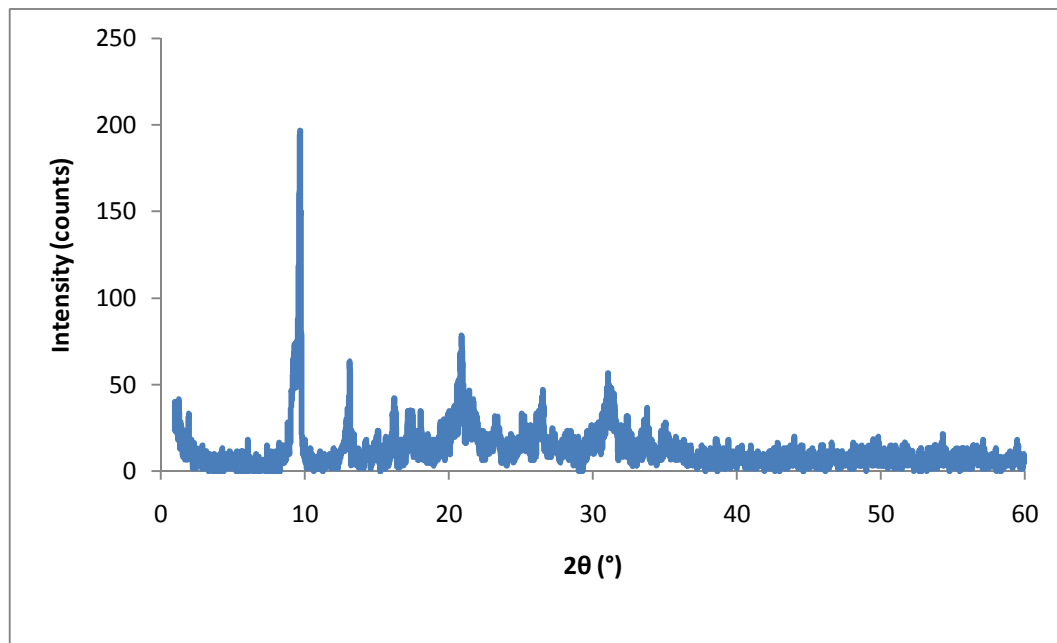


Figure 11. XRD pattern of SAPO-34 #14

On the other hand, as Figure 12 indicates the main peak intensity of SAPO-34 #19 was about 75 times higher than that of SAPO-34 #14. Thus, it can be concluded that SAPO-34 #19 had a higher crystallinity compared to SAPO-34 #14. Thus, the optimum synthesis condition for microporous SAPO-34 was achieved by adding phosphoric acid dropwise.

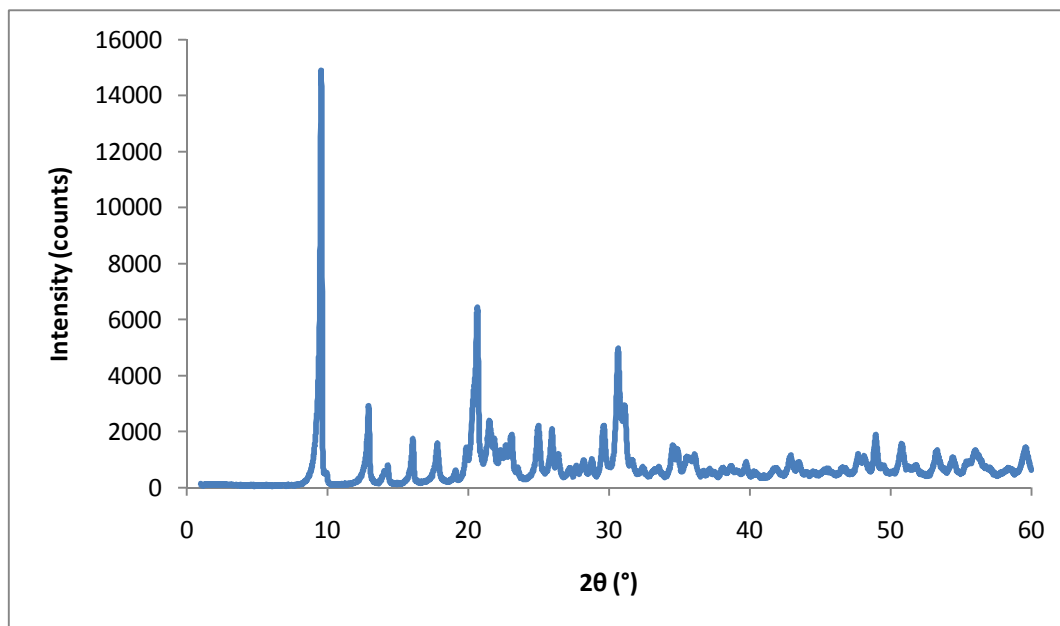


Figure 12. XRD pattern of SAPO-34 #19

To sum up, the optimum synthesis conditions for microporous SAPO-34 were found as shown in Table 9.

Table 9. Optimum synthesis parameters for microporous SAPO-34

Mixing temperature (°C)	40
Hydrothermal synthesis temperature (°C)	200
Hydrothermal synthesis time (days)	2
Initial and final pH	6.7 and 7.4
Addition rate of phosphoric acid	slow

Lastly, the synthesis of SAPO-34 #19 was repeated to check the reproducibility. The product obtained from the repeated synthesis was named as SAPO-34 #195 and its XRD pattern is shown in Figure 13.

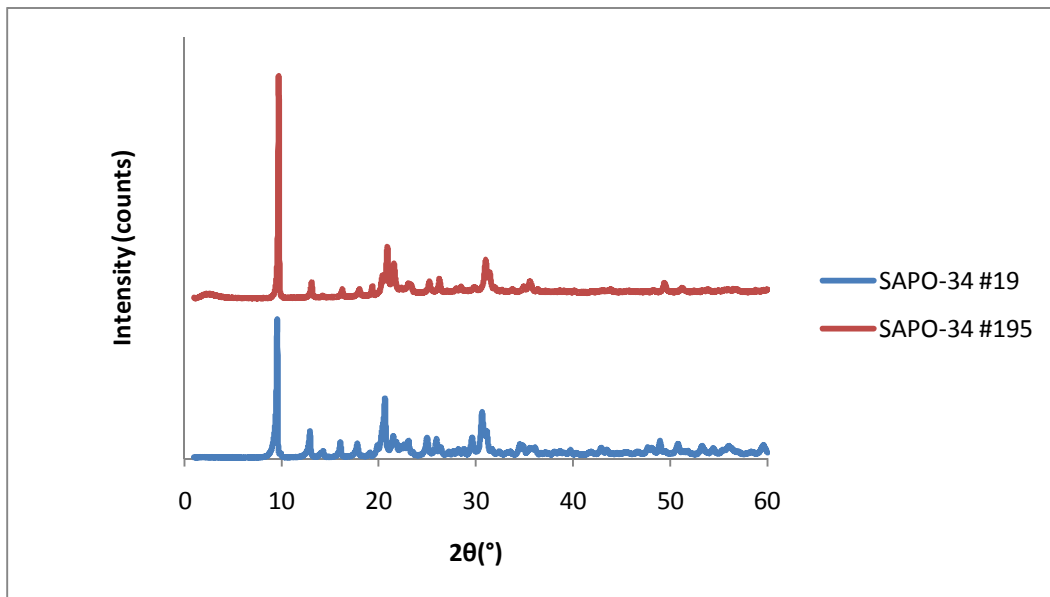


Figure 13. Comparison of XRD patterns of SAPO-34 #19 and SAPO-34 #195

As can be seen in Figure 13, XRD patterns of SAPO-34 #19 and SAPO-34 #195 were consistent with each other. Thus, microporous SAPO-34 was successfully synthesized.

6.1.2 Scanning Electron Microscopy (SEM)

Figures 14 and 15 show the SEM images of SAPO-34 #14 and SAPO-34 #19, respectively. In both of the samples, it was observed that cubic-like shaped structure was obtained as in the literature. However, these cubic-like shaped structures were more widespread in SAPO-34 #19 compared to SAPO-34 #14. In SAPO-34 #14, the irregular shaped structures, such as rod like structures, were more frequently seen. This was due to the lower crystallinity of SAPO-34 #14 compared to SAPO-34 #19 which was proved by XRD analysis results of them. Thus, it was observed that fast addition rate of phosphoric acid caused deterioration in crystallinity. From SEM image shown on the left top corner of Figure 14 and SEM image on the left bottom corner of Figure 15, the dimensions of SAPO-34 #14 and SAPO-34 #19 were measured as 36 x 30 x 20 μm and 11 x 13 x 6 μm , respectively. The surfaces of cubic-like shapes in SAPO-34 #14 were rough whereas those of cubic-like shapes in SAPO-34 #19 were smooth. This difference was probably caused by the crystallinity difference between these catalysts.

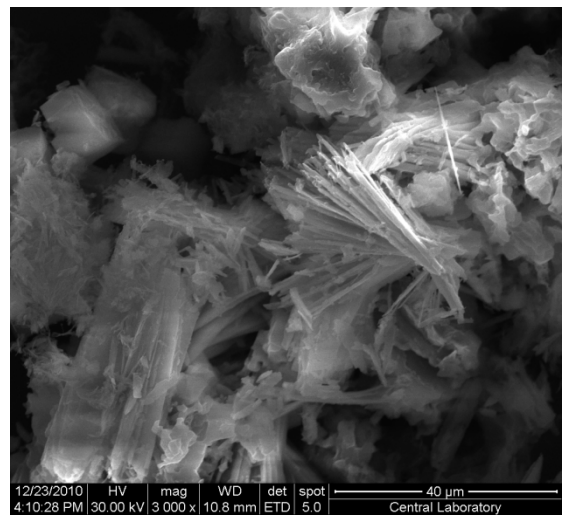
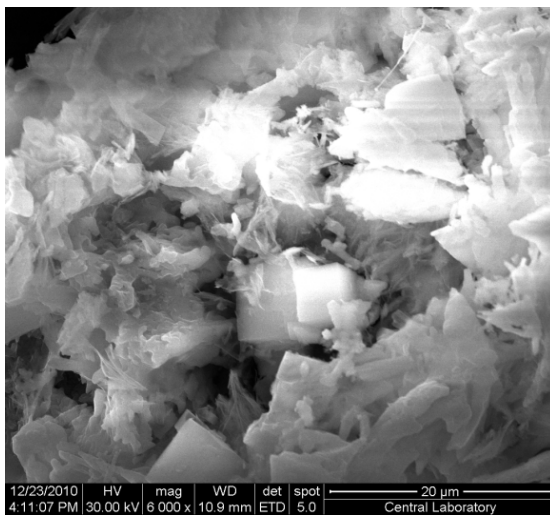
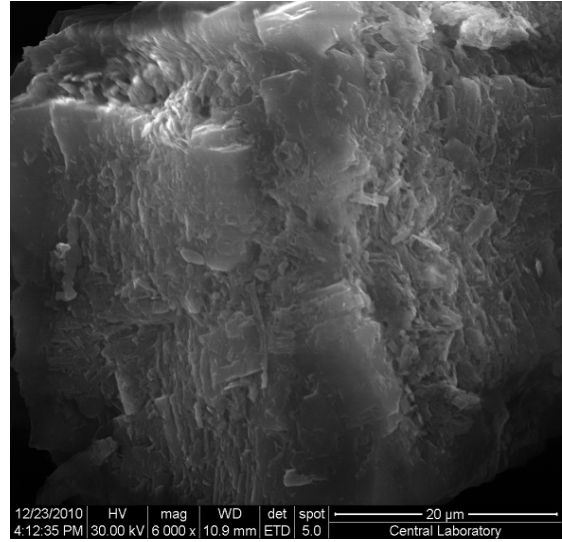
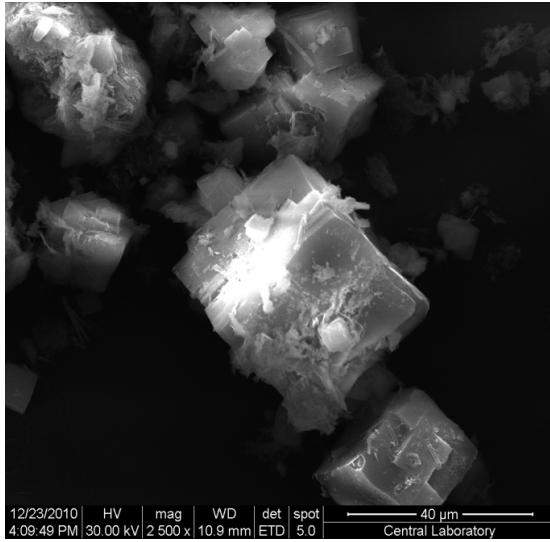


Figure 14. SEM images of SAPO-34 #14

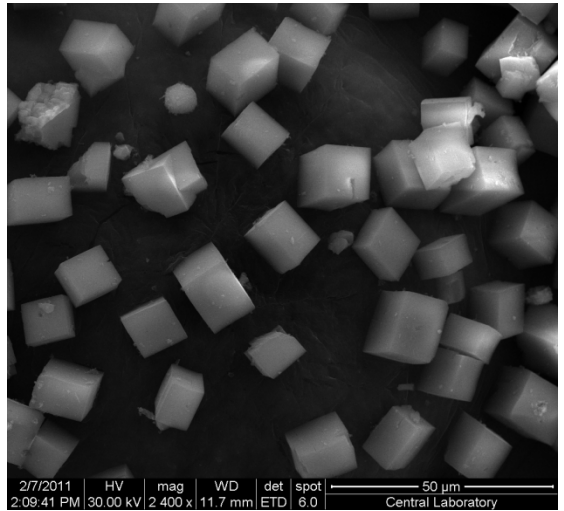
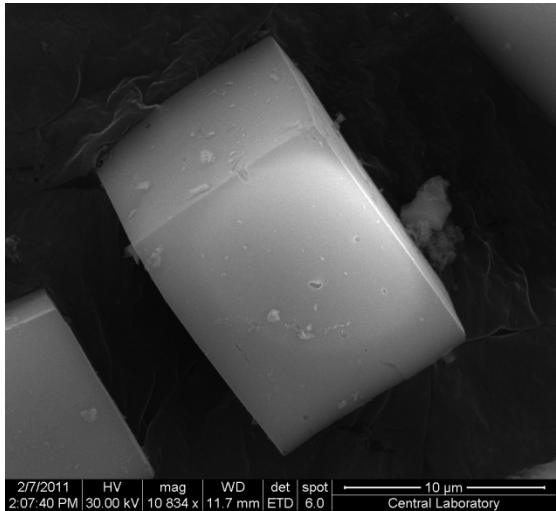
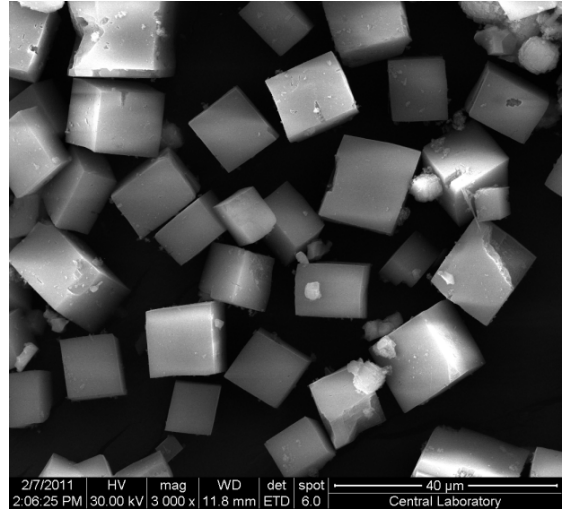
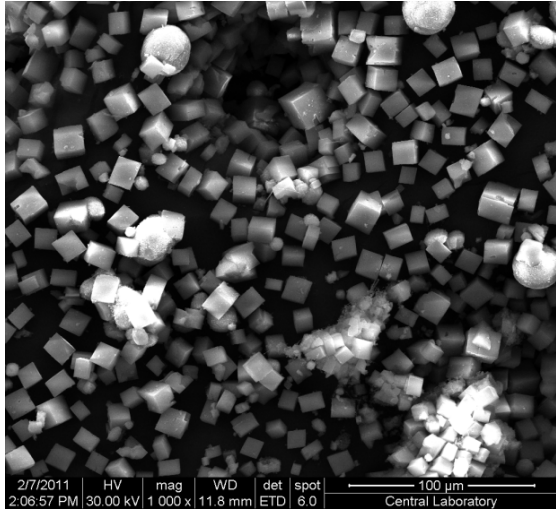


Figure 15. SEM images of SAPO-34 #19

6.1.3. Energy Dispersive X-Ray Spectroscopy (EDS)

The EDS analysis results of SAPO-34 #14 are shown in Table 10. The results show that a substantial amount of silicon was incorporated to the catalyst. During the synthesis steps such as centrifugation, Si, Al and P might be lost. It can be concluded from the EDS results that more phosphorus content was lost compared to aluminium throughout the steps of catalyst synthesis.

Table 10. EDS results for SAPO-34 #14

	Atomic Ratio (EDS)	Atomic Ratio (Initial Solution)
Si/Al	0.11	0.15
Si/P	0.13	0.15
Al/P	1.16	1

Table 11 indicates the EDS results of SAPO-34 #19. It can be deduced that silicon was successfully integrated into the catalyst structure. It is understood Al and P loss during the synthesis steps were significant that atomic ratios obtained from EDS differed much from that of utilized in the synthesis solution. Again, phosphorus loss was higher compared to Al loss. Detailed EDS data of mesoporous SAPO-34 like catalysts are given in Appendix C.

Table 11. EDS results for SAPO-34 #19

	Atomic Ratio (EDS)	Atomic Ratio (Initial Solution)
Si/Al	0.20	0.15
Si/P	0.30	0.15
Al/P	1.49	1

6.1.4. N₂ Physisorption

The microporous sample with the highest crystallinity, SAPO-34 #19, was characterized by N₂ physisorption in order to have information about the catalyst such as multipoint BET surface area, pore volume and average pore diameter. Those results are indicated in Table 12.

Table 12. Physical properties of SAPO-34 #19

Multipoint BET surface area (m²/g)	291
BJH method adsorption average pore diameter (nm)	0.6
BJH method desorption average pore diameter (nm)	2.1
BJH method cumulative adsorption pore volume (cm³/g)	6.1 x 10 ⁻²
BJH method cumulative desorption pore volume (cm³/g)	5.7 x 10 ⁻²
DR method micro pore volume (cm³/g)	1.127 x 10 ⁻¹

Nitrogen adsorption – desorption isotherms of SAPO-34 #19 is given in Figure

16.

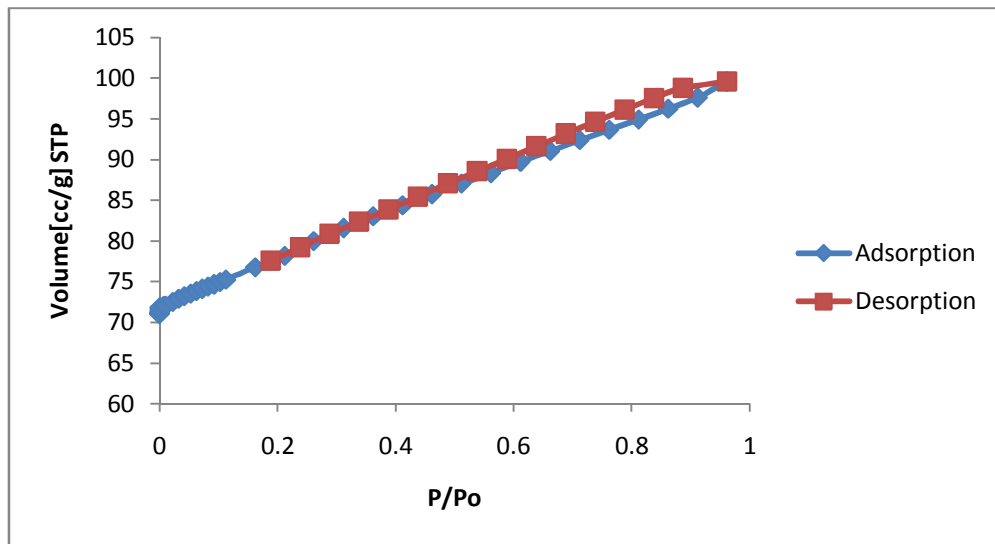


Figure 16. Nitrogen adsorption desorption isotherms of SAPO-34 #19

It can be concluded that the isotherms were similar to type I implying microporous structure but there was a slight hysteresis starting from P/P_0 value of about 0.45 with the type of H3. Thus, SAPO-34 #19 had both micropores and mesopores but micropores were overwhelming in the structure.

BJH adsorption and desorption pore size distributions of SAPO-34 #19 are shown in Figures 17 and 18, respectively. According to BJH adsorption data, the material had micropores and mesopores whereas BJH desorption data implied there were only mesopores. This difference was due to the irregular shapes of the pores in the structure. However, the pore size distributions were consistent with N_2 adsorption desorption isotherms. BJH adsorption data showed that most of the pores had diameters about 0.6 nm and some other pores had diameters around 2.2 nm with a lower frequency. According to BJH desorption data, pores were mostly 2.1 nm in size.

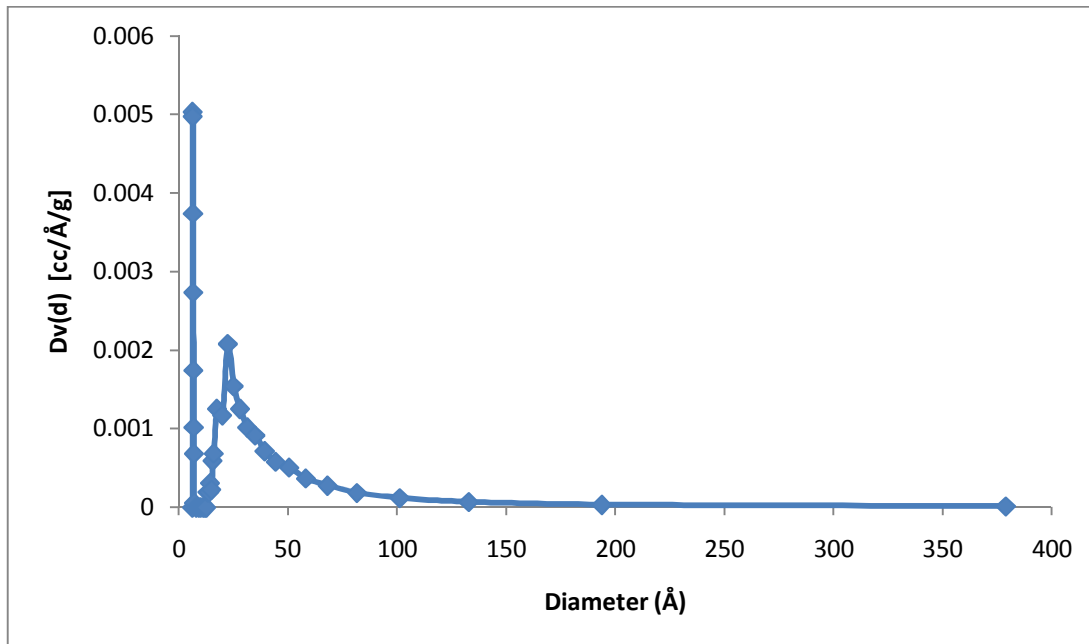


Figure 17. BJH adsorption pore size distribution of SAPO-34 #19

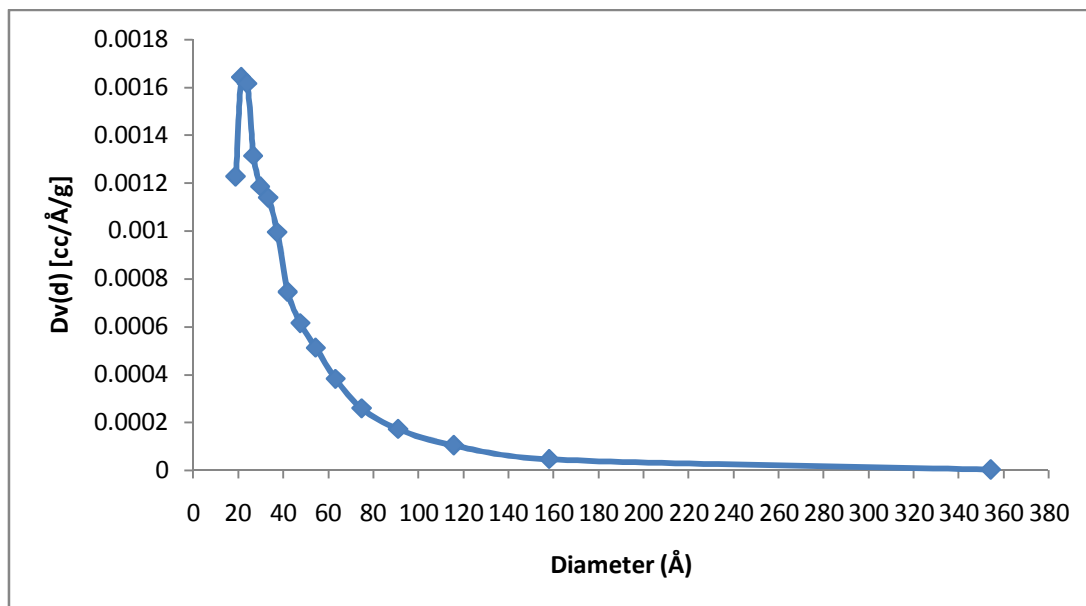


Figure 18. BJH desorption pore size distribution of SAPO-34 #19

6.1.5. TGA and DTA

The thermal analysis result of SAPO-34 #19 is shown in Figure 19. As shown in the figure, after 510°C, there was no substantial weight loss implying surfactant removal was almost completed at 510°C. Thus, the calcination temperature was selected as 550°C.

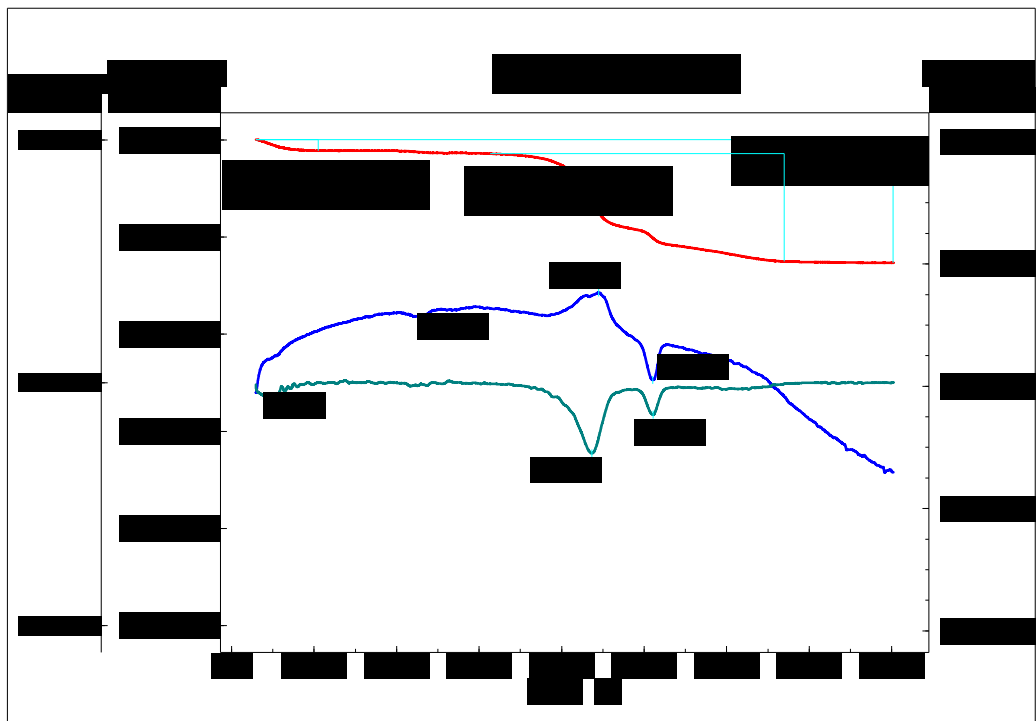


Figure 19. Thermal analysis of uncalcined SAPO – 34 # 19

6.1.6. Nuclear Magnetic Resonance (NMR)

^{27}Al and ^{29}Si NMR techniques were applied to SAPO-34 #19 to reveal the coordination environments of Al and Si. Figure 20 shows ^{27}Al NMR result of SAPO-34 #19 where around 30 ppm a sharp peak was observed which was attributed to tetrahedrally coordinated Al site. The broad peak around 7 ppm was assigned to pentacoordinated aluminum atom which was less seen. The broad peak around -15 ppm was assigned to octahedrally coordinated Al [46, 47]. Thus, aluminum atoms were mostly tetrahedrally coordinated. Other peaks were probably due to spinning sidebands [48].

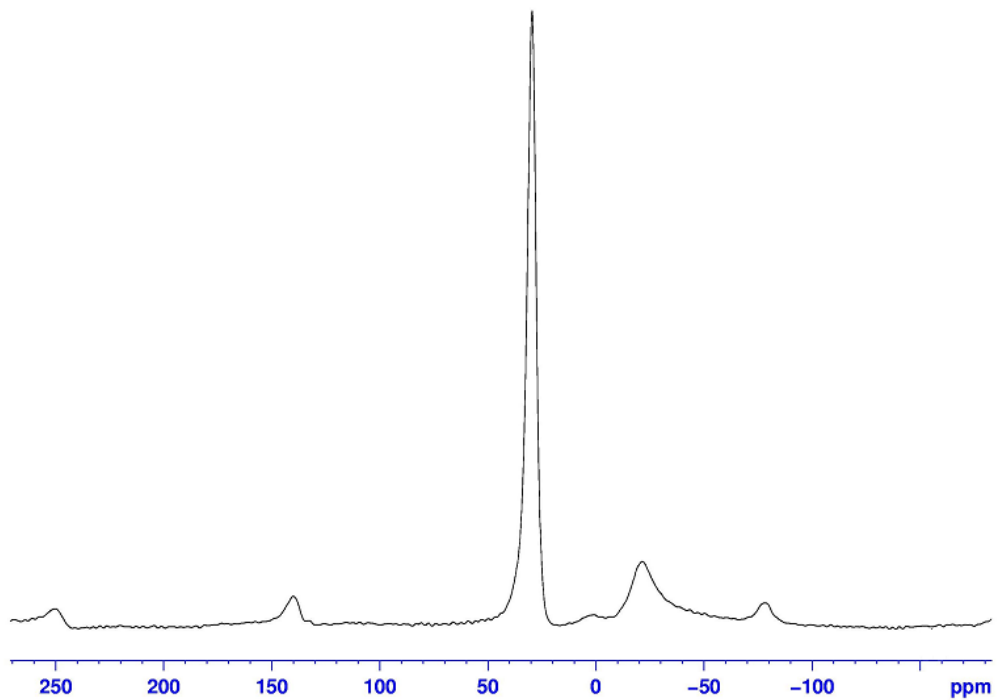


Figure 20. ^{27}Al NMR of SAPO-34 #19

Figure 21 illustrates the ^{29}Si NMR result of SAPO-34 #19. The signals with chemical shifts around -90, -95, -100, -105 and -110 were assigned to Si (4Al), Si (3Al), Si (2Al), Si (1Al) and Si (0Al), respectively [49].

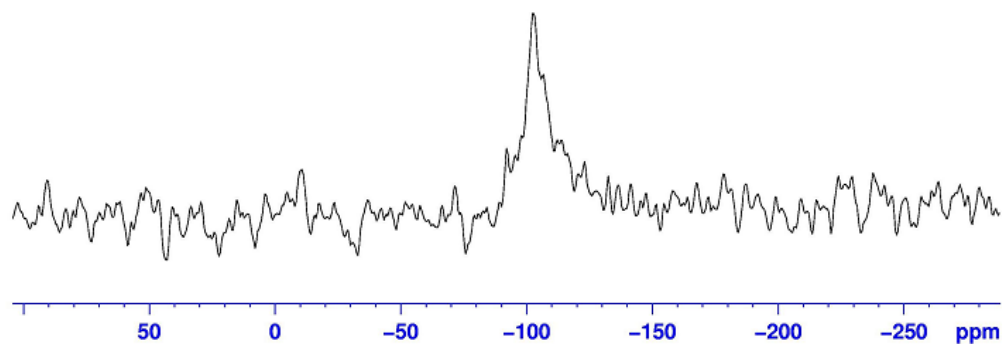


Figure 21. ^{29}Si NMR of SAPO-34 #19

6.2. CHARACTERIZATION OF MESOPOROUS SAPO-34 LIKE CATALYSTS

6.2.1. X-ray diffraction (XRD)

In the synthesis of mesoporous SAPO-34 like catalysts, three parameters, mixing temperature, initial pH and hydrothermal synthesis temperature, were changed. In order to synthesize SAPO-34 catalyst with mesoporous structure, totally 8 different synthesis procedures were applied. These procedures, which involved using a surfactant having longer alkyl chain length compared to TEAOH, were the slightly modified forms of the procedures utilized for microporous SAPO-34 synthesis. Although many procedures yielded mesoporous structure, all the materials synthesized with those modified procedures lost chabazitic structure of SAPO-34 whose main peak was around 10° [50, 51]. However, SiO_2 and AlPO_4 peaks were retained suggesting a silicoaluminophosphate (SAPO) structure. XRD patterns of several of these materials had only SiO_2 and AlPO_4 peaks and they were quite similar to each other whereas some other catalytic materials

had α -Al₂O₃ and Al(PO₃)₃ peaks in their XRD patterns as well. For instance, for SAPO-34 #26 and SAPO-34 #21 given in Figures 22 and 23, peaks at Bragg angle values of 22°, 36° belong to SiO₂ and AlPO₄ peaks. For SAPO-34 #20, peaks at 20°, 24°, 26°, 30°, 38°, 52° and 57° correspond to Al(PO₃)₃ whereas peaks at 22°, 36° belong to SiO₂ and AlPO₄ peaks. Lastly, peaks at 26°, 35°, 43°, 52° and 57° were attributed to α -Al₂O₃. Figures 49, 50, 51, 52 and 53 (Appendix A) present XRD patterns of SAPO-34 #22, SAPO-34 #24, SAPO-34 #25, SAPO-34 #27 and SAPO-34 #28, respectively. For SAPO-34 #22, SAPO-34 #25, SAPO-34 #27 and SAPO-34 #28, peaks at 20° and 30° were assigned to Al(PO₃)₃ while peaks at 21° and 35° were due to AlPO₄. Peaks at 22° and 35° were observed due to SiO₂ whereas peaks around 35°, 43° and 56° were assigned to α -Al₂O₃. For SAPO-34 #22, peak at 27° was also observed which was attributed to Al(PO₃)₃. For SAPO-34 #24, peaks at 20°, 23°, 27°, 30° and 38° were assigned to Al(PO₃)₃. Peaks around 22° and 36° were due to SiO₂ and AlPO₄. In Appendix A, low angle XRD patterns of SAPO-34 #20, SAPO-34 #26, SAPO-34 #27 and SAPO-34 #28 are given which showed characteristic low angle peaks that were typical of materials with mesoporous structure. Low Bragg angle peaks at 0.41°, 0.26°, 0.37° and 0.37° were observed for SAPO-34 #20, SAPO-34 #26, SAPO-34 #27 and SAPO-34 #28, respectively. Among them only in SAPO-34 #26 a reflection peak was observed which was at 2 θ value of 0.92°. pH is an important parameter for homogeneous micelle formation and it should be around 11 to observe apparent reflection peaks when CTMABr is used as surfactant [52]. Due to this fact, for the samples synthesized with initial pH values around 2, the reflection peaks might not be observed. The reason of having reflection peak in XRD pattern of SAPO-34 #26 might be neutral pH of its synthesis solution.

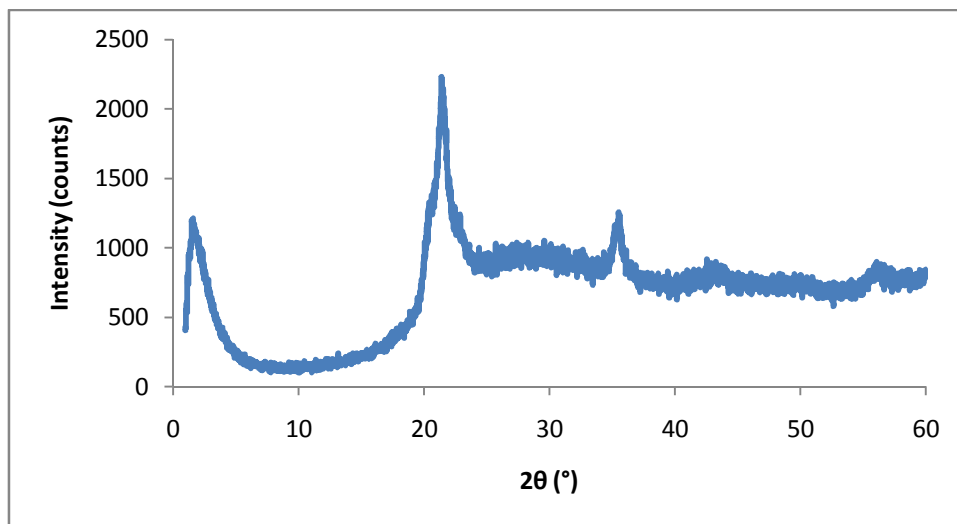


Figure 22. XRD pattern of SAPO-34 #26 (Mixing temperature: 40°C, initial pH: 6.70, hydrothermal synthesis temperature: 70°C)

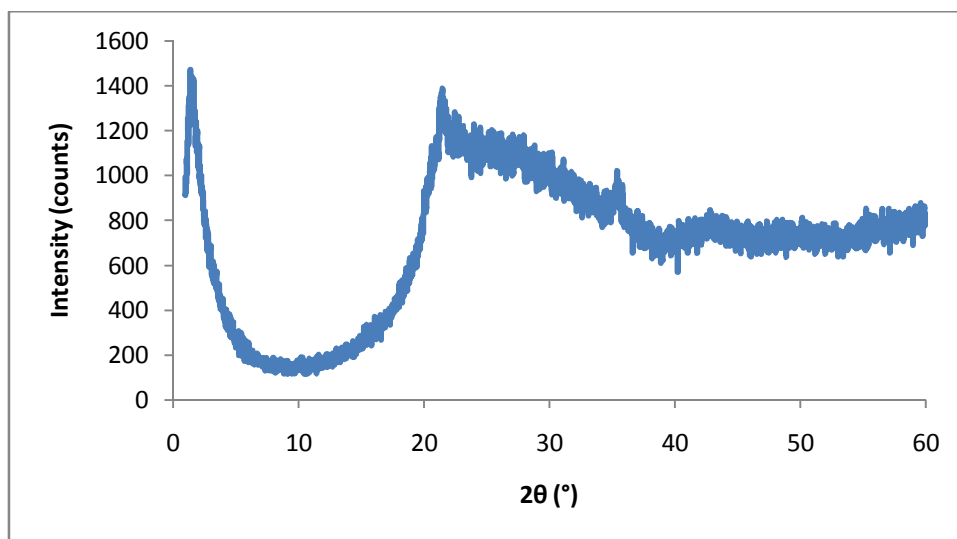


Figure 23. XRD pattern of SAPO-34 #21 (Mixing temperature: 30°C, initial pH: 2.33, hydrothermal synthesis temperature: 70°C)

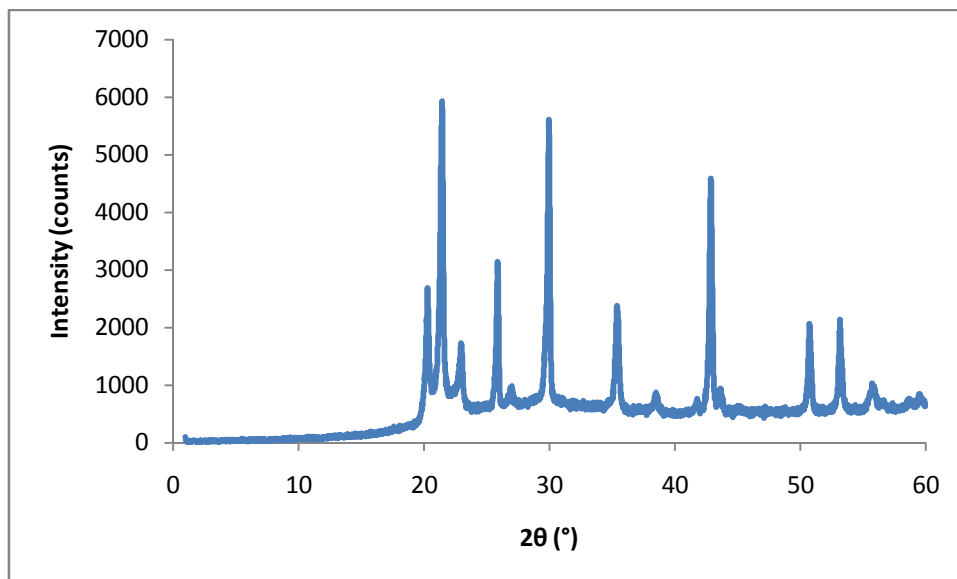


Figure 24. XRD pattern of SAPO-34 #20 (Mixing temperature: 30°C, initial pH: 2.28, hydrothermal synthesis temperature: 200°C)

Lastly, in order to see the effect of surfactant on the crystallographic structure, XRD patterns of SAPO-34 #19 and SAPO-34 #24 were compared. The only difference between these two samples was the surfactant used in the synthesis. Figure 25 shows the comparison of XRD patterns of these two samples. As seen in the figure, using cetyltrimethylammonium bromide instead of tetraethylammonium hydroxide caused distortion of SAPO-34 structure and loss of crystallinity.

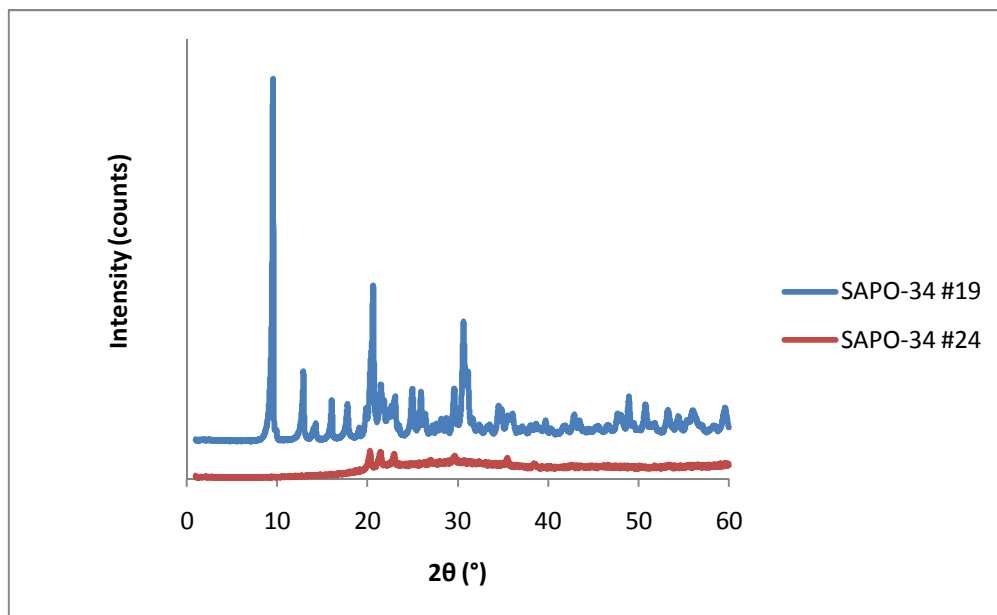


Figure 25. XRD pattern comparison of SAPO-34 #19 and SAPO-34 #24

6.2.2. N₂ Physisorption

Table 13 gives information about several physical properties of mesoporous SAPO-34 like catalysts, SAPO-34 #21, SAPO-34 #26 and SAPO-34 #28. All properties were found similar to each other except average pore diameter based on BJH method desorption. That property was measured as 2.1 nm, 17.4 nm, and 17.3 nm for SAPO-34 #21, SAPO-34 #26 and SAPO-34 #28, respectively. SAPO-34 #21 was synthesized at lower mixing temperature (30°C) compared to other two samples. At 30°C, the surfactant might not dissolve completely and be able to form homogeneous micelles causing lower pore diameter.

Table 13. Nitrogen adsorption desorption analysis results for SAPO-34 #21, SAPO-34 #26 and SAPO-34 #28

	SAPO-34 #21	SAPO-34 #26	SAPO-34 #28
Multipoint BET surface area (m²/g)	117	133	124
DR method micro pore area (m²/g)	95	87	232
BJH method adsorption average pore diameter (nm)	0.6	0.6	1.1
BJH method desorption average pore diameter (nm)	2.1	17.4	17.3
BJH method cumulative adsorption pore volume (cm³/g)	5.3 x 10 ⁻¹	5.1 x 10 ⁻¹	4.2 x 10 ⁻¹
BJH method cumulative desorption pore volume (cm³/g)	5.2 x 10 ⁻¹	4.9 x 10 ⁻¹	3.3 x 10 ⁻¹
DR method micro pore volume (cm³/g)	3.4 x 10 ⁻²	3.1 x 10 ⁻²	8.3 x 10 ⁻²

Figures 26-28 show nitrogen adsorption desorption isotherms of SAPO-34 #21, SAPO-34 #26, SAPO-34 #28, successively.

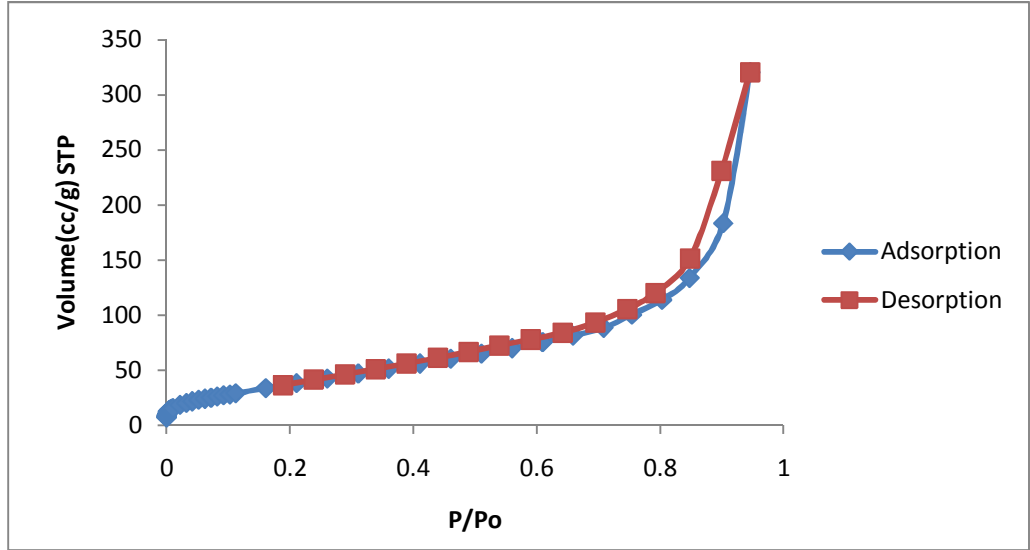


Figure 26. Nitrogen adsorption-desorption isotherms for SAPO-34 #21

Both isotherms behaved similar to type II isotherm with H3 hysteresis. The hysteresis of SAPO-34 #21 started around 0.7 whereas that of SAPO-34 #26 was seen to develop around 0.8. Type II isotherm is typical of macroporous structures.

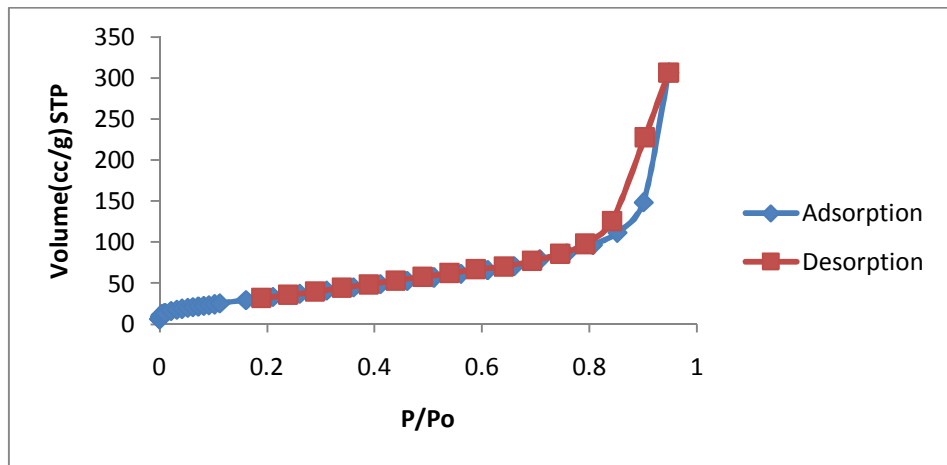


Figure 27. Nitrogen adsorption-desorption isotherms for SAPO-34 #26

Figure 28 illustrates the nitrogen adsorption-desorption isotherms for SAPO-34 #28 catalyst where the isotherms were also of type II with hysteresis type H3 showing macroporous structure. The hysteresis started around 0.8.

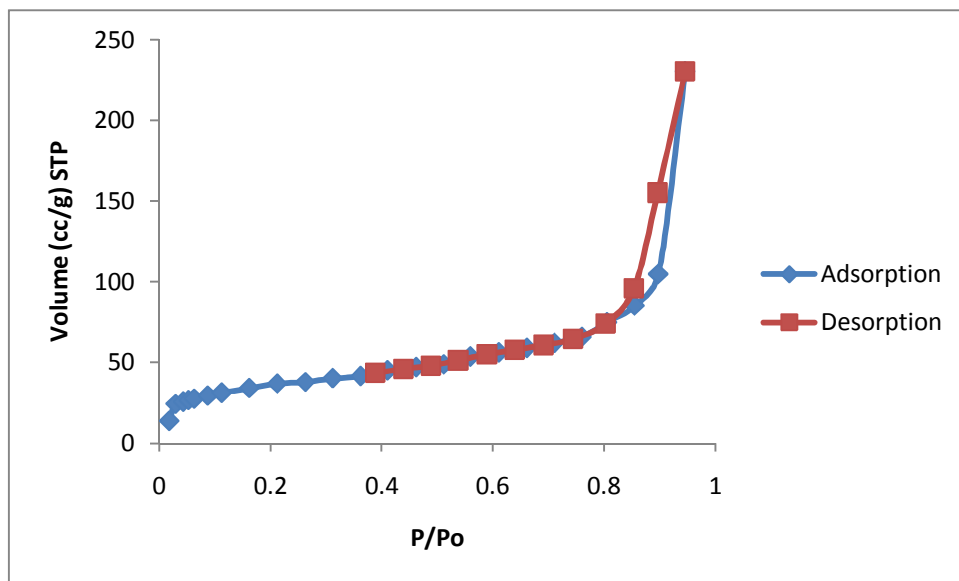


Figure 28. Nitrogen adsorption-desorption isotherms for SAPO-34 #28

Figures 29 and 30 depict pore size distributions of SAPO-34 #21 according to the application of BJH method to adsorption and desorption branches. Those graphs show the existence of micropores, mesopores.

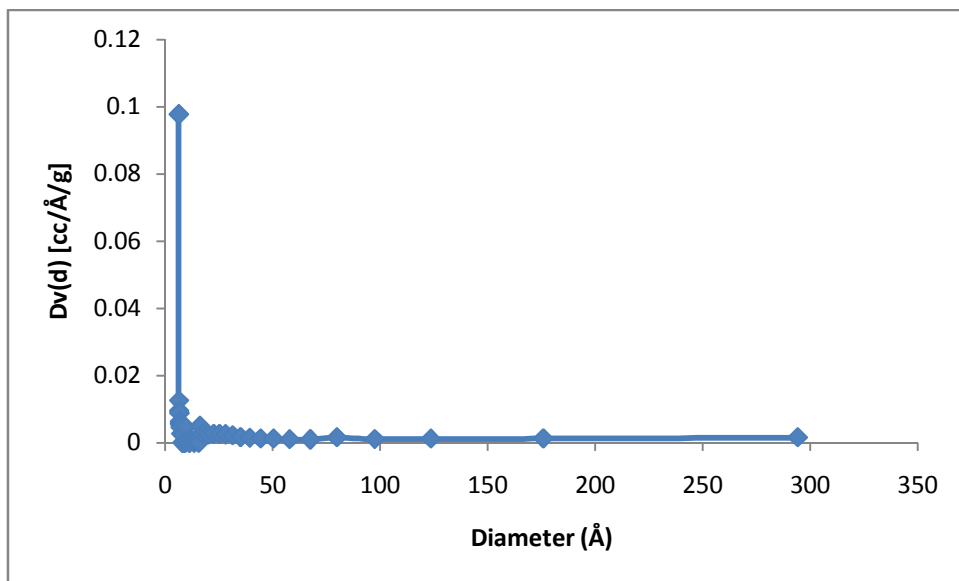


Figure 29. Pore size distribution of SAPO-34 #21 based on BJH adsorption

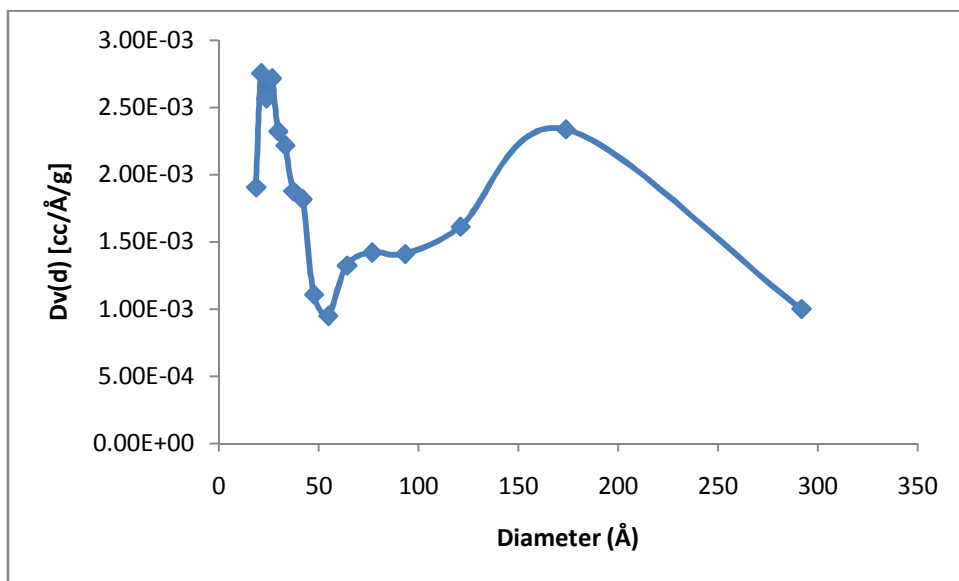


Figure 30. Pore size distribution of SAPO-34 #21 based on BJH desorption

The same phenomenon was valid for SAPO-34 #26, too. From Figures 31 and 32, it can be concluded that there were micropores, mesopores in the structure.

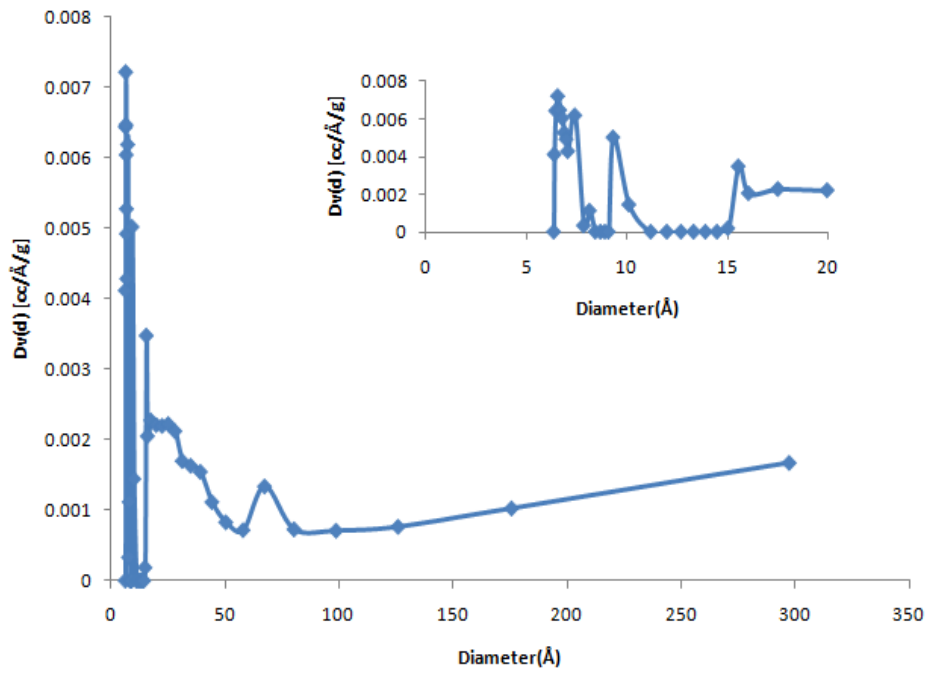


Figure 31. Pore size distribution of SAPO-34 #26 based on BJH adsorption

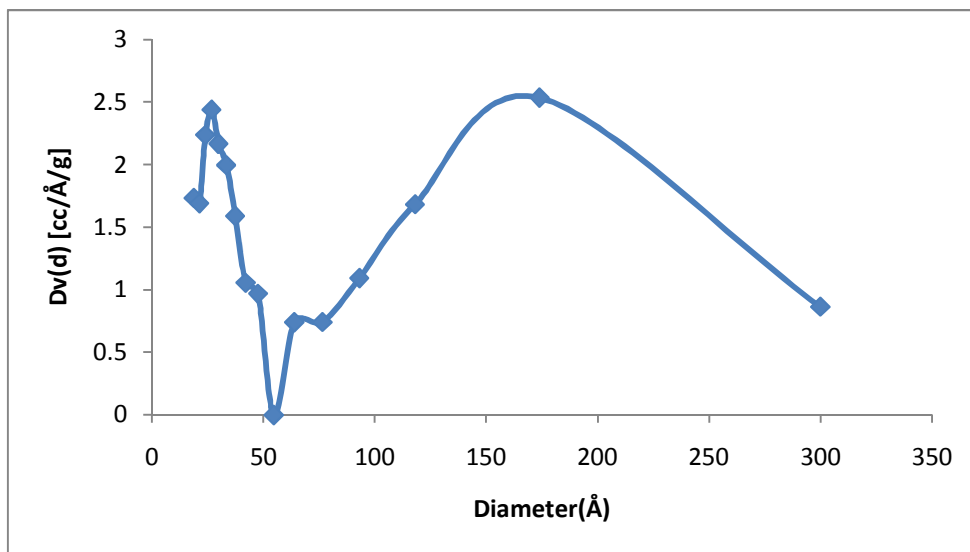


Figure 32. Pore size distribution of SAPO-34 #26 based on BJH desorption

Figures 33 and 34 depict pore size distributions of SAPO-34 #28 according to BJH method, respectively. Those graphs illustrate the existence of micropores and mesopores.

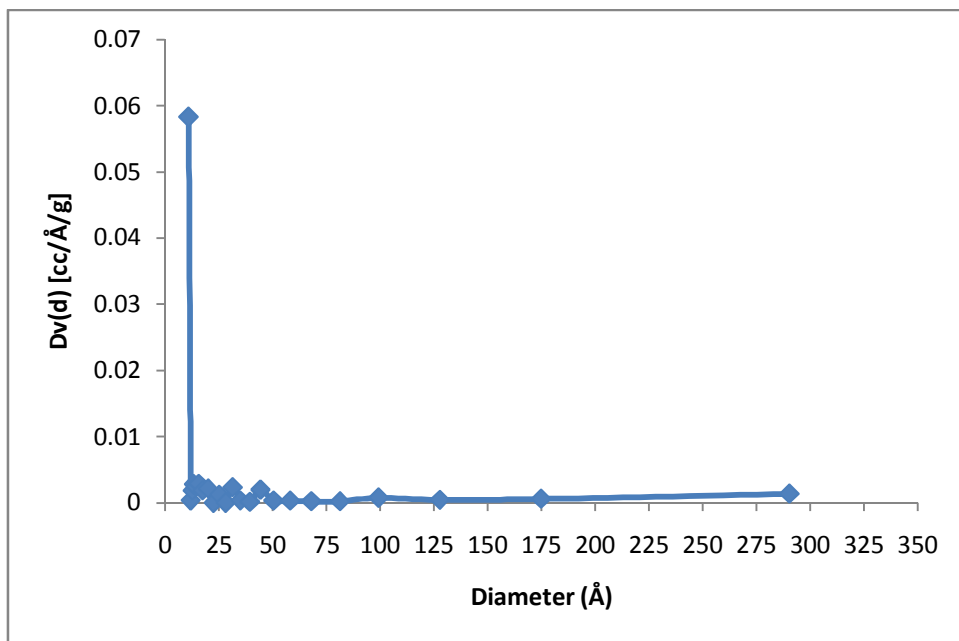


Figure 33. Pore size distribution of SAPO-34 #28 based on BJH adsorption

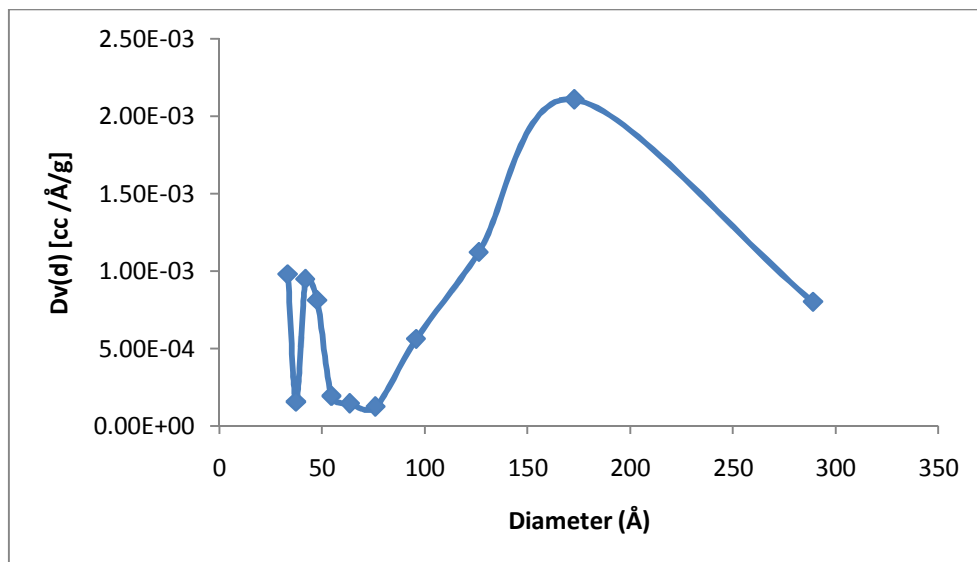


Figure 34. Pore size distribution of SAPO-34 #28 based on BJH desorption

6.2.3. Scanning Electron Microscopy (SEM)

Previously, it was observed that microporous SAPO-34 catalyst had cubic-like shaped structure. However, mesoporous SAPO-34 like catalysts exhibited structures with irregular shapes. Several examples of them are shown in Figure 35. SEM images of other samples are given in Appendix D. Among them, it can be seen that structures of SAPO-34 #20 and SAPO-34 #24 had apparent voids.

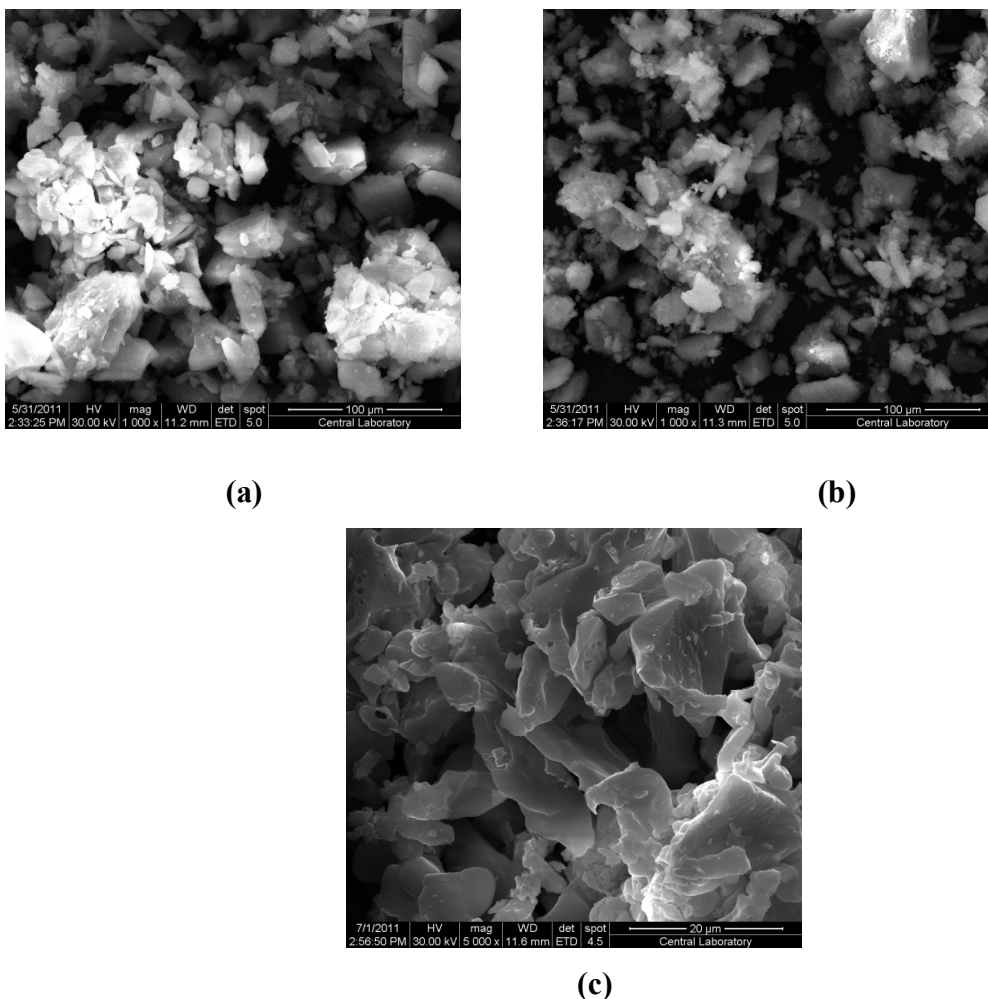


Figure 35. SEM images of (a) SAPO-34 #21, (b) SAPO-34 #26, (c) SAPO-34 #20 catalysts

6.2.4. Energy Dispersive X-Ray Spectroscopy (EDS)

EDS analysis results for SAPO-34 #21 and SAPO-34 #26 are shown in Table 14. These results show that a low amount of silicon was incorporated into SAPO-34 #21 structure. In SAPO-34 #26, a higher silicon proportion was observed. During the synthesis of both catalysts, phosphorus was lost in a considerable amount. EDS results for other samples are given in Appendix C.

Table 14. EDS results for SAPO-34 #21 and SAPO-34 #26

	Ratio	Atomic Ratio (EDS)	Atomic Ratio (Solution)
SAPO-34 #21	Si/Al	0.04	0.15
	Si/P	0.06	0.15
	Al/P	1.61	1
SAPO-34 #26	Si/Al	0.15	0.15
	Si/P	0.26	0.15
	Al/P	1.81	1

6.2.5. Nuclear Magnetic Resonance (NMR)

²⁷Al NMR technique was applied to SAPO-34 #28. The result of ²⁷Al NMR shown in Figure 36 indicated that about 30 ppm a sharp peak was attained. This peak was assigned to tetrahedrally coordinated Al site whereas the broad peak around -15 ppm was assigned to octahedrally coordinated Al [46, 47]. This showed that aluminium

was mainly tetrahedrally coordinated along with some octahedrally coordinated ones. Other peaks might be due to spinning sidebands. [48]

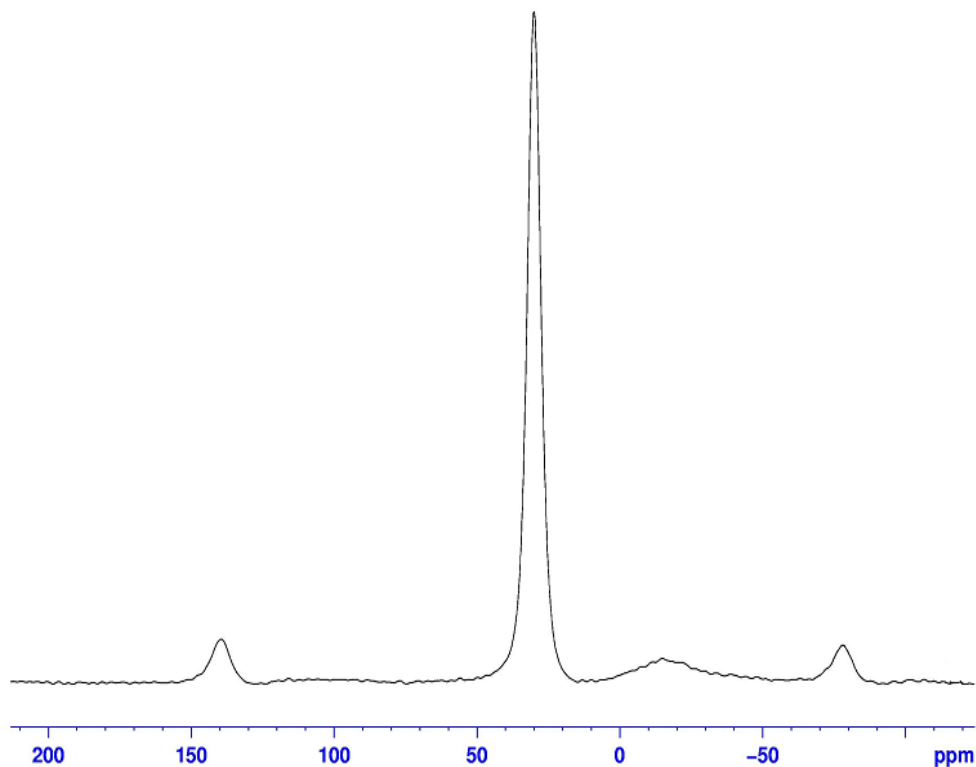


Figure 36. ^{27}Al NMR analysis result for SAPO-34 #28

6.3. ACTIVITY RESULTS OF SYNTHESIZED CATALYSTS

In this section, the results obtained from the testing of methanol dehydration reaction on several catalysts were discussed. The methanol conversion, selectivity and yield values were obtained with respect to temperature and activities of catalysts were compared. The yield, conversion and selectivity calculation results related to the

methanol dehydration reaction were shown in Appendix B. The tabulated form of the activity results of the catalysts are given in Appendix E and reaction raw data are presented in Appendix F. It was previously shown that methanol dehydration reaction was pressure insensitive and equilibrium conversion graph is presented in Appendix G [5]. For this reaction, firstly, microporous SAPO-34 catalyst was tested. Figure 37 shows the methanol conversion obtained by using SAPO-34 #19.

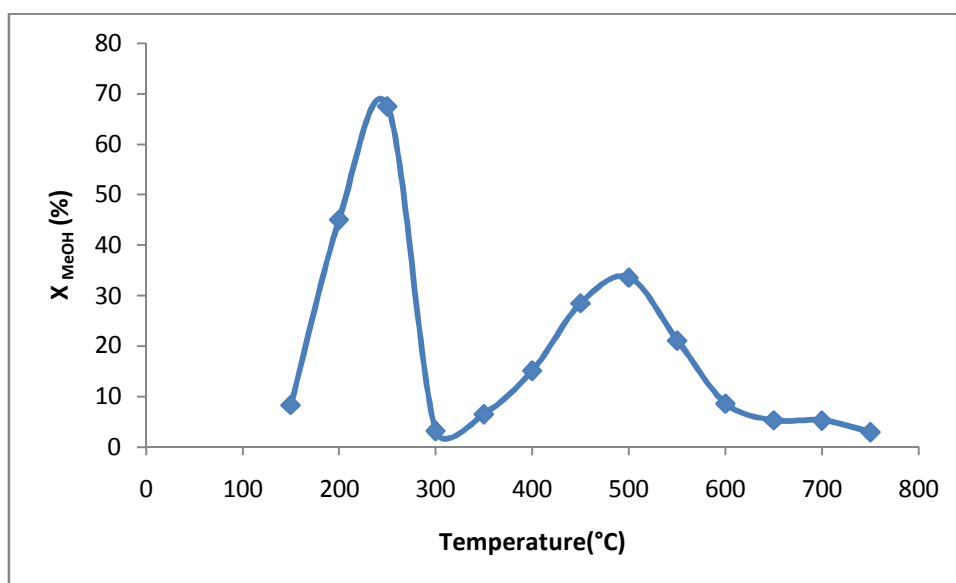


Figure 37. Methanol conversion on SAPO-34 #19 at 0.14 s.g/cm³

As seen in the figure, the maximum conversion was attained as 68% at 250°C. When the reaction temperature was increased to 300°C, the conversion decreased substantially. Further temperature increase caused methanol conversion to increase. At 500°C, a second highest methanol conversion was observed as 34%. Raising temperature above 500°C led to deactivation of the catalyst. This suggests that up to 300°C the reaction took place in the micropores of the catalyst where coke formation plugged them at 300°C. After 300°C, the reaction continued on mesopores of the

structure until they also were plugged by coke formation. The changes in selectivity and yield values were shown in Figures 38 and 39.

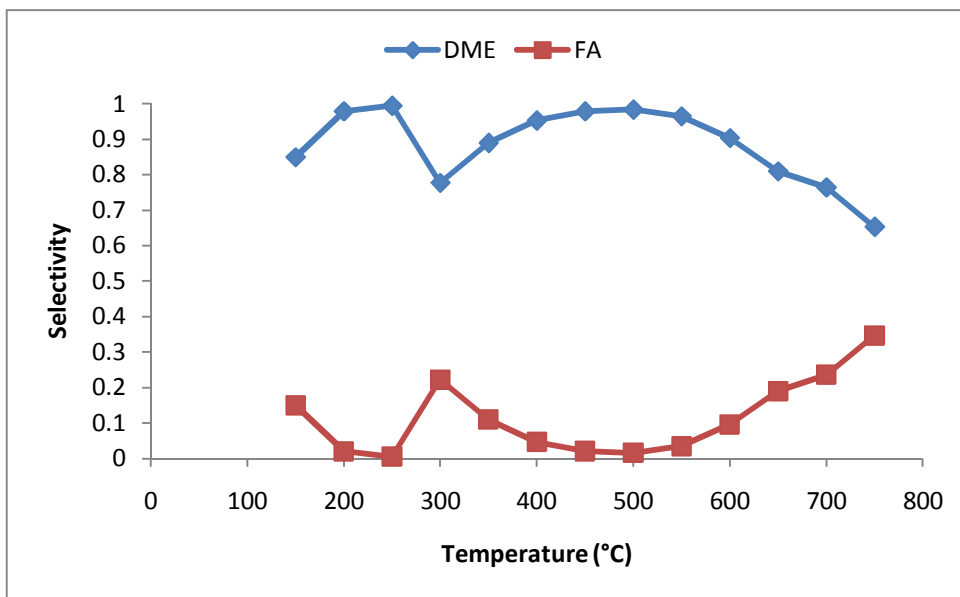


Figure 38. Selectivity values obtained by using SAPO-34 #19 at 0.14 s.g/cm³

Figure 38 shows that selectivity of DME was around 1 in a wide temperature range while formaldehyde selectivity became significant only after 600°C. Formaldehyde was formed by a side reaction shown below:



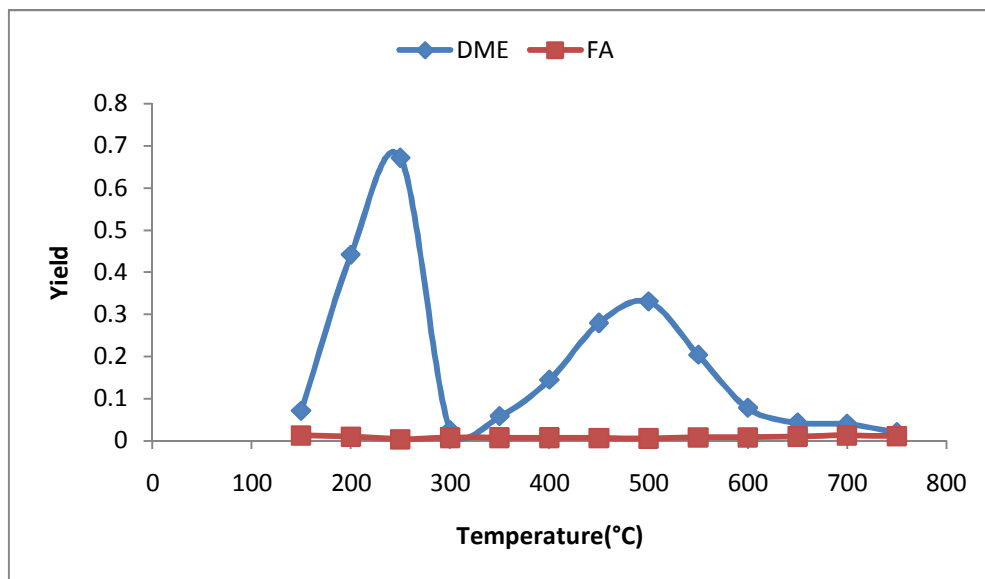


Figure 39. Yield values attained using SAPO-34 #19 catalyst at 0.14 s.g/cm³

The maximum dimethyl ether yield value was obtained at 250°C as 0.67 where the yield of formaldehyde was under 0.01 which are shown in Figure 39. The yield of DME showed a similar behavior to that of methanol conversion curve. Table 25 in Appendix E shows the activity test results of SAPO-34 #19.

A spent SAPO-34 #19 catalyst that was tested up to 300°C was characterized by XRD and TGA methods in order to understand the rapid decline in activity at 300°C. TGA analysis (Figure 40) showed that at around 600°C there was a substantial weight loss which was attributed to coke in graphitic form [53]. Besides, XRD of this spent catalyst (Figure 41) exhibited peaks at 2θ values of around 26° and 43° which might belong to deposited carbon. This implied, at 300°C, coke deposition occurred in SAPO-34 #19 catalyst probably blocking micropores of it. The reaction might continue in mesopores of the structure at higher temperatures. XRD data of carbon in graphite form were given in Appendix A.

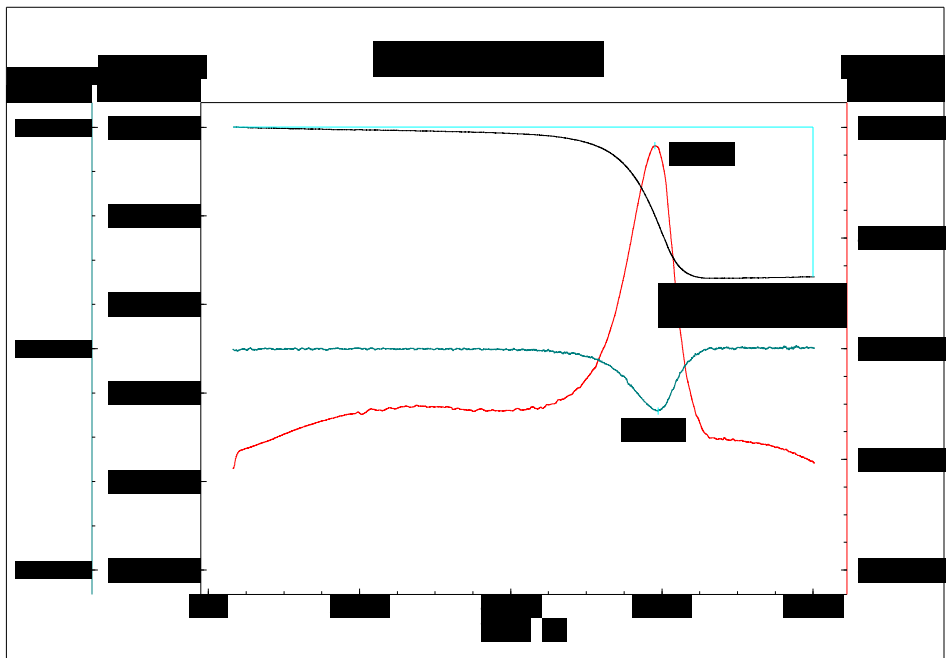


Figure 40. TGA analysis of spent SAPO-34 #19 catalyst

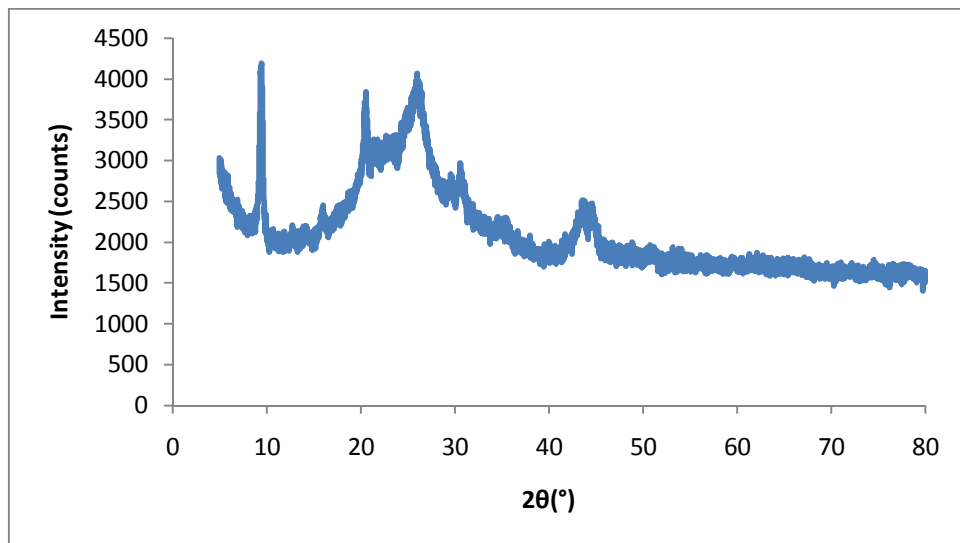


Figure 41. XRD pattern of spent SAPO-34 #19 catalyst

Activity test of SAPO-34 #19 was repeated two times. First one was the retesting of fresh SAPO-34 #19. Second one is the testing of regenerated SAPO-34 #19. The regenerated SAPO-34 #19 was obtained by calcining the used SAPO-34 #19 for 16 hours under air flow as described in Section 5.1. The activity results of them are shown in Figure 42. As seen from Figure 42, activity test result obtained by using fresh SAPO-34 #19 for the second time was very similar to that of attained by SAPO-34 #19, previously. However, the regenerated SAPO-34 #19 catalyst showed lower methanol conversions. This might imply that the pores of used SAPO-34 #19 were not opened up totally by calcination. The tabulated form of the activity results of them are given in Appendix E.

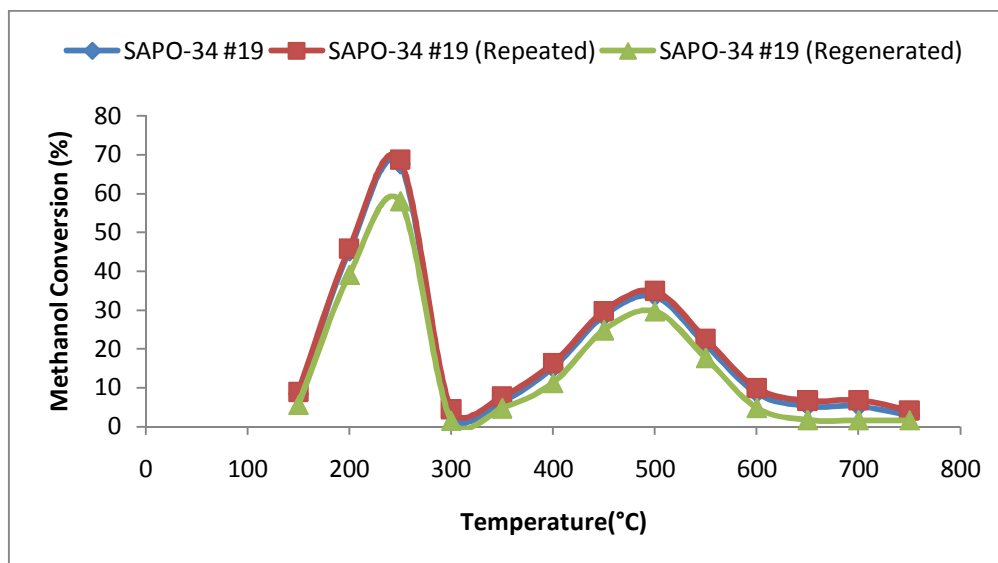


Figure 42. Activity test results of fresh and regenerated SAPO-34 #19 catalysts at 0.14 s.g/cm³

Activity results of mesoporous SAPO-34 like catalysts are depicted in Figures 43 and 44. They revealed that highest methanol conversion was achieved by using SAPO-34 #28 at 550°C around 49% (Figure 43). It had converted methanol to dimethyl ether

with selectivity value of 1 whereas dimethyl ether yield was about 0.49. The performance of SAPO-34 #21 was quite similar to that of SAPO-34 #28 (Figure 43). It gave 48% methanol conversion at 550°C with dimethyl ether selectivity of almost 1. The dimethyl ether yield was about 0.48. Trace amount of formaldehyde was also observed at 550°C. SAPO-34 #20 and SAPO-34 #24 showed the worst performances in the methanol dehydration reaction with methanol conversion less than 1% (Figure 44). No dimethyl ether formation was observed with the two catalysts. Usage of other catalysts led to methanol conversion about 20-30%. It can be concluded that catalysts synthesized at lower hydrothermal synthesis temperature (70°C) exhibited higher methanol conversion compared to the ones synthesized at higher hydrothermal synthesis temperature.

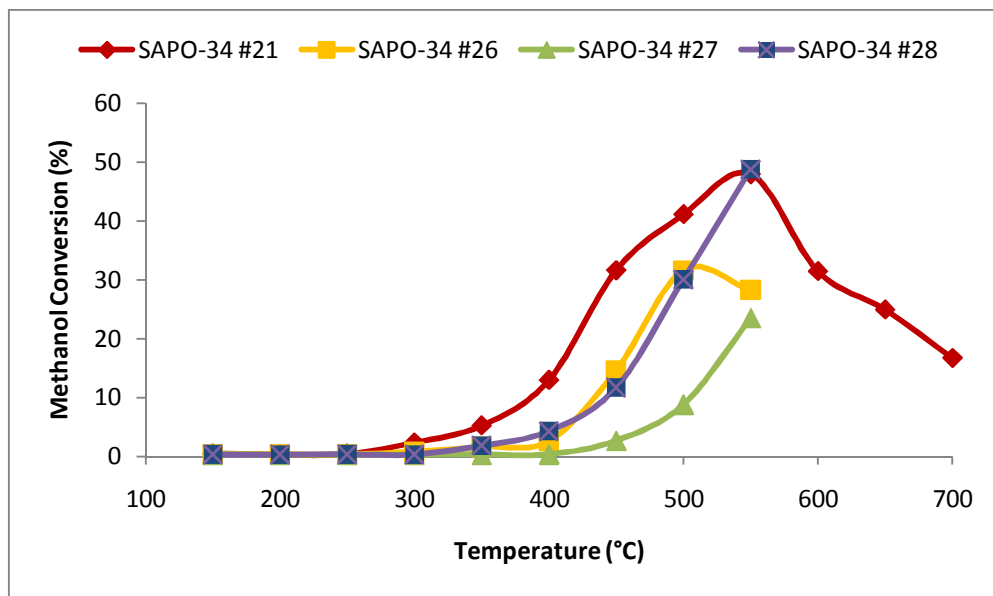


Figure 43. Activity results of SAPO-34 #21, SAPO-34 #26, SAPO-34 #27 and SAPO-34 #28 catalysts at 0.14 s.g/cm³

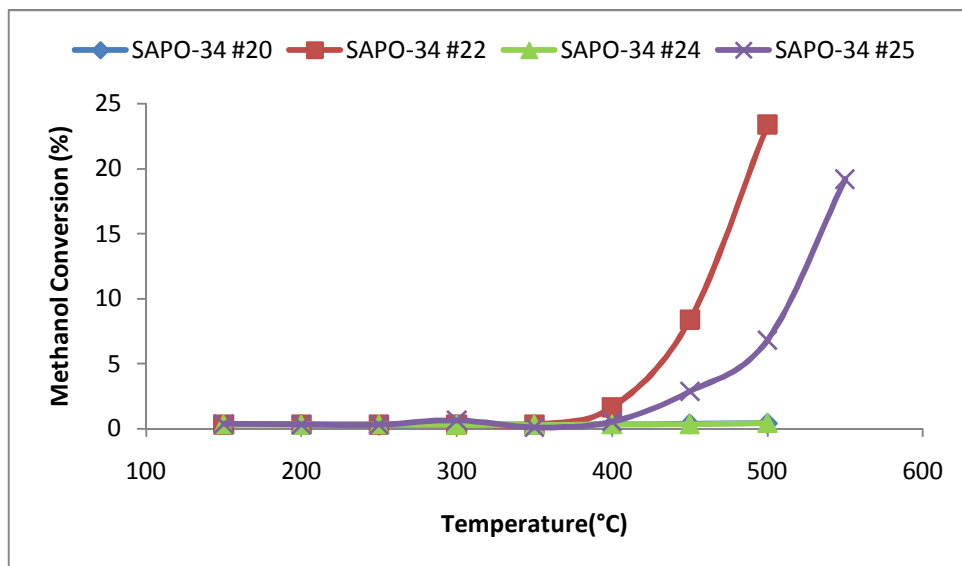


Figure 44. Activity results of SAPO-34 #20, SAPO-34 #22, SAPO-34 #24 and SAPO-34 #25 catalysts at 0.14 s.g/cm³

Figures 45, 46, 47 and 48 illustrate the selectivity and yield changes with respect to temperature for the mesoporous SAPO-34 like catalysts (SAPO-34 #21 and SAPO-34 #28) which gave the highest methanol conversions.

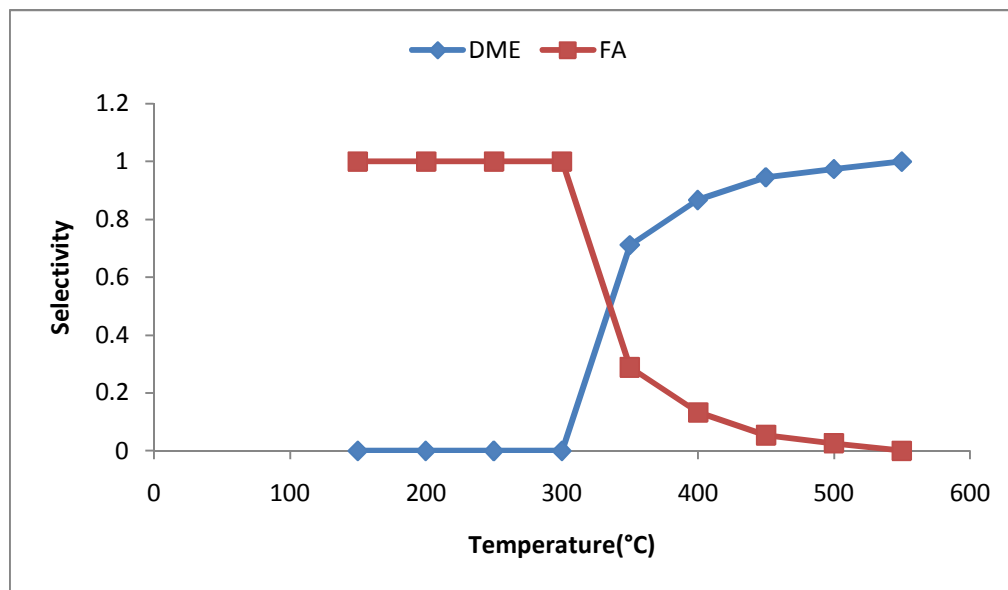


Figure 45. Selectivities obtained by using SAPO-34 #28 at 0.14 s.g/cm³

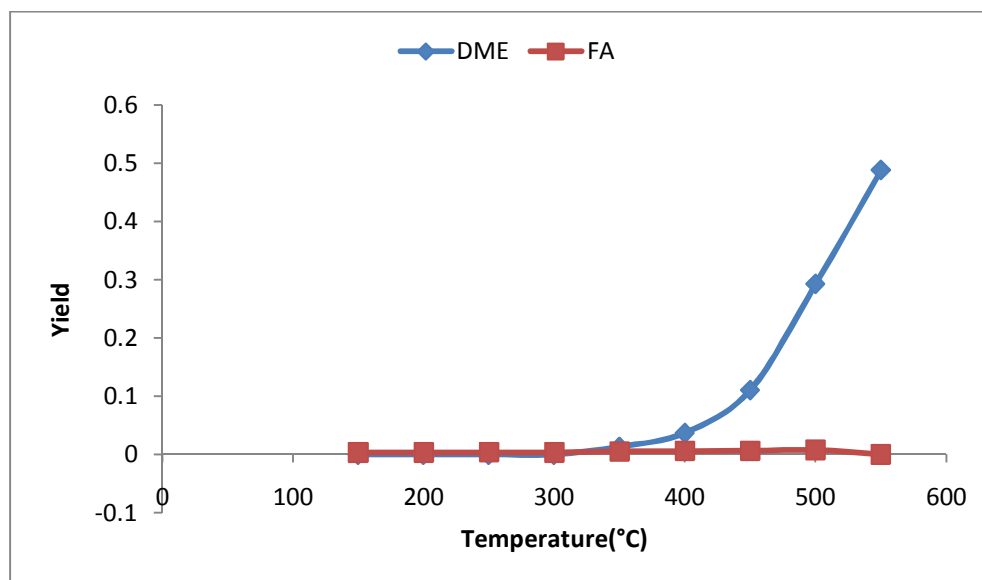


Figure 46. Yields obtained by using SAPO-34 #28 at 0.14 s.g/cm³

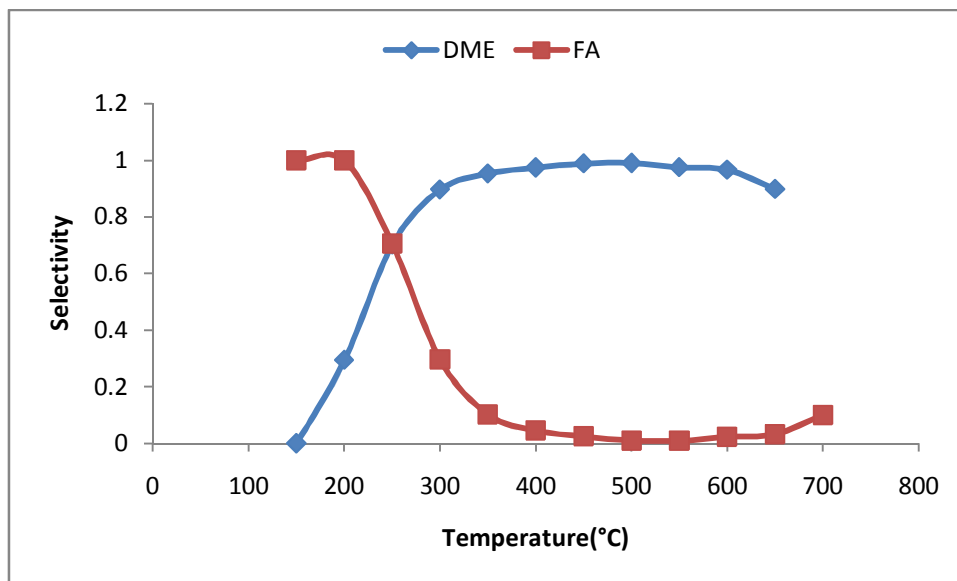


Figure 47. Selectivities obtained by using SAPO-34 #21 at 0.14 s.g/cm³

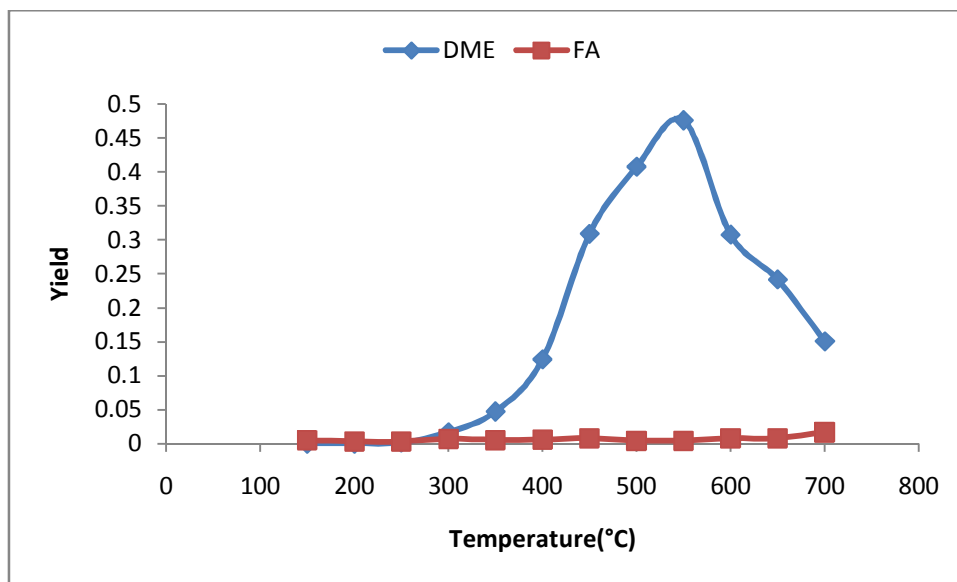


Figure 48. Yields obtained by using SAPO-34 #21 at 0.14 s.g/cm³

In the temperature range of 400-550°C, both catalysts produce dimethyl ether with high selectivity. They gave highest DME selectivity and yield values at 550°C.

CHAPTER 7

CONCLUSIONS AND RECOMMENDATIONS

In this thesis study, both microporous SAPO-34 and mesoporous SAPO-34 like catalytic materials were synthesized by following hydrothermal route. These catalysts were characterized by XRD, N₂ physisorption, SEM, EDS, NMR, TGA-DTA to reveal their structural properties. These catalysts were tested in vapor phase methanol dehydration reaction.

For the synthesis of microporous SAPO-34, it was found that the optimum mixing temperature was 40°C for the highest crystallinity. Besides, it was observed that keeping the temperature of the synthesis solution constant was crucial for crystallinity. The catalyst synthesized at constant mixing temperature, 40°C, had much higher crystallinity compared to the one synthesized without keeping the temperature constant at 40°C. The result of the activity test of microporous SAPO-34 catalyst implied that the reaction took place in both micropores and mesopores of the catalyst.

As the surfactant was changed from TEAOH to CTMABr for the synthesis of mesoporous SAPO-34 like catalyst, it was observed that the pore sizes increased as expected. However, the structure of SAPO-34 was distorted. It was observed that when mixing temperature was 30°C, SAPO-34 structure could not be attained by using either of the surfactants. The activity tests of mesoporous SAPO-34 like catalysts showed that methanol dehydration reaction took place at much higher temperatures compared to the ones for the case of microporous SAPO-34. Moreover, the maximum methanol conversion decreased to 49% which was 67% for microporous SAPO-34 catalyst. This shows that mesoporous structured catalysts might have lower acidity. It was observed

that the activities of all the catalysts synthesized in this thesis study were lower than the activities reported in the literature [54]. This might be due to the lower acidity of the catalysts synthesized in this study. To enhance the acidity of them, some active metal might be incorporated to the structure so that activity could be increased.

Since microporous SAPO-34 gave higher conversion at lower temperatures (67% conversion at 250°C), it appeared that mesoporous SAPO-34 like catalysts were not much appropriate for the reaction studied.

REFERENCES

- [1] Dogu, T., Varisli, D., “Alcohols as Alternatives to Petroleum for Environmentally Clean Fuels and Petrochemicals”, Turkish Journal of Chemistry, 2007, 31, 551-567.
- [2] Zhang, D., Wei, Y., Xu, L., Chang, F., Liu, Z., Meng, S., Su, B., Liu, Z., “MgAPSO-34 molecular sieves with various Mg stoichiometries: Synthesis, characterization and catalytic behavior in the direct transformation of chloromethane into light olefins” Microporous and Mesoporous Materials, 2008, 116, 684-692.
- [3] Marchese, L., Frache, A., Gatti, G., Coluccia, S., Lisi, L., Ruoppolo, G., Russo, G., Pastore, H.O., “Acid SAPO-34 Catalysts for Oxidative Dehydrogenation of Ethane” Journal of Catalysis, 2002, 208, 479-484.
- [4] Olah, G.A., Goeppert, A., Prakash, G.K.S., “Beyond Oil and Gas: The Methanol Economy”, Wiley- VCH, 2006, Weinheim.
- [5] Ciftci, A., “Nanocomposite Nafion and Heteropolyacid Incorporated Mesoporous Catalysts For Dimethyl Ether Synthesis From Methanol ”, M.S. Thesis, Middle East Technical University, Ankara, Turkey, August 2009.
- [6] U.S. DOE Energy Efficiency and Renewable Energy (EERE) Home Page, <http://www.eere.energy.gov/>,
http://www1.eere.energy.gov/vehiclesandfuels/pdfs/basics/jtb_diesel_engine.pdf, last visited on 1 August 2011.
- [7] Ertl, G., “Handbook of heterogeneous catalysis”, Volume 6, Wiley – VCH, 2008, Weinheim.

- [8] Wikipedia the Free Encyclopedia, http://www.wikipedia.org/Main_Page, http://en.wikipedia.org/wiki/Dimethyl_ether, last visited on 1 August 2011.
- [9] Semelsberger, T.A., Borup, R.L., Greene, H.L., “Dimethyl ether (DME) as an alternative fuel”, *Journal of Power Sources*, 2006, 156, 497-511.
- [10] DME - 21st Century Energy, <http://www.aboutdme.org>, <http://www.aboutdme.org/index.asp?sid=48>, last visited on 1 August 2011.
- [11] DME - 21st Century Energy, <http://www.aboutdme.org>, <http://www.aboutdme.org/index.asp?bid=275>, last visited on 1 August 2011.
- [12] Tokay, K.C., “Dimethyl Ether (DME) Synthesis Over Novel Mesoporous Catalysts”, M.S. Thesis, Middle East Technical University, Ankara, Turkey, August 2008.
- [13] Xu, M., Goodman, D.W., Bhattacharyya, A., “Catalytic dehydration of methanol to dimethyl ether (DME) over Pd/ Cab-O-Sil catalysts”, *Applied Catalysis A: General*, 1997, 149, 303-309.
- [14] Seo, Y.-H., Prasetyanto, E.A., Jiang, N., Oh, S.-M., Park, S.-E., “Catalytic dehydration of methanol over synthetic zeolite W”, *Microporous and Mesoporous Materials*, 2010, 128, 108-114.
- [15] Dai, W., Kong, W., Wu, G., Li, N., Li, L., Guan, N., “Catalytic dehydration of methanol to dimethyl ether over aluminophosphate and silico-aluminophosphate molecular sieves”, *Catalysis Communications*, 2011, 12, 535-538.
- [16] Liu, D., Yao, C., Zhang, J., Fang, D., Chen, D. “Catalytic dehydration of methanol to dimethyl ether over modified γ -Al₂O₃ catalyst”, *Fuel*, 2011, 90, 1738-1742.
- [17] Raouf, F., Taghizadeh, M., Eliassi, A., Yaripour, F., “Effects of temperature and feed composition on catalytic dehydration of methanol to dimethyl ether over γ -alumina”, *Fuel*, 2008, 87, 2967-2971.

- [18] Keshavarz, A.R., Rezaei, M., Yaripour, F., “Preparation of nanocrystalline γ -Al₂O₃ catalyst using different procedures for methanol dehydration to dimethyl ether”, *Journal of Natural Gas Chemistry*, 2011, 20, 334-338.
- [19] Ciftci, A., Sezgi, N.A., Doğu, T., “Nafion-Incorporated Silicate Structured Nanocomposite Mesoporous Catalysts for Dimethyl Ether Synthesis”, *Ind.Eng.Chem.Res.*, 2010, 49, 6753-6762
- [20] Varisli, D., Tokay, K.C., Ciftci, A., Dogu, T., Dogu, G., “Methanol dehydration reaction to produce clean diesel alternative dimethylether over mesoporous aluminosilicate-based catalysts”, *Turk. J. Chem.*, 2009, 33, 355-366.
- [21] Xu, L., Du, A., Wei, Y., Wang, Y., Yu, Z., He, Y., Zhang, X., Liu, Z., “Synthesis of SAPO-34 with only Si(4Al) species: Effect of Si contents on Si incorporation mechanism and Si coordination environment of SAPO-34”, *Microporous and Mesoporous Materials*, 2008, 115, 332-337.
- [22] Lok, B.M., Messina, C.A., Patton, R.L., Gajek, R.T., Cannan, T.R., Flanigen, E.M., “Silicoaluminophosphate Molecular Sieves: Another New Class of Microporous Crystalline Inorganic Solids”, *J.Am.Chem. Soc.*, 1984, 106, 6092-6093.
- [23] Wilson, S.T., “Synthesis of AlPO₄ – based molecular sieves”, *Studies in Surface Science and Catalysis*, Volume 58, 1991, 137-151.
- [24] Kulprathipanja, S., “Zeolites in Industrial Separation and Catalysis”, Wiley- VCH, 2010, Weinheim.
- [25] Liu, G., Tian, P., Zhang, Y., Li, J., Xu, L., Meng, S., Liu, Z., “Synthesis of SAPO-34 templated by diethylamine: Crystallization process and Si distribution in the crystals”, *Microporous and Mesoporous Materials*, 2008, 114, 416-423.
- [26] Nakatsuka, A., Okada, H., Fujiwara, K., Nakayama, N., Mizota, T., “Crystallographic configurations of water molecules and exchangeable cations in a

hydrated natural CHA-zeolite (chabazite)”, *Microporous and Mesoporous Materials*, 2007, 102, 188-195.

[27] Liu, Y., Wang, L., Zhang, J., “Preparation of floral mesoporous SAPO-34 with the aid of fluoride ion”, *Materials Letters*, 2011, 65, 2209-2212.

[28] Izadbakhsh, A., Farhadi, F., Khorasheh, F., Sahebdehfar, S., Asadi, M., Feng, Y.Z., “Effect of SAPO-34’s composition on its physico-chemical properties and deactivation in MTO process”, *Applied Catalysis A: General*, 2009, 364, 48-56.

[29] Zhang, D., Wei, Y., Xu, L., Chang, F., Liu, Z., Meng, S., Su, B.-L., Liu, Z., “MgAPSO-34 molecular sieves with various Mg stoichiometries: Synthesis, characterization and catalytic behavior in the direct transformation of chloromethane into light olefins”, *Microporous and Mesoporous Materials*, 2008, 116, 684-692.

[30] Nishiyama, N., Kawaguchi, M., Hirota, Y., Vu, D.V., Egashira, Y., Ueyama, K., “Size control of SAPO-34 crystals and their catalyst lifetime in the methanol-to-olefin reaction”, *Applied Catalysis A: General*, 2009, 362, 193-199.

[31] Y. Liu et al., *Micropor. Mesopor. Mater.* (2011), doi:10.1016/j.micromeso.2011.05.009

[32] Dubois, D.R., Obrzut, D.L., Liu, J., Thundimadathil, J., Adekkanattu, P.M., Guin, J.A., Punnoose, A., Seehra, M.S., “Conversion of methanol to olefins over cobalt-, manganese- and nickel-incorporated SAPO-34 molecular sieves”, *Fuel Processing Technology*, 2003, 83, 203-218.

[33] Lok, B.M., Messina, C.A., Patton, R.L., Gajek, R.T., Cannan, T.R., Flanigen, E.M., “Crystalline Silicoaluminophosphates”, US Patent 4,440,871, 1984

[34] Lin, S., Li, J., Sharma, R.P., Yu, J., Xu, R., “Fabrication of SAPO-34 Crystals with Different Morphologies by Microwave Heating”, *Top Catal*, 2010, 53, 1304-1310

- [35] Remy, T., Remi, J.C.S., Singh, R., Webley, P.A., Baron, G.V., Denayer, J.F.M., “Adsorption and Separation of C1-C8 Alcohols on SAPO-34”, *J.Phys.Chem.C*, 2011, 115, 8117-8125
- [36] PANalytical - XRD and XRF Analytical Instruments, <http://www.panalytical.com>, <http://www.panalytical.com/index.cfm?pid=135>, last visited on 1 August 2011
- [37] Niemantsverdriet, J.W., “Spectroscopy in Catalysis”, Wiley-VCH, 3rd Ed., 2007, Weinheim.
- [38] The A to Z of Materials and AZojomo – The “AZo Journal of Materials Online”, <http://www.azom.com>, <http://www.azom.com/article.aspx?ArticleID=4232>, last visited on 1 August 2011
- [39] Surface Area Analyzers, Pore Size Analyzers, Density Analyzers, Chemisorption Analyzers, Water Sorption Analyzers, Zeta Potential Analyzers, <http://www.quantachrome.com/>, <http://www.quantachrome.com/gassorption/>, last visited on 1 August 2011
- [40] SERC, <http://serc.carleton.edu/index.html>, http://serc.carleton.edu/research_education/geochemsheets/techniques/SEM.html, last visited on 1 August 2011
- [41] Intertek, <http://www.intertek.com>, <http://www.intertek.com/analysis/microscopy/edx/>, last visited on 1 August 2011
- [42] An Introduction to EDX (Energy Dispersive X-ray Analysis) and EPMA (Electron Probe Micro Analysis), <http://www.uksaf.org/>, <http://www.uksaf.org/tech/edx.html>, last visited on 1 August 2011
- [43] MEE - independent laboratory solving materials-related problems for a diverse clientele, <http://mee-inc.com/>, <http://mee-inc.com/eds.html>, last visited on 1 August 2011

- [44] Thermal Analysis, http://web.abo.fi/institut/biofuelsGS-2/kursen/%C3%85A/lectures/Lecture_Thermal%20Analysis.pdf, last visited on 1 August 2011
- [45] Cao, G., Shah, M.J., Brody, J.F., “Synthesis of Silicoaluminophosphates”, US Patent Application Publication, US 2005/0009691A1, 2005.
- [46] Yan, Z.M., Zhuang, J.Q., Xu, L., Han, X.W., Liu, Z.M., Bao, X.H., “Direct Observation of Various Al Sites in SAPO-34 by ^{27}Al Multiquantum (MQ) Magic Angle Spinning (MAS) NMR”, Chinese Chemical Letters, 2003, Vol. 14, No.1, pp 87-90
- [47] Buchholz, A., Wang, W., Arnold, A., Xu, M., Hunger, M., “Successive steps of hydration and dehydration of silicoaluminophosphates H-SAPO-34 and H-SAPO-37 investigated by in situ CF MAS NMR spectroscopy”, Microporous and Mesoporous Materials, 2003, 57, 157-168
- [48] Chakraborty, B., Pulikottil, A.C., Das, S., Viswanathan, B., “Synthesis and characterization of mesoporous silicoaluminophosphate”, Studies in Surface Science and Catalysis, 1998, 113, 631-636.
- [49] Wei, Y., He, Y., Zhang, D., Xu, L., Meng, S., Liu, Z., Su, B.-L., “Study of Mn incorporation into SAPO framework: Synthesis, characterization and catalysis in chloromethane conversion to light olefins”, Microporous and Mesoporous Materials, 2006, 90, 188-197
- [50] Hirota, Y., Murata, K., Tanaka, S., Nishiyama, N., Egashira, Y., Ueyama, K., “Dry gel conversion synthesis of SAPO-34 nanocrystals”, Materials Chemistry and Physics, 2010, 123, 507-509.
- [51] Venna, S.R., Carreon, M.A., “Synthesis of SAPO-34 crystals in the presence of crystal growth inhibitors”, J. Phys. Chem. B, 2008, 112, 16261-16265.

[52] Sener, C., “Synthesis and Characterization of Pd-MCM-Type Mesoporous Nanocomposite Materials”, M.S. Thesis, Middle East Technical University, Ankara, Turkey, January 2006.

[53] Cerritos, R.C., Ramirez, R.F., Alvarado, A.F.A., Rosales, J.M.M, Garcia, T.V., Esquivel, R.G., “Steam Reforming of Ethanol over Ni/Al₂O₃-La₂O₃ Catalysts Synthesized by Sol-Gel”, doi: 10.1021/ie100636f

[54] Pop, G., Bozga, G., Ganea, R. Natu, N., “Methanol Conversion to Dimethyl Ether over H-SAPO-34 Catalyst”, *Ind.Eng.Chem.Res.*, 2009, 48, 7065-7071.

[55] International Centre for Diffraction Data, “Selected Powder Diffraction Data for Education & Training : Search Manual and Data Cards”, The Centre – Swartmore, 1988, PA

APPENDIX A

XRD DATA AND PATTERNS

A1. XRD DATA OF SAPO-34

Table 15. Generalized X-ray powder diffraction data of SAPO-34 [33]

2θ (°)	d (Å)	$100 \times I/I_0$
9.45-9.65	9.36-9.17	81-100
12.8-13.05	6.92-6.78	8-20
13.95-14.2	6.35-6.24	8-23
16.0-16.2	5.54-5.47	25-54
17.85-18.15	4.97-4.89	11-76
19.0	4.67	0-2
20.55-20.9	4.32-4.25	44-100
22.05-22.5	4.03-3.95	0-5
23.0-23.15	3.87-3.84	2-10
24.95-25.4	3.57-3.51	12-87
25.8-26.0	3.45-3.43	14-26
27.5-27.7	3.243-3.220	1-4
28.05-28.4	3.181-3.143	1-12
29.2-29.6	3.058-3.018	3-9

30.5-30.7	2.931-2.912	19-75
31.05-31.4	2.880-2.849	15-28
32.2-32.4	2.780-2.763	1-5
33.4-33.85	2.683-2.648	0-6
34.35-34.65	2.611-2.589	4-15
36.0-36.5	2.495-2.462	2-11
38.8-38.9	2.321-2.315	0-2
39.6-39.7	2.276-2.270	2-4
43.1-43.5	2.099-2.080	3-6
47.4-47.7	1.918-1.907	2-6
48.8-49.2	1.866-1.852	4-7
49.9-50.45	1.828-1.809	0-2
50.65-51.3	1.802-1.781	1-8
53.0-53.25	1.728-1.720	2-7
54.25-54.7	1.691-1.678	0-4
55.7-55.9	1.650-1.645	2-5

A2. XRD PATTERNS OF THE SYNTHESIZED CATALYSTS

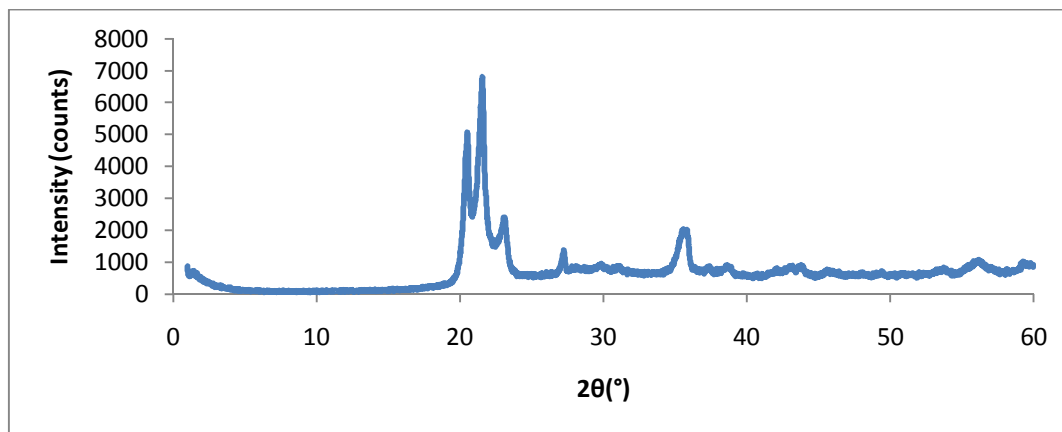


Figure 49. XRD pattern of SAPO-34 #22 (Mixing temperature: 40°C, initial pH: 2.14, hydrothermal synthesis temperature: 200°C)

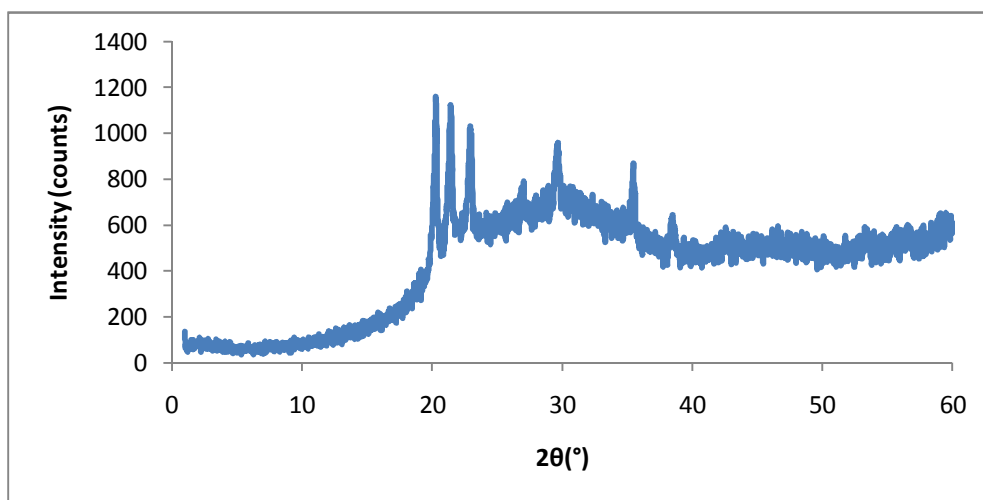


Figure 50. XRD pattern of SAPO-34 #24 (Mixing temperature: 40°C, initial pH: 6.70, hydrothermal synthesis temperature: 200°C)

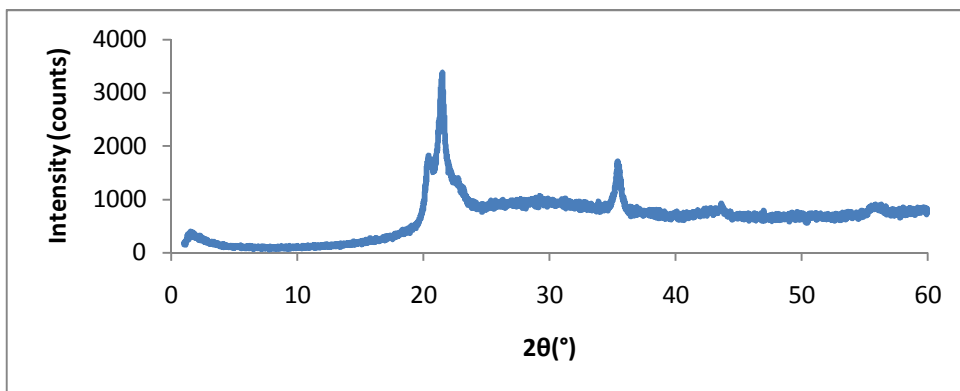


Figure 51. XRD pattern of SAPO-34 #25 (Mixing temperature: 30°C, initial pH: 6.71, hydrothermal synthesis temperature: 200°C)

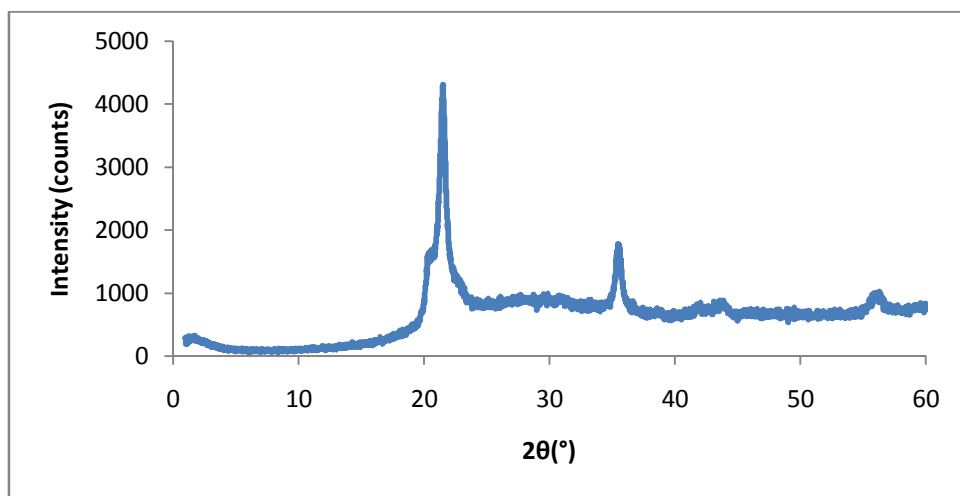


Figure 52. XRD pattern of SAPO-34 #27 (Mixing temperature: 30°C, initial pH: 6.71, hydrothermal synthesis temperature: 70°C)

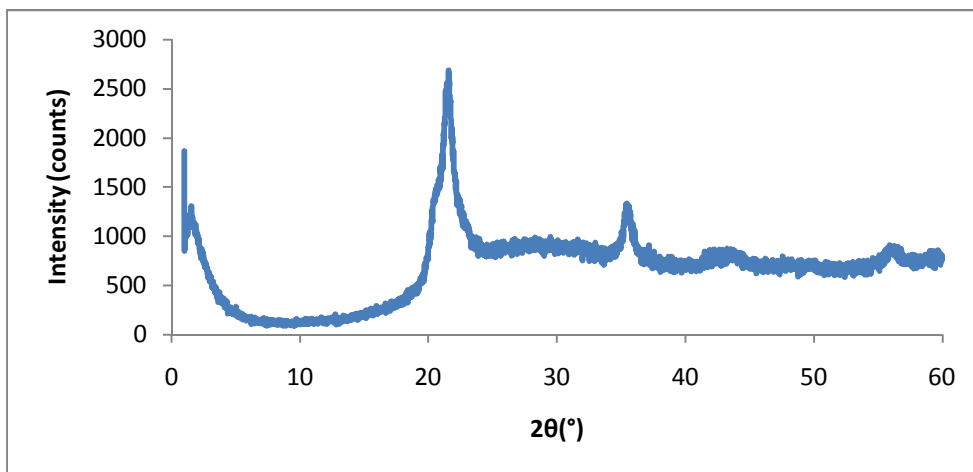


Figure 53. XRD pattern of SAPO-34 #28 (Mixing temperature: 40°C, initial pH: 2.13, hydrothermal synthesis temperature: 70°C)

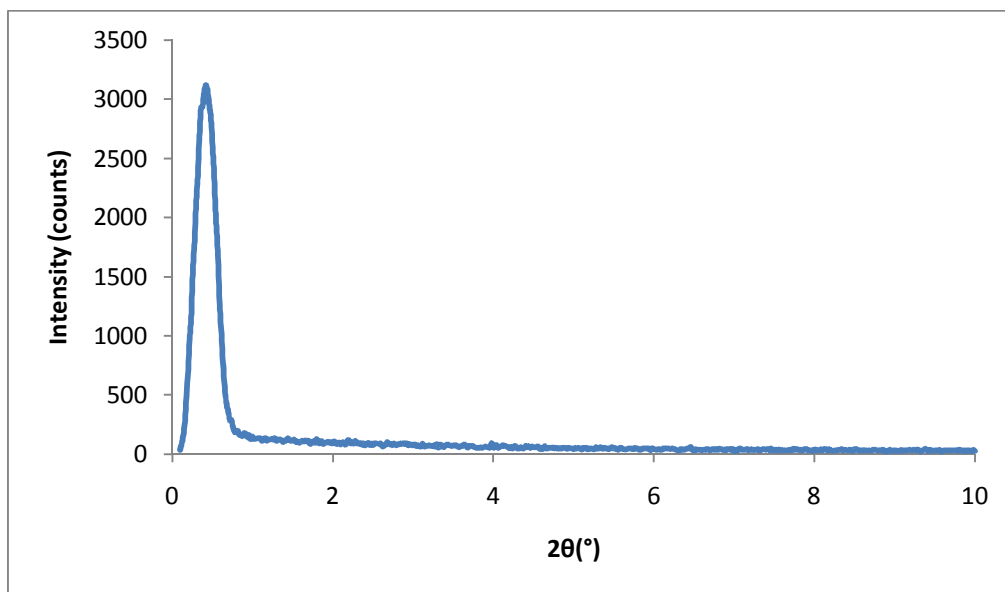


Figure 54. Low angle XRD pattern of SAPO-34 #20 (Mixing temperature: 30°C, initial pH: 2.28, hydrothermal synthesis temperature: 200°C)

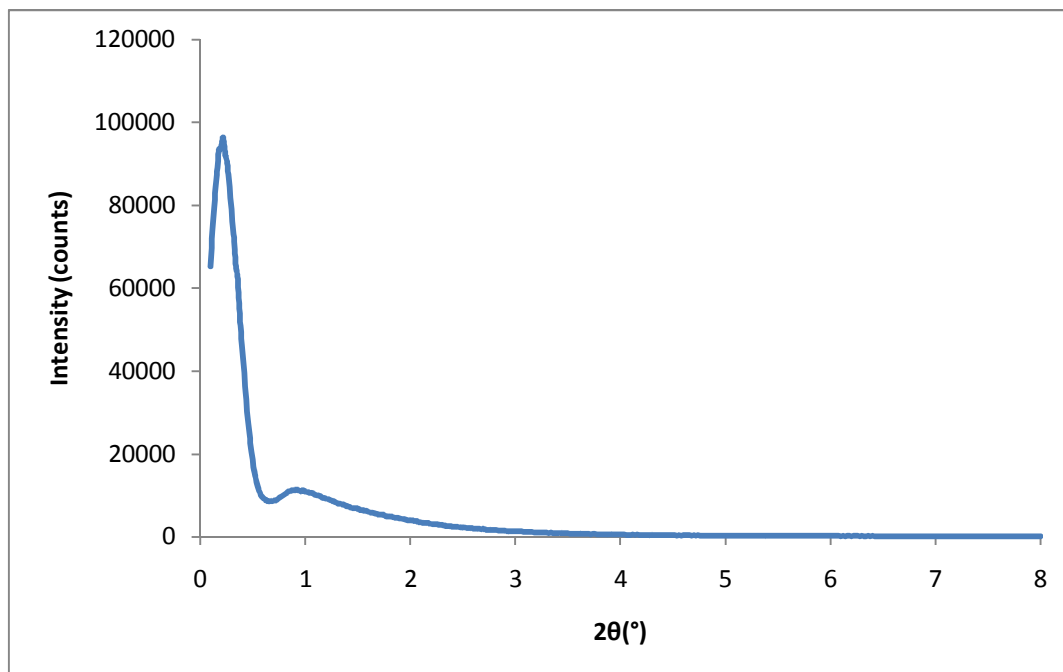


Figure 55. Low angle XRD pattern of SAPO-34 #26 (Mixing temperature: 40°C, initial pH: 6.70, hydrothermal synthesis temperature: 70°C)

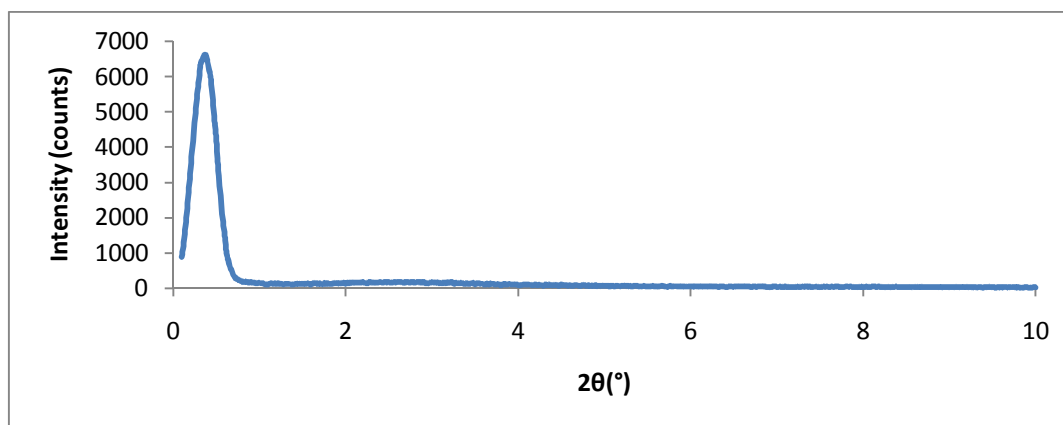


Figure 56. Low angle XRD pattern of SAPO-34 #27 (Mixing temperature: 30°C, initial pH: 6.71, hydrothermal synthesis temperature: 70°C)

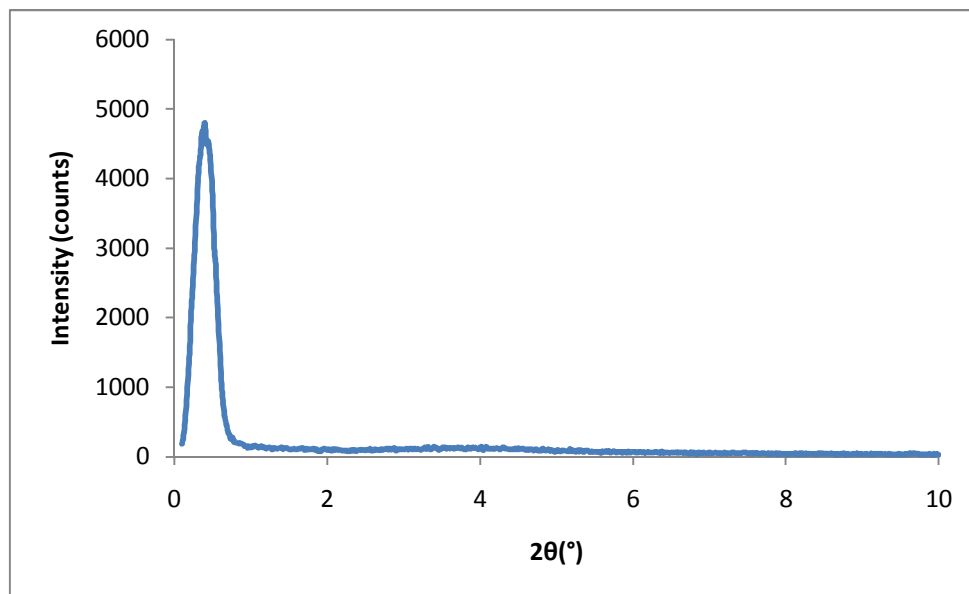


Figure 57. Low angle XRD pattern of SAPO-34 #28 (Mixing temperature: 40°C, initial pH: 2.13, hydrothermal synthesis temperature: 70°C)

Table 16. XRD data of SiO₂ [55]

d (Å)	2 θ (°)	Int	hkl
4.05	21.9272	100	101
3.53	25.2068	4	110
3.135	28.4457	11	111
2.841	31.4618	13	102
2.485	36.1136	20	200
2.465	36.4169	5	112
2.34	38.4364	1	201
2.118	42.6513	5	211
2.019	44.8533	3	202
1.929	47.0689	5	113
1.87	48.6483	7	212
1.757	52.0023	<1	220
1.73	52.8763	1	004
1.69	54.2289	3	203
1.634	56.249	1	104
1.612	57.0866	5	301
1.6	57.5546	3	213
1.571	58.7197	<1	310
1.567	58.8843	<1	222
1.533	60.3239	3	311
1.494	62.0701	5	302
1.431	65.1305	3	312
1.419	65.7505	3	204
1.398	66.8666	3	223
1.379	67.9121	<1	320
1.365	68.7054	3	214
1.352	69.4602	3	321
1.346	69.8147	<1	303
1.333	70.5964	3	105
1.299	72.7341	3	313
1.281	73.9244	3	322
1.242	76.657	<1	400
1.233	77.3197	1	224
1.223	78.0713	3	401
1.21	79.0731	3	205
1.206	79.3872	3	410
1.188	80.8359	1	411
1.183	81.249	1	323

Table 17. XRD data of AlPO₄ [55]

d (Å)	2 θ(°)	Int	hkl
5.012	17.68	1	110
4.077	21.78	100	111
3.553	25.04	3	020
3.539	25.14	3	200
3.496	25.46	3	002
3.162	28.20	10	021
2.867	31.17	10	112
2.506	35.80	20	220
2.491	36.02	5	022
2.135	42.30	5	311
2.038	44.41	3	222
1.949	46.56	7	023
1.888	48.15	5	132
1.779	51.31	<1	040
1.77	51.59	3	400
1.749	52.26	3	004
1.707	53.65	3	223
1.651	55.62	1	114
1.625	56.59	5	331
1.6163	56.92	3	133
1.5823	58.26	3	042
1.5452	59.80	3	421
1.5074	61.46	5	332
1.4431	64.52	3	422
1.4341	64.97	3	224
1.4101	66.22	1	403
1.3789	67.92	3	134
1.363	68.82	1	511
1.3582	69.10	1	333
1.3474	69.73	3	115
1.3104	72.00	3	423
1.2913	73.24	3	512
1.2443	76.49	<1	404
1.2333	77.30	1	441
1.2151	78.68	1	530
1.1977	80.05	<1	531
1.1936	80.38	1	513
1.1866	80.95	1	315
1.1794	81.55	<1	442

Table 18. XRD data of α -Al₂O₃ [55]

d (Å)	2 θ(°)	Int	hkl
3.479	25.58	75	012
2.552	35.13	90	104
2.379	37.78	40	110
2.165	41.68	<1	006
2.085	43.36	100	113
1.964	46.18	2	202
1.74	52.55	45	024
1.601	57.52	80	116
1.546	59.76	4	211
1.514	61.16	6	122
1.51	61.34	8	018
1.404	66.54	30	214
1.374	68.19	50	300
1.337	70.35	2	125
1.276	74.26	4	208
1.239	76.88	16	1010
1.2343	77.22	8	119
1.1898	80.69	8	220
1.16	83.21	<1	306
1.147	84.37	6	223
1.1382	85.18	2	131
1.1255	86.37	6	312
1.1246	86.46	4	128
1.0988	89.01	8	0210
1.0831	90.66	4	0012
1.0781	91.20	8	134
1.0426	95.25	14	226
1.0175	98.40	2	042
0.9976	101.09	12	2110
0.9857	102.78	<1	1112
0.9819	103.34	4	404
0.9431	109.52	<1	321
0.9413	109.83	<1	1211
0.9345	111.02	4	318
0.9178	114.12	4	229
0.9076	116.13	14	324
0.9052	116.62	4	0114
0.8991	117.89	8	410
0.8884	120.23	<1	235
0.8804	122.06	4	413
0.8698	124.64	2	048
0.858	127.72	12	1310
0.8502	129.91	4	3012
0.846	131.14	4	2014
0.8303	136.15	22	146
0.8137	142.38	4	1115
0.8072	145.19	11	4010
0.7988	149.27	7	054
0.797	150.23	14	1016
0.7931	152.43	13	330

Table 19. XRD data of Al(PO₃)₃ [55]

d(Å)	2 θ(°)	Int	hkl
5.61	15.78	25	211
4.85	18.28	18	220
4.34	20.45	100	310
3.67	24.23	55	321
3.432	25.94	60	400
3.07	29.06	30	420
2.927	30.51	45	332
2.801	31.92	6	422
2.692	33.25	30	510
2.507	35.79	14	521
2.354	38.20	20	530
2.227	40.47	18	611
2.171	41.56	12	620
2.118	42.65	6	541
2.024	44.74	2	631
1.981	45.76	10	444
1.941	46.76	8	710
1.903	47.75	6	640
1.869	48.68	18	721
1.835	49.64	2	642
1.743	52.45	14	651
1.69	54.23	2	741
1.6648	55.12	14	820
1.6412	55.98	6	653
1.6179	56.86	12	660
1.5963	57.70	18	750
1.5549	59.39	2	752
1.5349	60.24	2	840
1.4986	61.86	12	842
1.4803	62.71	10	761
1.4473	64.31	12	930
1.4161	65.90	8	932
1.4013	66.69	4	844
1.387	67.47	6	941
1.373	68.25	2	860
1.3594	69.03	2	772
1.3462	69.80	6	1020
1.3333	70.58	2	943
1.3092	72.08	10	1031

Table 20. XRD data of C [55]

d (Å)	2 θ(°)	Int	hkl
3.36	26.5048	100	002
2.13	42.3994	10	100
2.03	44.5972	50	101
1.8	50.6708	5	102
1.678	54.6489	80	004
1.544	59.8501	10	103
1.232	77.3942	30	110
1.158	83.3885	50	112
1.138	85.1952	5	105
1.12	86.9003	20	006
1.054	93.9049	5	201
0.994	101.592	40	114
0.841	132.66	10	
0.829	136.6	40	116
0.801	148.145	5	211

APPENDIX B

CONVERSION, YIELD AND SELECTIVITY CALCULATIONS ABOUT METHANOL DEHYDRATION REACTION SYSTEM

B1. RELATIONS FOR THE CALCULATIONS OF CONVERSION, SELECTIVITY AND YIELD

Total carbon atoms were found from

$$n_{Total} = 2 \times \beta_{DME} \times A_{DME} + \beta_{MeOH} \times A_{MeOH} + \beta_{FA} \times A_{FA}$$

Conversion, selectivity and yield calculations were done on carbon basis.

$$X_{MeOH} = \frac{n_{Total} - \beta_{MeOH} \times A_{MeOH}}{n_{Total}}$$

$$S_{DME} = \frac{2 \times \beta_{DME} \times A_{DME}}{n_{Total} - \beta_{MeOH} \times A_{MeOH}}$$

$$S_{FA} = \frac{\beta_{FA} \times A_{FA}}{n_{Total} - \beta_{MeOH} \times A_{MeOH}}$$

$$Y_{DME} = X_{Methanol} \times S_{DME}$$

$$Y_{FA} = X_{Methanol} \times S_{FA}$$

B2. CALCULATION OF METHANOL FLOW RATE

The flow rate of liquid methanol was set as 2.1 mL/hr. Thus, the flow rate of gaseous methanol at room temperature was

$$\rho = \frac{PM}{RT} = \frac{1.013 \text{ bar} \times 32.04 \text{ g/mol}}{83.14 \text{ cm}^3 \cdot \frac{\text{bar}}{\text{mol} \cdot \text{K}} \times 298 \text{ K}} = 1.31 \times 10^{-3} \text{ g/cm}^3$$

$$\frac{\rho_{liquid}}{\rho_{vapor}} = \frac{0.7918}{1.31 \times 10^{-3}} = 604$$

$$\frac{2.1 \text{ mL}}{h} \times \frac{1 \text{ hr}}{60 \text{ min}} \times 604 = 21.14 \text{ mL/min}$$

B3. CALCULATION OF HELIUM FLOW RATE

Helium flow rate was adjusted as 10 mL/26 seconds. Thus,

$$\frac{10 \text{ mL}}{26 \text{ sec}} \times \frac{60 \text{ sec}}{1 \text{ min}} = 23 \text{ mL/min}$$

B4. CALCULATION OF TOTAL FLOW RATE

$$F_{\text{total}} = F_{\text{methanol}} + F_{\text{helium}} = 21.14 \text{ mL/min} + 23 \text{ mL/min} = 44.14 \text{ mL/min}$$

Then, the ratio of methanol flow rate to the total flow rate was

$$\frac{F_{\text{methanol}}}{F_{\text{total}}} = \frac{21.14 \text{ mL/min}}{44.14 \text{ mL/min}} = 0.48$$

B5. GC CALIBRATION FACTORS AND RETENTION TIMES OF COMPONENTS

The table below indicates gas chromatography calibration factors and retention times of components included in the methanol dehydration reaction.

Table 21. Calibration factors and retention times for the species obtained

	Calibration Factor	Retention Time (min)
Dimethyl ether	0.76	5.2
Methanol	1	7.7
Formaldehyde	1.33	7.4
Water	2.53	6.9

APPENDIX C

EDS RESULTS OF THE SYNTHESIZED CATALYSTS

For all samples, Si/Al, Si/P and Al/P were 0.15, 0.15 and 1 in the initial synthesis solution, respectively.

Table 22. EDS analysis results of several catalysts

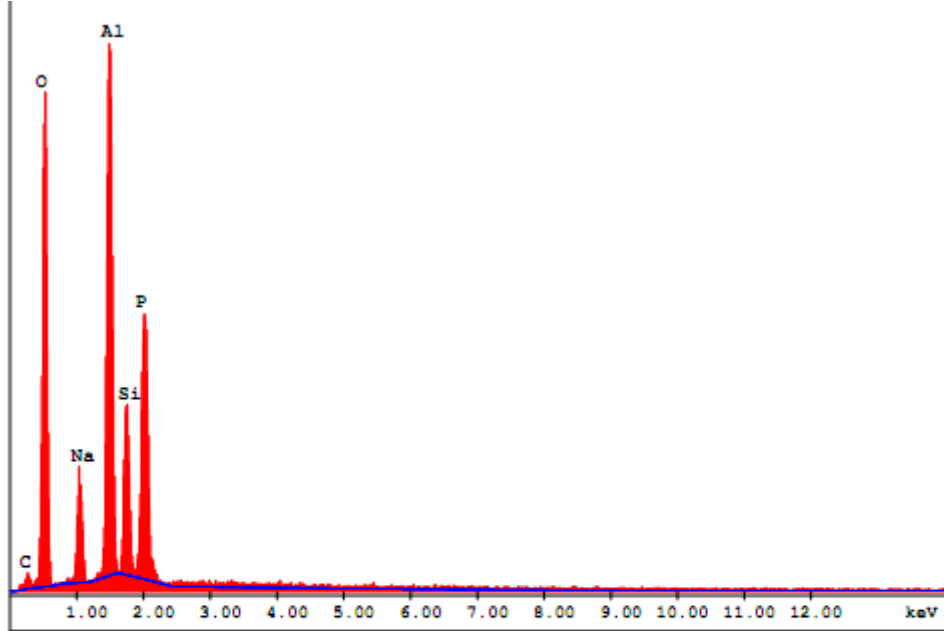
EDS Result	SAPO-34 #195	SAPO-34 #20	SAPO-34 #22	SAPO-34 #24	SAPO-34 #25	SAPO-34 #27	SAPO-34 #28
Si/Al	0.24	0.12	0.12	0.08	0.16	0.23	0.37
Si/P	0.31	0.15	0.17	0.08	0.23	0.31	0.63
Al/P	1.27	1.29	1.43	1.1	1.44	1.35	1.68

Table 23. Atomic percentages of Al, Si and P in several catalysts obtained by EDS

Atomic Percentage (%)	SAPO-34 #14	SAPO-34 #19	SAPO-34 #195	SAPO-34 #20	SAPO-34 #21	SAPO-34 #22
Al	10.8	9.4	15.2	13.5	15.0	17.7
Si	1.2	1.9	3.7	1.6	0.6	2.1
P	9.3	6.3	12.0	10.5	9.3	12.4

Table 24. Atomic percentages of Al, Si and P in several catalysts obtained by EDS

Atomic Percentage (%)	SAPO-34 #24	SAPO-34 #25	SAPO-34 #26	SAPO-34 #27	SAPO-34 #28
Al	13.2	13.3	19.9	16.3	12.6
Si	1.0	2.1	2.9	3.7	4.7
P	12.1	9.2	11.0	12.1	7.5



EDAX ZAF Quantification (Standardless)
 Element Normalized
 SEC Table : Default

Element	Wt %	At %	K-Ratio	Z	A	F
C K	9.12	14.33	0.0124	1.0393	0.1312	1.0006
O K	47.00	55.46	0.1280	1.0247	0.2656	1.0006
NaK	6.58	5.40	0.0188	0.9826	0.2953	1.0045
AlK	17.97	12.57	0.0878	0.9599	0.5061	1.0059
SiK	7.03	4.73	0.0308	0.9889	0.4404	1.0055
P K	12.31	7.50	0.0586	0.9571	0.4973	1.0000
Total	100.00	100.00				

Element	Net Inte.	Bkgd Inte.	Inte. Error	P/B
C K	13.11	2.51	8.47	5.22
O K	447.07	4.76	1.25	94.00
NaK	120.06	12.43	2.61	9.66
AlK	635.89	22.69	1.07	28.02
SiK	217.96	26.63	1.97	8.18
P K	392.04	21.67	1.39	18.09

Figure 58. EDS spectrum and data of SAPO-34 #28

APPENDIX D

SEM IMAGES OF SYNTHESIZED CATALYSTS

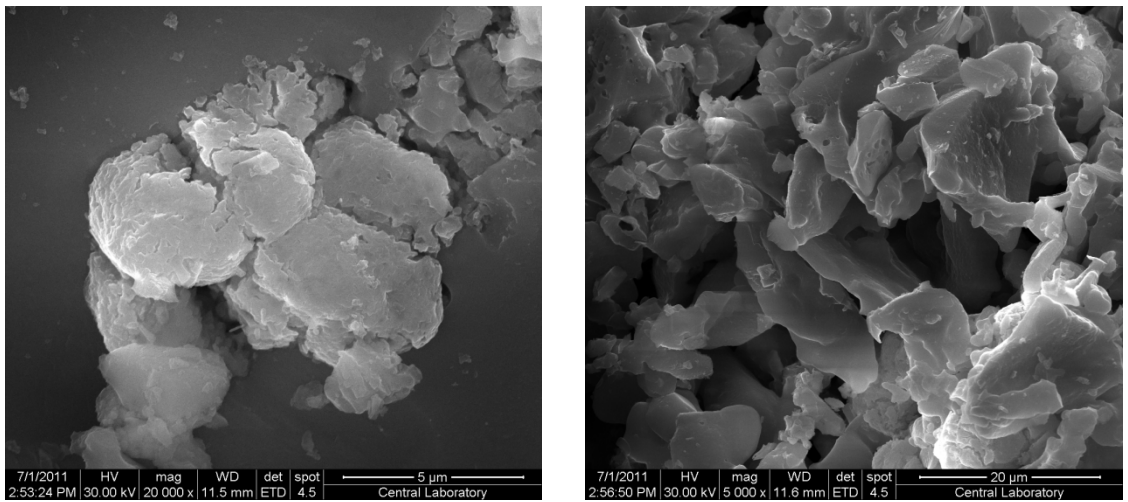


Figure 59. SEM images of SAPO-34 #20

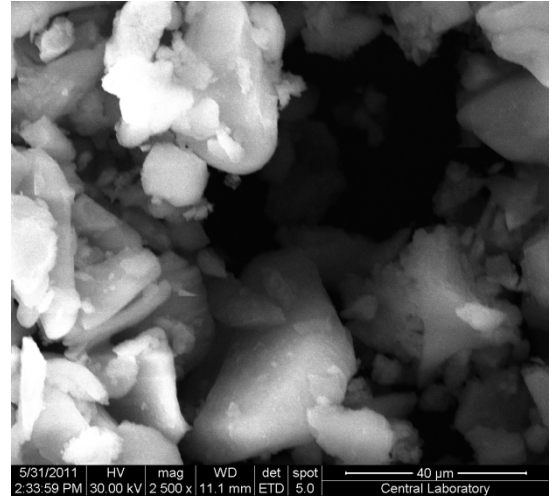
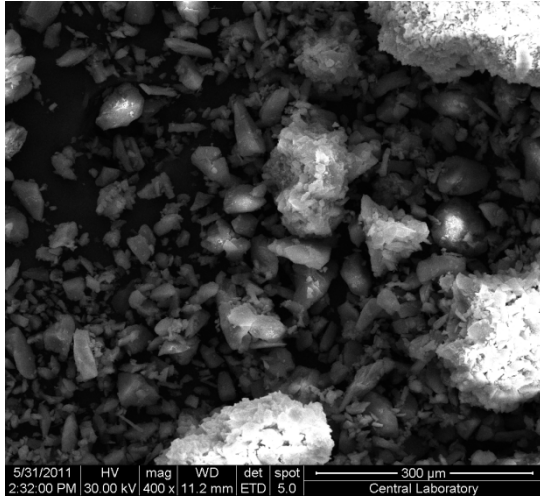


Figure 60. SEM images of SAPO-34 #21

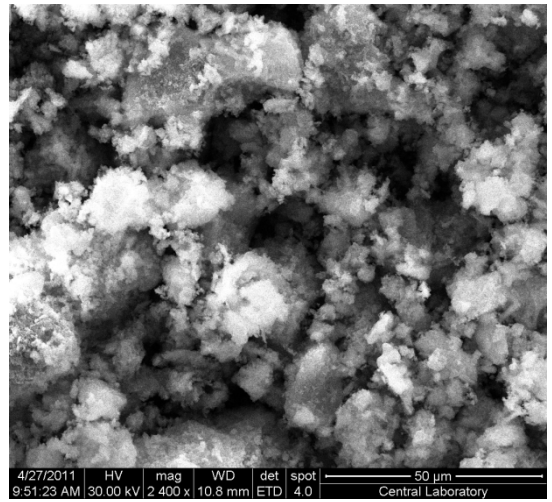
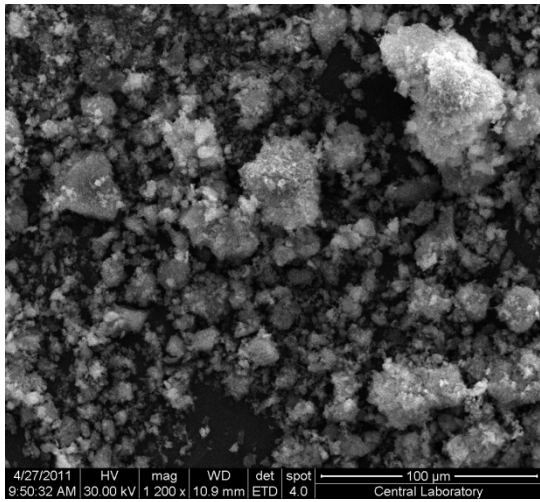


Figure 61. SEM images of SAPO-34 #22

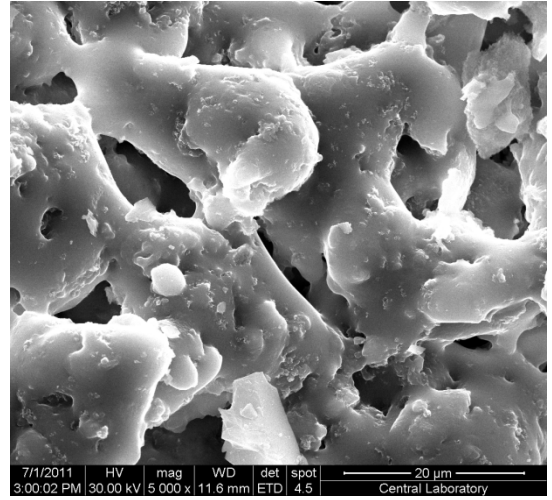
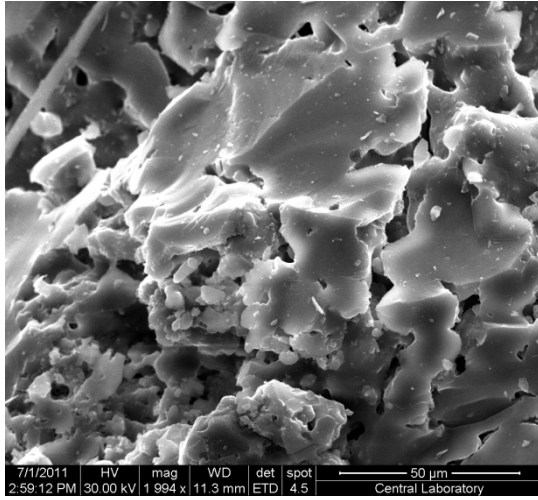


Figure 62. SEM images of SAPO-34 #24

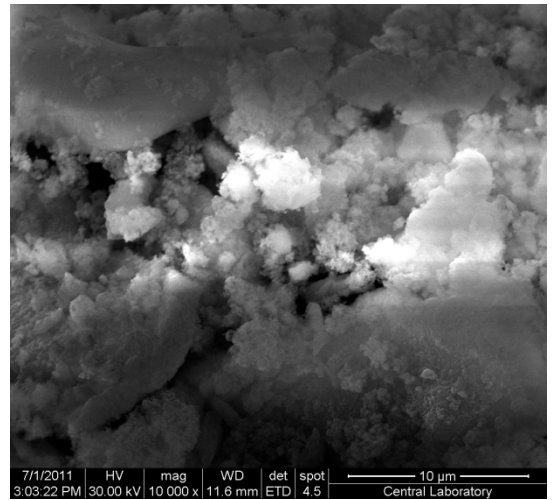
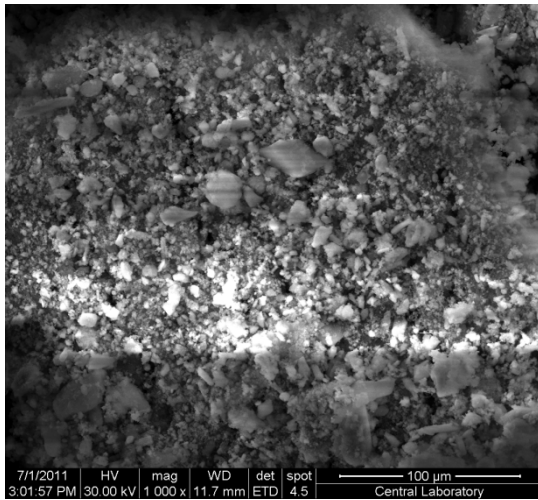


Figure 63. SEM images of SAPO-34 #25

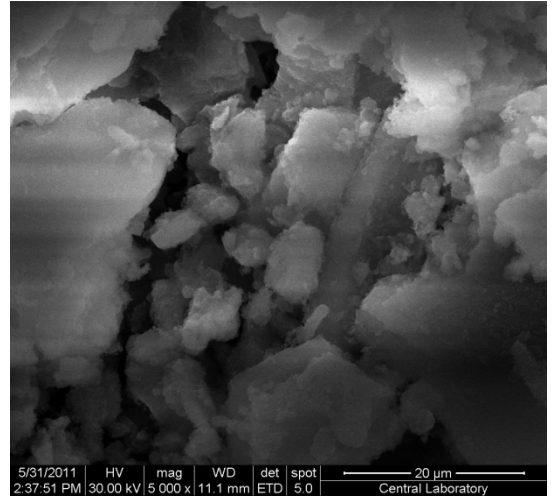
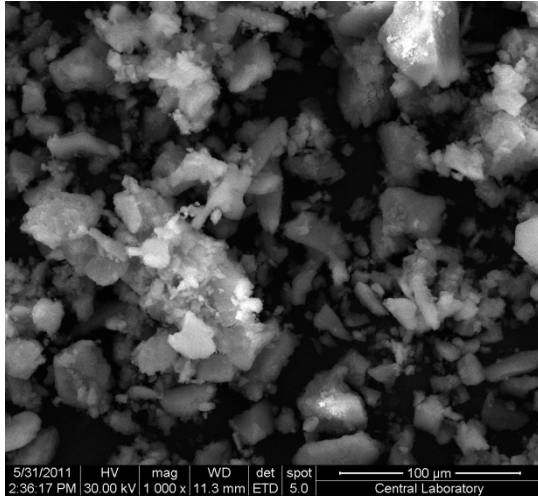


Figure 64. SEM images of SAPO-34 #26

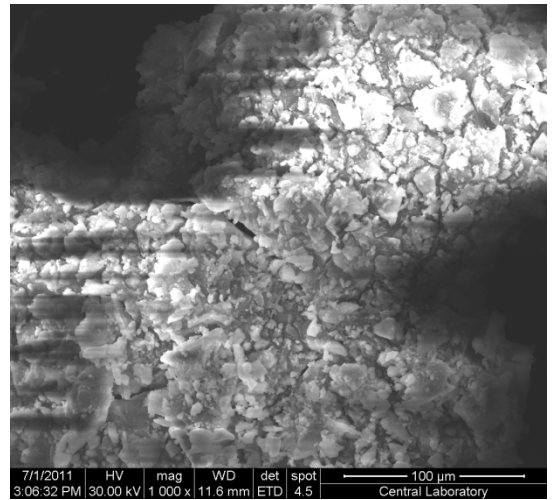
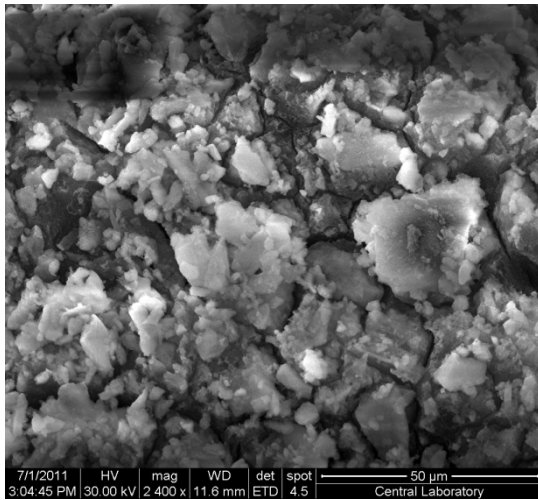


Figure 65. SEM images of SAPO-34 #27

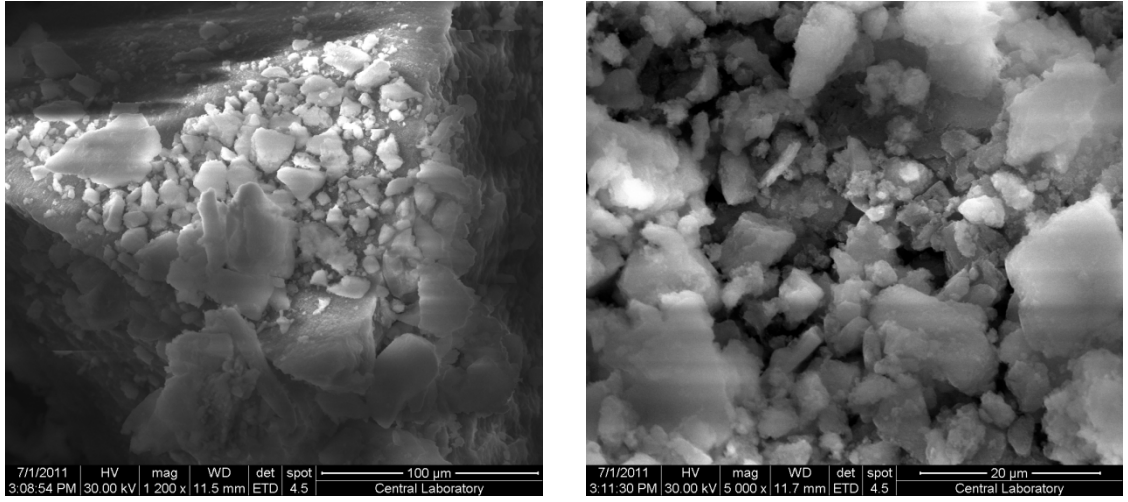


Figure 66. SEM images of SAPO-34 #28

APPENDIX E

CONVERSION, SELECTIVITY AND YIELD VALUES

Table 25. Conversion, selectivity and yield obtained by SAPO-34 #19

Temperature (°C)	Conversion (%)	S _{DME}	S _{FA}	Y _{DME}	Y _{FA}
150	8.3	0.849	0.151	0.071	0.013
200	45.1	0.979	0.021	0.441	0.009
250	67.5	0.994	0.006	0.671	0.004
300	3.3	0.777	0.223	0.025	0.007
350	6.5	0.890	0.110	0.058	0.007
400	15.1	0.953	0.047	0.144	0.007
450	28.5	0.979	0.021	0.279	0.006
500	33.6	0.984	0.016	0.330	0.006
550	21.1	0.965	0.035	0.204	0.007
600	8.6	0.903	0.097	0.078	0.008
650	5.3	0.810	0.190	0.043	0.010
700	5.3	0.764	0.236	0.040	0.012
750	3.0	0.653	0.347	0.020	0.010

Table 26. Conversion, selectivity and yield obtained by SAPO-34 #19 (repeated)

Temperature (°C)	Conversion (%)	S_{DME}	S_{FA}	Y_{DME}	Y_{FA}
150	8.9	0.852	0.148	0.076	0.013
200	45.9	0.982	0.018	0.451	0.008
250	68.7	0.996	0.004	0.684	0.003
300	4.5	0.778	0.222	0.035	0.010
350	7.8	0.890	0.110	0.069	0.009
400	16.3	0.954	0.046	0.156	0.007
450	29.7	0.980	0.020	0.291	0.006
500	34.9	0.985	0.015	0.344	0.005
550	22.6	0.970	0.030	0.219	0.007
600	9.9	0.905	0.095	0.090	0.009
650	6.7	0.815	0.185	0.055	0.012
700	6.8	0.773	0.227	0.053	0.015
750	4.2	0.658	0.342	0.028	0.014

Table 27. Conversion, selectivity and yield obtained by SAPO-34 #19
(regenerated)

Temperature (°C)	Conversion (%)	S_{DME}	S_{FA}	Y_{DME}	Y_{FA}
150	5.6	0.840	0.160	0.047	0.009
200	39	0.970	0.030	0.378	0.012
250	58	0.990	0.010	0.574	0.006
300	1.5	0.768	0.232	0.012	0.003
350	4.7	0.880	0.120	0.041	0.006
400	11.2	0.940	0.060	0.105	0.007
450	24.8	0.970	0.030	0.241	0.007
500	29.7	0.972	0.028	0.289	0.008
550	17.7	0.955	0.045	0.169	0.008
600	4.8	0.891	0.109	0.043	0.005
650	1.7	0.792	0.208	0.013	0.004
700	1.6	0.752	0.248	0.012	0.004
750	1.6	0.642	0.358	0.010	0.006

Table 28. Conversion, selectivity and yield obtained by SAPO-34 #20

Temperature (°C)	Conversion (%)	S _{DME}	S _{FA}	Y _{DME}	Y _{FA}
150	0.3	0.000	1.000	0.000	0.003
200	0.3	0.000	1.000	0.000	0.003
250	0.3	0.000	1.000	0.000	0.003
300	0.3	0.000	1.000	0.000	0.003
350	0.3	0.000	1.000	0.000	0.003
400	0.3	0.000	1.000	0.000	0.003
450	0.4	0.000	1.000	0.000	0.004
500	0.4	0.000	1.000	0.000	0.004

Table 29. Conversion, selectivity and yield obtained by SAPO-34 #21

Temperature (°C)	Conversion (%)	S _{DME}	S _{FA}	Y _{DME}	Y _{FA}
150	0.5	0.000	1.000	0.000	0.005
200	0.3	0.000	1.000	0.000	0.003
250	0.4	0.295	0.706	0.001	0.003
300	2.4	0.703	0.297	0.017	0.007
350	5.2	0.897	0.103	0.047	0.005
400	13.0	0.954	0.046	0.124	0.006
450	31.7	0.975	0.025	0.309	0.008
500	41.2	0.990	0.011	0.407	0.004
550	48.0	0.991	0.009	0.476	0.004
600	31.5	0.976	0.024	0.308	0.008
650	25.0	0.967	0.033	0.241	0.008
700	16.7	0.899	0.101	0.150	0.017

Table 30. Conversion, selectivity and yield obtained by using SAPO-34 #22

Temperature (°C)	Conversion (%)	S _{DME}	S _{FA}	Y _{DME}	Y _{FA}
150	0.3	0.000	1.000	0.000	0.003
200	0.3	0.000	1.000	0.000	0.003
250	0.3	0.000	1.000	0.000	0.003
300	0.3	0.000	1.000	0.000	0.003
350	0.3	0.000	1.000	0.000	0.003
400	1.7	0.753	0.247	0.013	0.004
450	8.4	0.930	0.070	0.078	0.006
500	23.4	0.956	0.044	0.224	0.010

Table 31. Conversion, selectivity and yield obtained by using SAPO-34 #24

Temperature (°C)	Conversion (%)	S _{DME}	S _{FA}	Y _{DME}	Y _{FA}
150	0.4	0.000	1	0.000	0.004
200	0.3	0.000	1	0.000	0.003
250	0.4	0.000	1	0.000	0.004
300	0.3	0.000	1	0.000	0.003
350	0.3	0.000	1	0.000	0.003
400	0.3	0.000	1	0.000	0.003
450	0.4	0.000	1	0.000	0.004
500	0.5	0.000	1	0.000	0.005

Table 32. Conversion, selectivity and yield obtained by using SAPO-34 #25

Temperature (°C)	Conversion (%)	S_{DME}	S_{FA}	Y_{DME}	Y_{FA}
150	0.4	0.000	1.000	0.000	0.004
200	0.3	0.000	1.000	0.000	0.003
250	0.3	0.000	1.000	0.000	0.003
300	0.7	0.000	1.000	0.000	0.007
350	0.1	0.000	1.000	0.000	0.001
400	0.6	0.615	0.385	0.003	0.002
450	2.9	0.791	0.209	0.023	0.006
500	6.8	0.915	0.085	0.062	0.006
550	19.2	0.986	0.014	0.189	0.003

Table 33. Conversion, selectivity and yield obtained by using SAPO-34 #26

Temperature (°C)	Conversion (%)	S_{DME}	S_{FA}	Y_{DME}	Y_{FA}
150	0.4	0.000	1.000	0.000	0.004
200	0.4	0.000	1.000	0.000	0.004
250	0.3	0.000	1.000	0.000	0.003
300	0.8	0.574	0.426	0.005	0.004
350	1.6	0.631	0.369	0.010	0.006
400	2.6	0.647	0.353	0.017	0.009
450	14.6	0.941	0.060	0.137	0.009
500	31.6	0.967	0.033	0.306	0.010
550	28.3	0.989	0.012	0.279	0.003

Table 34. Conversion, selectivity and yield obtained by using SAPO-34 #27

Temperature (°C)	Conversion (%)	S _{DME}	S _{FA}	Y _{DME}	Y _{FA}
150	0.3	0.000	1.000	0.000	0.003
200	0.3	0.000	1.000	0.000	0.003
250	0.3	0.000	1.000	0.000	0.003
300	0.3	0.000	1.000	0.000	0.003
350	0.3	0.000	1.000	0.000	0.003
400	0.3	0.000	1.000	0.000	0.003
450	2.7	0.808	0.193	0.021	0.005
500	8.8	0.907	0.093	0.080	0.008
550	23.5	0.981	0.019	0.230	0.005

Table 35. Conversion, selectivity and yield obtained by using SAPO-34 #28

Temperature (°C)	Conversion (%)	S _{DME}	S _{FA}	Y _{DME}	Y _{FA}
150	0.3	0.000	1.000	0.000	0.003
200	0.3	0.000	1.000	0.000	0.003
250	0.4	0.000	1.000	0.000	0.004
300	0.3	0.000	1.000	0.000	0.003
350	1.8	0.712	0.289	0.013	0.005
400	4.3	0.867	0.133	0.037	0.006
450	11.7	0.946	0.054	0.111	0.006
500	30.1	0.974	0.026	0.293	0.008
550	48.8	1.000	0.000	0.488	0.000

APPENDIX F

REACTION RAW DATA

Tables below show the average areas for dimethyl ether, formaldehyde and methanol obtained from gas chromatography analyses.

Table 36. Experimental data for SAPO-34 #19

Temperature (°C)	A _{DME}	A _{FA}	A _{MeOH}
150	39.9	8.1	784.8
200	254.3	6.2	481.0
250	324.0	2.1	238.3
300	14.1	4.6	821.0
350	31.5	4.5	768.0
400	90.0	5.1	804.7
450	159.4	3.9	620.5
500	218.3	4.2	667.0
550	107.1	4.5	630.0
600	30.6	3.7	545.7
650	13.5	3.6	451.7
700	10.3	3.6	367.7
750	5.3	3.2	403.0

Table 37. Experimental data for SAPO-34 #19 (repeated)

Temperature (°C)	A_{DME}	A_{FA}	A_{MeOH}
150	42.9	6.3	754.2
200	248.3	5.4	453.2
250	309	1.4	215.1
300	21.2	4	803.6
350	36.6	3.7	720.5
400	98.2	4.2	794.1
450	165.3	3.2	604.2
500	223.7	3.2	642.9
550	113.6	3.3	606.5
600	35.9	3	533.4
650	17.8	2.9	432.7
700	14.1	2.6	343.2
750	9.1	2.5	392.8

Table 38. Experimental data for SAPO-34 #19 (regenerated)

Temperature (°C)	A_{DME}	A_{FA}	A_{MeOH}
150	23.7	5.7	741.1
200	183.2	5.1	446.6
250	189.8	1.1	209.6
300	5.2	3.4	789.3
350	19.9	3.1	702.4
400	62.4	3.3	783.2
450	125.9	2.7	591.8
500	170.4	2.6	622.3
550	82.3	2.7	598.1
600	15.1	2.4	521.9
650	2.7	2.3	421.6
700	1.7	2.2	332.6
750	2.0	2.2	378.2

Table 39. Experimental data for SAPO-34 #20

Temperature (°C)	A_{DME}	A_{FA}	A_{MeOH}
150	0.0	2.4	949.3
200	0.0	2.3	906.5
250	0.0	2.3	1058.5
300	0.0	2.4	924.0
350	0.0	2.4	935.0
400	0.0	2.2	895.0
450	0.0	2.1	717.0
500	0.0	1.7	524.0

Table 40. Experimental data for SAPO-34 #21

Temperature (°C)	A_{DME}	A_{FA}	A_{MeOH}
150	0.0	1.9	531.0
200	0.0	1.8	734.3
250	0.7	2.0	916.0
300	8.0	3.9	719.0
350	27.4	3.6	840.0
400	71.3	3.9	761.5
450	170.0	4.9	572.0
500	197.5	2.4	433.5
550	252.5	2.7	419.5
600	147.5	4.1	499.5
650	102.0	4.0	482.0
700	25.0	3.2	210.5

Table 41. Experimental data for SAPO-34 #22

Temperature (°C)	A_{DME}	A_{FA}	A_{MeOH}
150	0.0	2.1	832.3
200	0.0	2.1	904.3
250	0.0	2.0	828.5
300	0.0	2.1	900.0
350	0.0	2.1	897.0
400	6.6	2.5	796.5
450	38.5	3.3	685.5
500	34.7	1.8	180.5

Table 42. Experimental data for SAPO-34 #24

Temperature (°C)	A_{DME}	A_{FA}	A_{MeOH}
150	0.0	2.7	967.5
200	0.0	2.3	940.5
250	0.0	2.3	819.5
300	0.0	2.3	966.0
350	0.0	2.2	921.5
400	0.0	2.1	838.0
450	0.0	1.8	676.0
500	0.0	1.6	443.0

Table 43. Experimental data for SAPO-34 #25

Temperature (°C)	A_{DME}	A_{FA}	A_{MeOH}
150	0.0	2.6	931.7
200	0.0	2.2	931.0
250	0.0	2.3	972.0
300	0.0	4.5	909.0
350	0.0	0.7	876.0
400	1.2	0.9	540.0
450	11.9	3.6	777.5
500	27.7	2.9	627.5
550	31.9	0.5	207.0

Table 44. Experimental data for SAPO-34 #26

Temperature (°C)	A_{DME}	A_{FA}	A_{MeOH}
150	0.0	2.2	801.0
200	0.0	2.3	846.5
250	0.0	2.2	863.5
300	2.4	2.1	791.5
350	5.2	3.5	772.0
400	8.6	5.4	753.0
450	63.9	4.6	604.0
500	109.0	4.3	371.0
550	98.9	1.3	386.0

Table 45. Experimental data for SAPO-34 #27

Temperature (°C)	A_{DME}	A_{FA}	A_{MeOH}
150	0.0	2.2	869.7
200	0.0	2.1	902.0
250	0.0	2.1	918.0
300	0.0	2.0	956.0
350	0.0	2.1	904.0
400	0.0	2.0	840.0
450	11.4	3.1	788.0
500	30.4	3.6	527.5
550	36.8	0.8	186.0

Table 46. Experimental data for SAPO-34 #28

Temperature (°C)	A_{DME}	A_{FA}	A_{MeOH}
150	0.0	2.4	907.3
200	0.0	2.3	888.5
250	0.0	2.2	846.0
300	0.0	2.2	874.0
350	8.1	3.7	918.0
400	22.4	3.9	876.5
450	58.8	3.8	711.5
500	124.0	3.7	450.0
550	121.0	0.0	193.0

APPENDIX G

EQUILIBRIUM CONVERSION FOR METHANOL DEHYDRATION REACTION

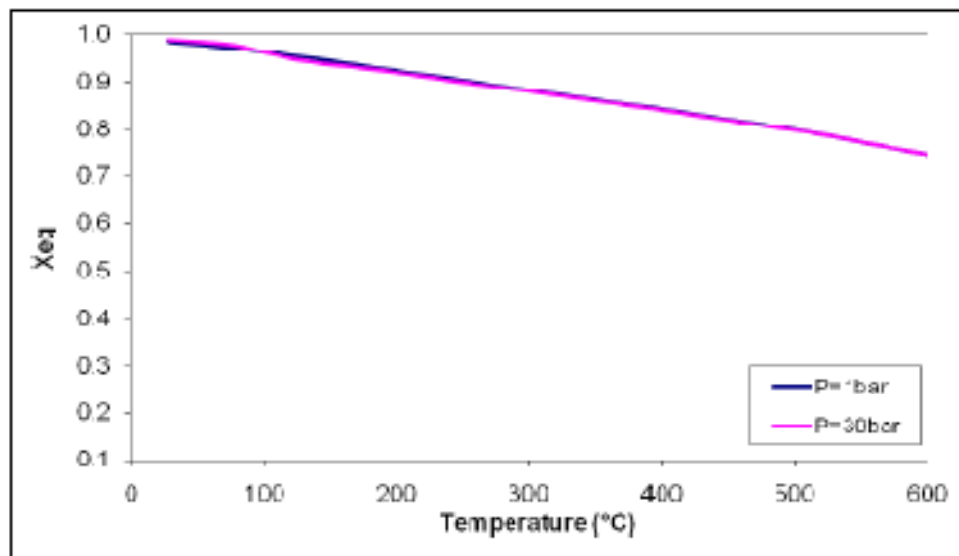


Figure 67. Effect of temperature on equilibrium conversion for methanol dehydration reaction [5]